

New Chronology for El Teniente, Chilean Andes, from U-Pb, $^{40}\text{Ar}/^{39}\text{Ar}$, Re-Os, and Fission-Track Dating: Implications for the Evolution of a Supergiant Porphyry Cu-Mo Deposit

VICTOR MAKSAEV,[†] FRANCISCO MUNIZAGA,

Departamento de Geología, Universidad de Chile, Casilla 13518, Correo 21, Santiago, Chile

MICHAEL MCWILLIAMS,

Department of Geological and Environmental Sciences, Stanford University, Stanford, California 94305-2115

MARK FANNING,

Research School of Earth Sciences, Australian National University, Canberra ACT 0200, Australia

RYAN MATHUR,

Geology Department, Juniata College, 1700 Moore Street, Huntingdon, Pennsylvania 16652

JOAQUIN RUIZ,

Department of Geosciences, University of Arizona, Gould-Simpson Building, 1040E Fourth Street, Tucson, Arizona 85721-0077

AND MARCOS ZENTILLI

Department of Earth Sciences, Dalhousie University, Halifax, Nova Scotia, Canada B3H 3J5

Abstract

Combined isotopic dating indicates five episodes of felsic intrusion within the El Teniente orebody: (1) Sewell stock and other quartz diorite-tonalite intrusions of the eastern part crystallized from 6.46 ± 0.11 to 6.11 ± 0.13 Ma (zircon U-Pb); (2) quartz diorite-tonalite, immediately southeast of the orebody, with biotite $^{40}\text{Ar}/^{39}\text{Ar}$ plateau ages of 5.63 ± 0.12 and 5.47 ± 0.12 Ma—these ages agree with a hydrothermal overprint on zircons from the intrusions of the previous episode at 5.67 ± 0.19 to 5.48 ± 0.19 Ma (U-Pb); (3) Teniente dacite porphyry crystallized at 5.28 ± 0.10 Ma (zircon U-Pb); (4) a dacite ring dike encircling the Braden pipe crystallized at 4.82 ± 0.09 Ma (zircon U-Pb); and (5) minor dacite intrusions and dikes yielded a biotite $^{40}\text{Ar}/^{39}\text{Ar}$ plateau age of 4.58 ± 0.10 Ma, and sericite $^{40}\text{Ar}/^{39}\text{Ar}$ plateau ages of 4.56 ± 0.12 to 4.46 ± 0.10 Ma. All these felsic intrusions were emplaced within country rocks of late Miocene according to an apatite fission-track age of 8.9 ± 2.8 Ma for a mafic sill, in accord with previous K-Ar ages of 12.0 ± 0.7 to 6.6 ± 0.4 Ma for volcanic rocks from the district.

Molybdenite Re-Os dating at El Teniente revealed ore deposition at 6.30 ± 0.03 , 5.60 ± 0.02 , 5.01 to 4.96 , 4.89 ± 0.08 to 4.78 ± 0.03 , and 4.42 ± 0.02 Ma, concurrent with the five intrusive episodes. The Re-Os system for molybdenite was unaffected by the various hydrothermal episodes. In contrast, the $^{40}\text{Ar}/^{39}\text{Ar}$ system of micas was reset by high-temperature ($>350^\circ\text{C}$) fluid circulation and provides only a partial record of the latest history of development of this supergiant ore-forming system; biotite, sericite, and altered whole-rock samples collected throughout the orebody yielded 40 $^{40}\text{Ar}/^{39}\text{Ar}$ plateau ages ranging from 5.06 ± 0.12 to 4.37 ± 0.10 Ma. These ages reveal a period of hydrothermal activity, which extended either continuously or episodically, for at least 0.69 ± 0.22 m.y. ($\pm 2\sigma$) and that comprises a succession of three episodes of ore deposition. Separate hydrothermal episodes are thus interpreted to have lasted $<0.69 \pm 0.22$ m.y.

The Braden breccia pipe in the center of the deposit was formed as a single synmineralization event, probably related in time to the injection of the dacite ring dikes at 4.82 ± 0.09 Ma (zircon U-Pb). It was followed by quartz-sericite alteration within and peripheral to, the pipe from 4.81 ± 0.12 to 4.37 ± 0.10 Ma (sericite $^{40}\text{Ar}/^{39}\text{Ar}$).

The successive intrusions of felsic bodies and their respective crystallization processes were immediately followed by genetically related, short-lived episodes of ore deposition, each associated with hydrothermal alteration. This multistage evolution, inferred from systematic dating, was not apparent from previous geochronologic data and is inferred to have contributed to the enormous volume and richness of the El Teniente. Thermal modeling of apatite fission-track data suggests that the porphyry system cooled very rapidly to temperatures below $105^\circ \pm 20^\circ\text{C}$, most likely before the intrusion of a postore hornblende-rich andesitic dike at 3.85 ± 0.18 Ma (hornblende $^{40}\text{Ar}/^{39}\text{Ar}$). This dike cuts the southern part of the El Teniente deposit and marks the end of igneous activity in the orebody.

[†]Corresponding author: e-mail, vmaksaev@cec.uchile.cl

Resumen

Cinco episodios de intrusiones félsicas en El Teniente se evidencian por una combinación de dataciones isotópicas: (1) El stock Sewell y otras intrusiones de diorita cuarcífera-tonalita del sector oriental cristalizaron de $6,46 \pm 0,11$ Ma a $6,11 \pm 0,13$ Ma (U-Pb en circón); (2) diorita cuarcífera-tonalita, inmediatamente al sureste del cuerpo mineralizado, con edades plateau $^{40}\text{Ar}/^{39}\text{Ar}$ en biotita de $5,63 \pm 0,19$ y $5,47 \pm 0,12$ Ma; estas edades coinciden con una sobreimposición hidrotermal en los circones de los intrusivos del episodio anterior de $5,67 \pm 0,19$ a $5,48 \pm 0,19$ Ma (U-Pb); (3) el pórfido dacítico Teniente cristalizó a los $5,28 \pm 0,19$ Ma (U-Pb en circón); (4) un dique dacítico anular, que rodea a la chimenea de brecha Braden, cristalizó a los $4,82 \pm 0,09$ Ma (U-Pb en circón); (5) intrusivos dacíticos menores y diques dieron una edad plateau $^{40}\text{Ar}/^{39}\text{Ar}$ en biotita de $4,58 \pm 0,10$ Ma y edades plateau $^{40}\text{Ar}/^{39}\text{Ar}$ en sericita de $4,56 \pm 0,12$ a $4,46 \pm 0,10$ Ma. Todas estas intrusiones félsicas fueron emplazadas en rocas encajadoras del Mioceno tardío de acuerdo a una datación de trazas de fisión en apatita de un sill máfico de $8,9 \pm 2,8$ Ma, coincidente con edades previas K-Ar de $12,0 \pm 0,7$ a $6,6 \pm 0,4$ de rocas volcánicas del distrito.

Dataciones Re-Os en molibdenita revelaron precipitación de menas a los $6,30 \pm 0,03$ Ma, $5,60 \pm 0,02$ Ma, $5,01$ a $4,96$ Ma, $4,89 \pm 0,08$ a $4,78 \pm 0,03$ Ma y $4,42 \pm 0,02$ Ma, coincidentes con los cinco episodios intrusivos. El sistema Re-Os de las molibdenitas no fue afectado por los varios episodios hidrotermales, mientras que el sistema $^{40}\text{Ar}/^{39}\text{Ar}$ de las micas fue rejuvenecido por la circulación de fluidos a alta temperatura ($>350^\circ\text{C}$) y provee solo un registro parcial de la historia más reciente del desarrollo de este sistema mineralizador supergigante; biotita, sericita y rocas alteradas recolectadas en todo el yacimiento entregaron 40 edades plateau $^{40}\text{Ar}/^{39}\text{Ar}$ en el rango desde $5,06 \pm 0,12$ Ma hasta $4,37 \pm 0,10$ Ma. Estas dataciones revelan un período de actividad hidrotermal, el cual se extendió, ya sea continuamente o en forma episódica, por al menos $0,69 \pm 0,22$ millones de años ($\pm 2\sigma$) y que comprende una sucesión de tres episodios separados de precipitación de menas, los cuales, en consecuencia, deben haber durado menos de $0,69 \pm 0,22$ millones de años.

La chimenea de brecha Braden en el centro del depósito se formó en un evento sinmineralización, probablemente relacionado en el tiempo a la inyección de diques anulares a los $4,82 \pm 0,09$ Ma (U-Pb en circón). Subsecuentemente ocurrió alteración hidrotermal cuarzo-sericítica dentro y en la periferia de la chimenea de $4,81 \pm 0,12$ a $4,37 \pm 0,10$ Ma ($^{40}\text{Ar}/^{39}\text{Ar}$ en sericita).

La sucesiva intrusión de cuerpos félsicos y su cristalización fueron seguidas inmediatamente por episodios de mineralización, genéticamente relacionados, de corta duración, cada uno asociado con alteración hidrotermal. La evolución con múltiples etapas inferidas por datación sistemática, no era obvia de los datos geocronológicos previos, pero se infiere que contribuyó al enorme volumen y riqueza del yacimiento El Teniente. El modelo termal de datos trazas de fisión en apatito sugiere que el sistema porfírico se enfrió muy rápido a temperaturas por debajo de $105 \pm 20^\circ\text{C}$, probablemente antes de la intrusión de un dique postmineral de andesita rica en hornblenda de $3,85 \pm 0,18$ Ma ($^{40}\text{Ar}/^{39}\text{Ar}$ en hornblenda). Este dique corta la sección sur del cuerpo mineralizado de El Teniente y marca el fin de la actividad ígnea en el yacimiento.

Introduction

EL TENIENTE (Fig. 1) is the youngest porphyry Cu-Mo deposit of the Chilean Andes and the largest deposit in the world. It has continuously been mined since 1906, producing 15.71 million metric tons (Mt) of copper; the mineral reserves inventory in 1999 was 1,252 Mt at 1.0 percent Cu (Camus, 2003). The deposit currently sustains an exceptionally large underground bulk mining operation with daily production of 98,000 t of ore at 1.2 percent Cu and 0.026 percent Mo; expansion is underway to 130,000 t/d by 2005. Mining operations take place between levels 1,980 (transport level) and 2,625 m, but the premine surface was at 3,120 m above sea level. Remarkably, much of the supergiant orebody is hypogene, with copper grades mostly ranging from 0.65 to 1.50 percent Cu (Skewes et al., 2002), with even higher primary grades occurring within parts of dense stockwork or mineralized hydrothermal breccia. The uppermost 50 to 150 m of the deposit was leached and oxidized. It grades downward to a secondary enriched zone 100 to 500 m thick, typified by supergene chalcocite (Howell and Molloy, 1960; Cuadra, 1986). The enriched ore amounted to 956 Mt at 1.68 percent Cu but is now largely exhausted; the secondary enrichment was 2.4 times the average primary Cu grade (Camus, 2003).

Previous K-Ar ages for altered rocks and hydrothermal micas, ranging from 7.4 ± 1.5 to 4.0 ± 0.4 Ma, established that

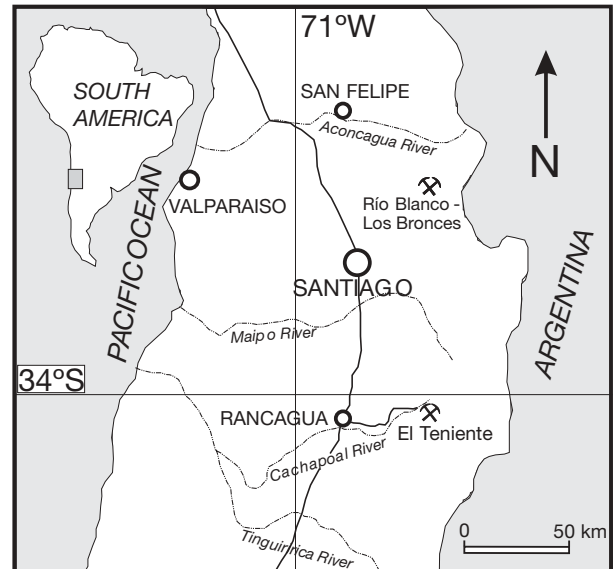


FIG. 1. Location map of the El Teniente mine.

the El Teniente deposit was formed by a late Miocene to Pliocene magmatic-hydrothermal system (Clark et al., 1983; Cuadra, 1986). The peak of the K-Ar ages for micas at 4.6 to

4.7 Ma, presumably formed in association with the ore, was interpreted to represent the main-stage ore deposition (Cuadra, 1986). Although the K-Ar data provided a first chronology for the deposit, the precise age of mineralization remained uncertain and subject to further interpretations (e.g., Skewes et al., 2002). The determination of the precise age of mineralization within an ore-forming system is essential for understanding genetic processes and locating economic deposits. We used a combination of SHRIMP U-Pb, Re-Os, $^{40}\text{Ar}/^{39}\text{Ar}$, and fission-track geochronology to resolve the timing of mineralizing events and the duration of hydrothermal activity at El Teniente. In this contribution we provide a new detailed chronologic framework for the El Teniente orebody and discuss the implications of the geochronologic data for its evolution.

Metallogenic Setting

The supergiant El Teniente porphyry Cu-Mo deposit (resources of 75 Mt of contained Cu) is the southernmost known economic mineralized center in a north-south-trending Neogene metallogenic belt that extends along the upper western slopes of the Andean Cordillera in Chile and Argentina (Fig. 2). The belt includes other enormous Cu-Mo porphyries, such as Río Blanco-Los Bronces (50 Mt of contained Cu) and Los Pelambres-El Pachón (25 Mt of contained Cu), located 100 and 260 km north of El Teniente, respectively. Farther north, the Neogene metallogenic belt includes world-class Miocene epithermal precious metal deposits and less important Au, Cu, and Cu-Au porphyries in the El Indio-Mariquina belt (Davidson and Mpodozis, 1991; Sillitoe, 1991; Fig. 2). In central Chile, the Neogene metallogenic belt coincides with the position of Miocene volcanic centers and associated flat-lying volcanic rocks, sills, and dikes. The Miocene volcanic sequence, with an average thickness of 2,500 m, comprises andesite, basalt (lavas and sills), dacite, and intercalations of rhyolitic tuff, which constitute a north-south belt ~20 km wide (Farellones Formation; Thiele, 1980; Rivano et al., 1990). Eruption of these volcanic rocks occurred at a number of volcanic centers, possibly localized by intersections of regional structures. These volcanic rocks unconformably overlie folded Oligocene to early Miocene andesitic volcanic and continental sedimentary rocks (Abanico and Coya-Machalí Formations; Thiele, 1980; Charrier et al., 2002). The Miocene to Pliocene porphyry Cu-Mo deposits occur within hydrothermal alteration zones related to multiphase porphyritic stocks with compositions ranging from quartz diorite to granodiorite. These intrusions and their country rocks host dense networks of sulfide-bearing veins and associated hydrothermal breccia complexes. The country rocks are late Miocene basaltic and andesitic volcanic rocks, diabase sills, and gabbro at El Teniente, Miocene andesite and a middle Miocene granodioritic batholith at Río Blanco-Los Bronces (San Francisco batholith; Serrano et al., 1996), and folded Early Cretaceous volcanic and sedimentary rocks at Los Pelambres (Atkinson et al., 1996).

The El Teniente deposit occurs within an arc-related late Miocene to Pliocene volcano-plutonic complex (e.g., Howell and Molloy, 1960; Camus, 1975, 2003; Cuadra, 1986; Skewes and Stern, 1995). Although late Pliocene dikes and lavas are documented in the region (Charrier and Munizaga, 1979;

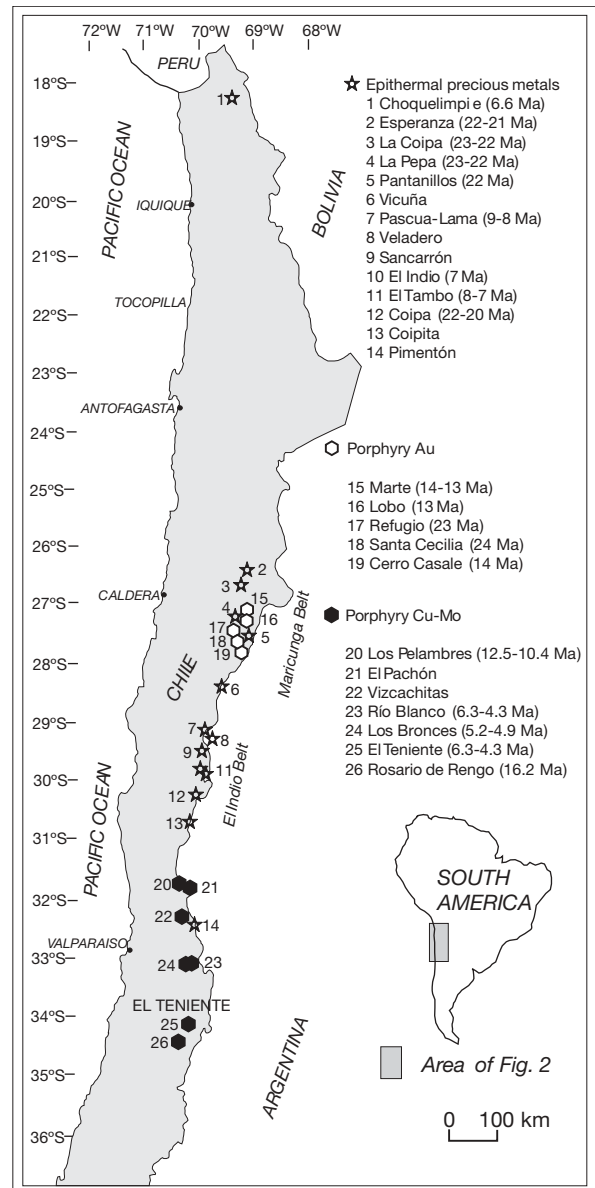


FIG. 2. Neogene metallogenic belt in the Andes of northern Chile. Ages of ore deposits compiled from Gröpper et al. (1991), Sillitoe et al. (1991), Kay and Kurtz (1995), Moscoso et al. (1993), McKee et al. (1994), Serrano et al. (1996), Bissing et al. (2001, 2002), Muntean and Einaudi (2001), Bertens et al. (2003), and Deckart et al. (2003).

Cuadra, 1986; Godoy and Köppen, 1993), El Teniente is now located in the forearc of the northernmost segment of the currently active Andean southern volcanic zone, which extends from latitude 33° to 46° S. The locus of subduction-related arc magmatism therefore migrated some 50 km east after the formation of the deposit (Kay and Kurtz, 1995).

Geologic Background

The El Teniente deposit is genetically related to late Miocene-early Pliocene magmatic-hydrothermal processes (Howell and Molloy, 1960; Camus, 1975, 2003; Cuadra, 1986; Skewes and Stern, 1995; Skewes et al., 2002). The mineralized body

(at $>0.5\%$ Cu) is $\sim 2,700$ m long in a north-south direction, 1,000 to 1,700 m wide (roughly triangular in plan; Fig. 3), and possesses a recognized vertical extent of about 1,800 m, excluding a funnel-shaped, centrally located, and poorly mineralized diatreme ($\sim 0.3\%$ Cu; Ortega, 1981). Some 20 percent of the copper and molybdenum resources at El Teniente occur within altered felsic stocks and dikes, but much of the orebody is hosted by pervasively altered, dark-gray to black basalt, andesite, diabase sills, and gabbro intrusions. K-Ar ages for unaltered volcanic rocks from beyond the mine in the El Teniente district range from 12.0 ± 0.7 to 6.6 ± 0.4 Ma ($\pm 2\sigma$; Cuadra, 1986; Godoy and Köepfen, 1993).

Lithologic units

The main lithologic units that host the El Teniente deposit (Fig. 4) are the following:

Andesites of the mine: This name is customarily given to the dark-colored, mostly porphyritic country rocks. Nearly all of the primary characteristics of these country rocks are obliterated by biotite-dominated hydrothermal alteration and locally superimposed chloritization and sericitization. Macroscopically, plagioclase crystals are recognized as white laths within a microcrystalline black groundmass. Microscopically, plagioclase phenocrysts are normally the only remnant of the primary igneous minerals; these are partially replaced by fine-grained biotite and anhydrite. Most of the original minerals have been replaced by a microcrystalline hydrothermal aggregate of biotite, anhydrite, opaque minerals (sulfides \pm magnetite), and minor actinolite. These pervasively altered host rocks have traditionally been considered as a volcanic section including lava, agglomerate, and volcanic breccia of the Miocene Farellones Formation (Howell and Molloy, 1960; Camus, 1975; Villalobos, 1975; Cuadra, 1986; Skewes

and Stern, 1995). The same altered units have recently been interpreted as a mineralized basic intrusive complex composed of gabbro, diabase, and basalt (Skewes and Arévalo, 1997, 2000; Skewes et al., 2002), as first recognized by Lindgren and Bastin (1922).

Sewell quartz diorite-tonalite: It is the largest felsic composite intrusive body at El Teniente (Fig. 4), and has a modal composition ranging from quartz diorite to tonalite (Fig. 5). The intrusion is about 1 km in diameter in the southeastern part of the underground mine (2,284-m level) but abruptly tapers upward to a maximum dimension of 200 m at surface (3,100 m a.s.l.). The upper altered part of the Sewell stock includes a stockwork of chalcopyrite-bearing veins, which gradually diminish in intensity and copper grade with depth. In addition, an irregular north-northeast-trending body of hydrothermal breccias is hosted by this pluton in the easternmost part of the deposit (Fig. 4); the breccia matrix has a pegmatite appearance and is composed of coarse-grained aggregates of anhydrite, biotite, chalcopyrite, and molybdenite. The mineralized portion of the Sewell stock is mainly porphyritic and originally included a breccia carapace with tourmaline-bearing matrix (Camus, 1975). However, much of the pluton is medium grained and equigranular and this rock type extends irregularly outside the orebody for ~ 5 km to the southwest. According to Reich (2001), beyond the economic limits of the orebody the Sewell stock is considerably less altered, preserving much of the original magmatic texture and mineralogy. However, our geochronologic data suggest that this fresh equigranular quartz diorite is a distinct intrusion (see below). The porphyritic facies includes ~ 50 to 60 percent phenocrysts composed of plagioclase (up to 4 mm long), biotite, and relict amphibole in a groundmass composed of quartz, plagioclase microlites, and minor K-feldspar. The

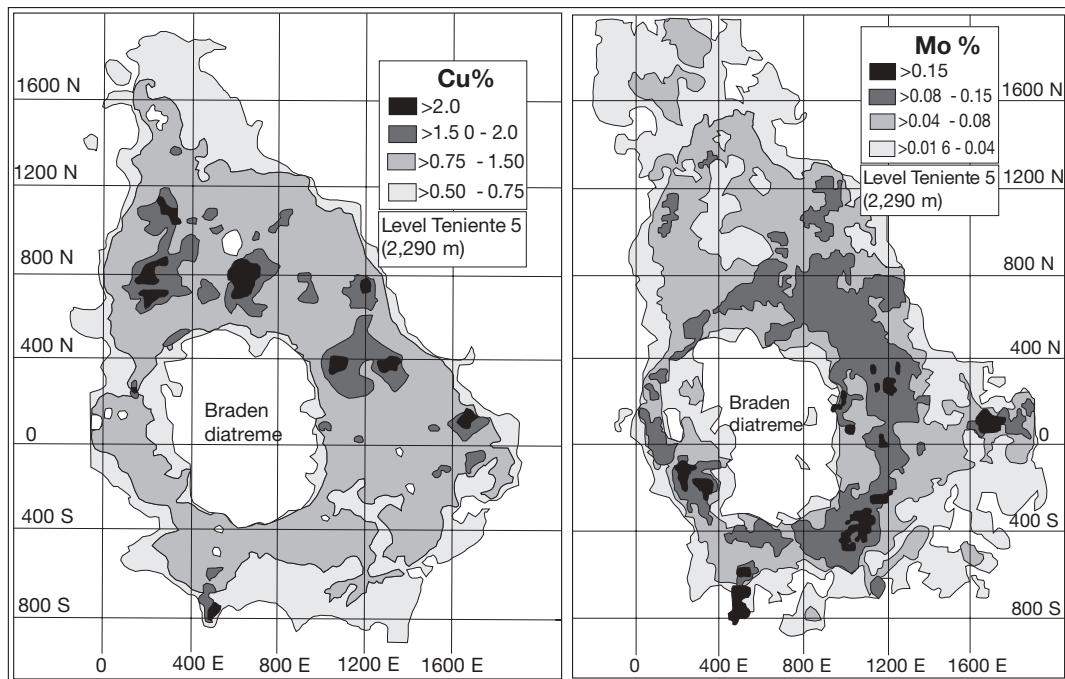


FIG. 3. Cu- and Mo-grade distribution in the Teniente 5 level (2,290 m) of the El Teniente orebody (after Skewes et al., 2002, and Valenzuela, 2003). Local mine grid (metric) is shown.

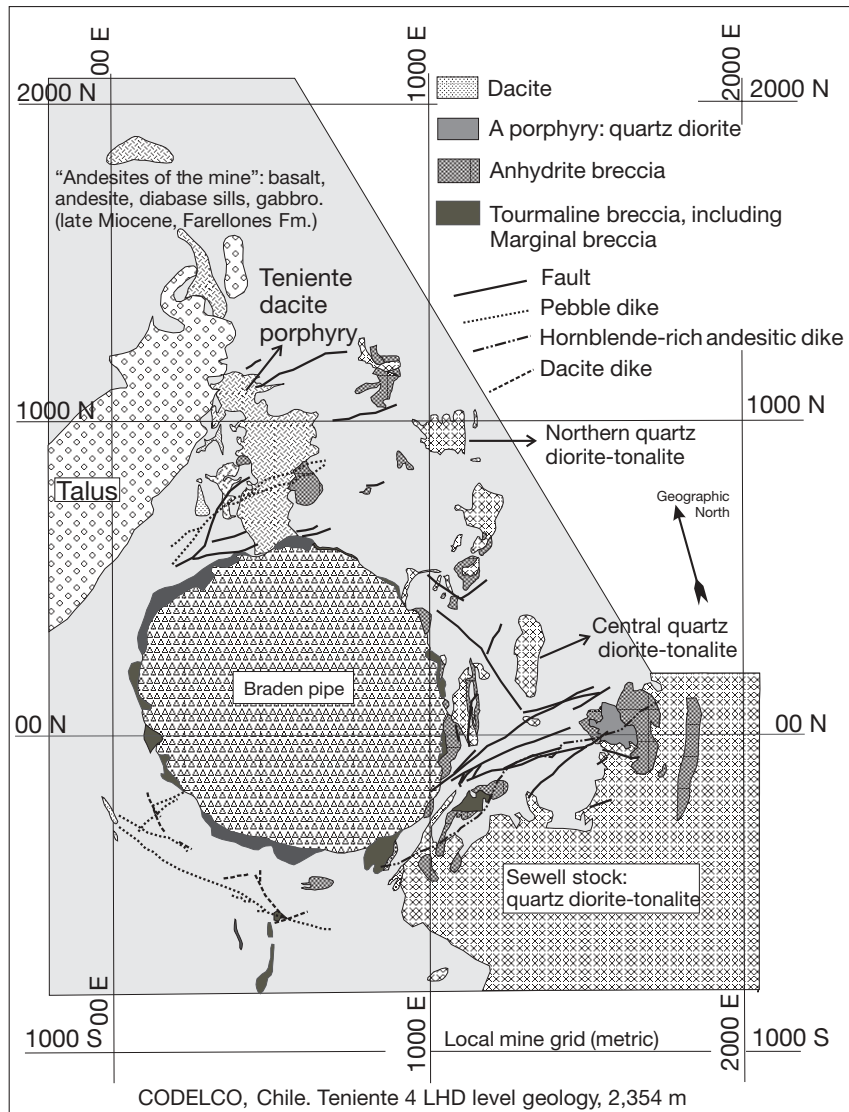


FIG. 4. Geology of the Teniente 4 LHD level (2,354 m) of the El Teniente mine (provided by El Teniente Division of CODELCO-Chile).

granular facies displays hypidiomorphic-granular aggregates of 60 to 70 vol percent plagioclase, 5 to 7 percent chloritized hornblende, and 1 to 5 percent biotite with 10 to 25 percent fine-grained interstitial quartz and 2 to 4 percent K-feldspar (Faunes, 1981; Reich, 2001). It is uncertain whether the porphyritic parts of the Sewell stock, and other apophyses of similar lithology to the north, represent rapidly cooled parts of the same stock or distinct porphyry intrusions (Camus, 1975; Faunes, 1981; Guzmán, 1991). Transitional contacts within porphyritic and equigranular facies of the Sewell stock were described by Faunes (1981), suggesting that the Sewell stock taken as a whole is a composite intrusion.

Central and Northern quartz diorite-tonalite stocks: These are porphyritic apophyses that occur in the eastern part of the orebody north of the Sewell stock. These separate minor intrusive bodies (Fig. 4) are customarily correlated with the Sewell stock (e.g., Cuadra, 1986). The quartz diorite-tonalite stocks of the eastern portion of El Teniente, including the

northernmost portion of the Sewell stock, contain a dense stockwork of chalcopyrite-bearing veins and are pervasively sericitized in their upper parts, whereas biotite-dominated potassic alteration occurs at depth (Cuadra, 1986).

Various interpretations of the role of these intrusions in the mineralizing processes at El Teniente have been published. The early study of Lindgren and Bastin (1922) concluded that alteration of quartz diorite was accompanied by sparse deposition of sulfides, but Howell and Molloy (1960) pointed out the clear relationship between the quartz diorite and sulfide ores. Further studies by Camus (1975) and, especially, Cuadra (1986) related the earliest stage of significant mineralization and potassic and quartz-sericite alteration events to the emplacement of this north-south corridor of quartz diorite-tonalite intrusions. In contrast, Skewes et al. (2002) postulated that the emplacement of quartz diorite-tonalite intrusions postdated main-stage ore deposition and that these intrusions were altered and mineralized by subsequent

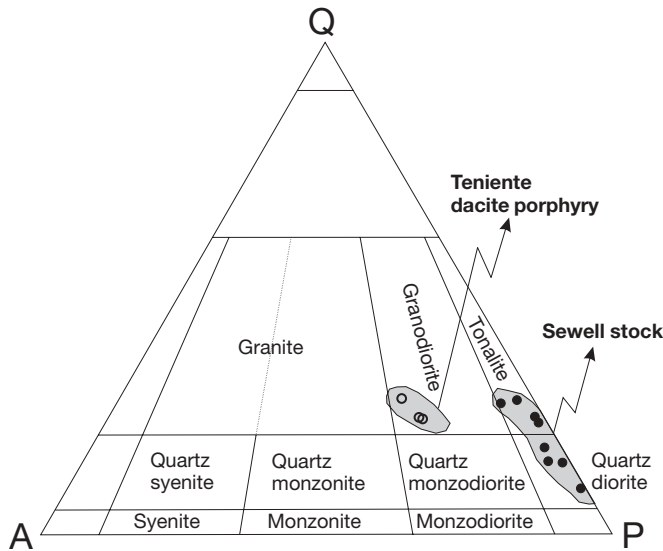


FIG. 5. Modal composition of the Sewell stock and the Teniente dacite porphyry in the QAP ternary diagram (after Streckeisen, 1976). Data from Ossandón (1974), and Reich (2001).

hydrothermal brecciation in their peripheral parts. Actually, stockwork mineralization is superimposed on biotite-bearing breccia with decimeter-scale tonalite fragments, adjacent to the Northern quartz diorite-tonalite stock.

A porphyry: This is gray, fine-grained quartz diorite porphyry that intrudes the Sewell stock and adjacent andesitic wall rocks in the southeastern part of the deposit. It characteristically contains centimeter- to decimeter-scale enclaves of equigranular quartz diorite-tonalite. The A porphyry contains plagioclase phenocrysts largely altered to smectite, sericite, and siderite, and a groundmass completely replaced by microcrystalline aggregates of anhydrite, quartz, partly chloritized hydrothermal biotite, and abundant sulfides. Its diameter is ~100 m, with subvertical axis, and it is surrounded by a 100- to 200-m-wide, irregular rim of richly mineralized, polymictic hydrothermal breccia, characterized by a coarse-grained matrix of anhydrite, tourmaline, chalcocopyrite, molybdenite, quartz, and biotite. According to Arredondo (1994) this hydrothermal breccia was formed by multistage processes: (1) initial rock fragmentation, potassic alteration, and deposition of the abundant matrix of anhydrite, biotite, and sulfides; (2) superimposed veins accompanied by potassic alteration; and (3) further brecciation, introduction of tourmaline, and new crosscutting veins with sericitic halo overprinted on the breccia.

Teniente dacite porphyry: This unit forms a ~200-m-wide, vertical north-south-trending tabular intrusion that transects the dark biotitized andesitic country rocks and extends for ~1.5 km in the northern part of El Teniente (Fig. 4). This porphyry is light gray to white and possesses a granodioritic modal composition (Fig. 5); phenocrysts include plagioclase up to 4 mm long (40–60%), biotite (5%) normally partly altered to white mica, chlorite, and calcite, and rare quartz eyes. The groundmass is composed of a microcrystalline aggregate of quartz, K-feldspar, minor plagioclase microlites,

and fine-grained disseminations of secondary biotite. Perthitic K-feldspar partly replaces plagioclase and irregular parts of the groundmass. Disseminated bornite and chalcocopyrite associated with anhydrite form 1 to 2 percent of the rock. Detailed mapping by Rojas (2002) concluded that the Teniente dacite porphyry is a composite intrusion formed by two intrusive pulses of dacitic composition from a common magma source.

The Teniente dacite porphyry has traditionally been regarded as representative of the main mineralizing intrusion at El Teniente, because the main concentration of hypogene bornite-bearing stockwork veins and bornite dissemination, associated with pervasive potassic alteration, occurs within this porphyry and adjacent andesites. In addition, the bornite/chalcocopyrite ratio decreases steadily away from the porphyry, as does the intensity of biotite alteration of the andesite host rocks (Howell and Molloy, 1960; Ossandón, 1974; Camus, 1975; Zúñiga, 1982; Cuadra, 1986; Ip, 1987a, b; Camus, 2003). In contrast, Skewes et al. (2002) argued that the Teniente dacite porphyry is a late, copper-poor felsic intrusion that merely redistributed earlier copper from the biotitized country rocks and biotite-bearing hydrothermal breccias.

At its southern end, the Teniente dacite porphyry is cut by the Marginal Breccia and Braden pipe (see below) but also by an irregular, richly mineralized (2% Cu) body of hydrothermal breccia along its eastern side (Arredondo, 1994); the mostly biotitized andesitic fragments of this latter breccia contain prebrecciation quartz-chalcocopyrite-bornite veins accompanied by potassic alteration. The matrix comprises anhydrite, quartz, and bornite, but the entire breccia, including fragments and matrix, is also crosscut by mineralized veins with potassic alteration selvages (Arredondo, 1994). The characteristics of this hydrothermal breccia body suggest a complex evolution involving early stockwork veining, followed by brecciation, sealing with hydrothermal minerals, and further veining, all related to potassic alteration.

Braden breccia pipe: This enormous breccia body forms a funnel-shaped pipe in the center of the orebody, 1,200 m in diameter at the surface and tapering to about 600 m at a depth of 1,800 m (Cuadra, 1986). It contains ~3 billion metric tons (Bt) of fragmented and milled rock. The main fragmental unit filling the pipe is typically poorly sorted, matrix-supported, polymictic breccia with milled rock fragments supported by abundant altered tuffisitic groundmass (cf., Sillitoe, 1985). The clasts are well rounded to subrounded and are formed by a mixture of all rock types that occur within the deposit, as well as extraneous accidental fragments of atypical porphyry, jasper, and aphanitic lithic clasts, probably carried from depth (Vega, 2004). These characteristics are typical of a diatreme vent generated by cataclysmic phreatomagmatic explosions (Sillitoe, 1985; Morales, 1997; Vega and Maksaev, 2003).

The Braden pipe is asymmetric, with a vertically dipping eastern border and other walls dipping about 60° to 70° inward. Much of the pipe is poorly mineralized (overall ~0.3% Cu; Ortega, 1981; Camus, 2003). However, ~96 Mt of ore at 1.16 percent copper have been estimated within certain parts of the breccia possessing a tourmalinized matrix (0.7% Cu cutoff; Valenzuela, 2003). It appears that this breccia was not a favorable locus for ore deposition because of the abundant

clayey matrix and the near absence of fracture planes (Lindgren and Bastin, 1922). Although clasts of the Teniente dacite porphyry with sulfide-bearing veins occur within the breccia, indicating that fragmentation affected previously mineralized porphyry, late veins with sericitic halos, various hydrothermal breccias, voids coated by sulfide and sulfate crystals, and disseminations of chalcopyrite, tennantite-tetrahedrite, molybdenite, sphalerite, and/or galena also occur within the pipe (Vega, 2004). Thus, fragmentation affected all known rock types in the mine area but further hydrothermal circulation and mineralization obviously persisted after diatreme formation.

The occurrence of obsidian and tuffaceous material within the Braden pipe was first described by Camus (1975), who suggested volcanic explosion vent. Unfortunately, the occurrence of juvenile material within it is uncertain, owing to pervasive alteration to various associations of sericite, chlorite, smectite, calcite, and siderite with subordinate dravite (Ortega, 1981; Vega and Makshev, 2003).

Marginal breccia: The Braden pipe is surrounded by a distinct, 50- to 60-m-wide, irregular rim (tapering to 5–10 m at depth) of well-mineralized magmatic-hydrothermal breccia known as the Marginal breccia. This unit is characteristically clast supported, with angular fragments and sulfide-rich, fine-grained black tourmaline matrix. The clasts, typically correspond to the adjacent wall rocks, are variably bleached and altered to quartz-sericite-chlorite assemblages.

Late dacite intrusions: A series of dikes of dacitic composition was emplaced during the late evolutionary stages at El Teniente. These are 2 to 15 m thick, some of them forming discontinuous concentric inward-dipping, cone sheetlike dikes that encircle the Braden pipe, whereas others are parallel to the main northeast and northwest structural orientations within the orebody (Riveros, 1991). The ring dikes are interpreted to represent magmatic injections along cone fractures generated by an overpressured body of volatile-rich felsic magma at depth (e.g., Phillips, 1973). A barren dacite stock also occurs immediately north of the Braden pipe; it is brecciated at its contact with the pipe, and according to deepest drill hole data, the breccia pipe itself is irregularly rooted within a barren dacite at a depth of ~2,000 m (Zúñiga, 1982). In addition, dacite blocks and megablocks up to hundreds of meters across, some even internally brecciated, occur within the Braden pipe in its upper part (Howell and Molloy, 1960).

Dacite dikes and stocks are typically light colored or white and characterized by a relatively small amount of phenocrysts (20–40%) of plagioclase, biotite, and quartz in an aplitic groundmass (Riveros, 1991). Although texturally distinct, major element chemistry suggests that, compositionally, they do not differ from other felsic intrusive rocks at El Teniente (Riveros, 1991; Skewes et al., 2002).

The late dacite intrusions show moderate to strong quartz-sericite-calcite and only minor biotite-quartz-chlorite alteration at deep levels and contain variable amounts of copper-bearing sulfides. Most dacite dikes show only scarce pyrite veins, but some contain veins with the sulfide association typical of the latest stage of mineralization at El Teniente, with chalcopyrite, molybdenite, tennantite-tetrahedrite, sphalerite, galena, and pyrite (Cuadra, 1986).

Hornblende-rich andesite dike: After hydrothermal mineralization had ceased, the southern part of the deposit

was cut by a 0.5- to 2-m-thick hornblende-rich andesite dike (referred to as lamprophyre at the mine), which has yielded a hornblende $^{40}\text{Ar}/^{39}\text{Ar}$ age of 3.85 ± 0.18 Ma (Makshev et al., 2002), identical to the whole-rock K-Ar age of 3.8 ± 0.3 Ma presented by Cuadra (1986). This northeast-trending dike marks the local termination of igneous activity, postdating all hydrothermal alteration and mineralization in the deposit (Cuadra, 1986).

Hydrothermal alteration and mineralization: Hypogene sulfides at El Teniente are mostly distributed within a dense stockwork of mineralized veins and within a variety of magmatic-hydrothermal breccia bodies that developed mainly along or near the vertical contacts of intrusive bodies as well as around the margins of the Braden pipe (Camus, 1975, 2003; Cuadra, 1986; Morales, 1997; Skewes et al., 2002; Salazar, 2003). Hydrothermal breccia constitute ~15 vol percent of the deposit according to mine reserve estimations (Camus, 2003), but this assessment does not include the unmapped biotite breccia bodies interpreted by Skewes et al. (2002).

Valenzuela (2003) described 13 types of veins within the orebody, but those composed of quartz-sulfides-anhydrite \pm biotite (chlorite) are dominant within pervasively potassic-altered wall rocks. Some of them have no noticeable alteration halos, but others show dark biotitized halo superimposed on the altered wall rocks. Commonly, discontinuous and irregular veins occur, which are similar to the A-type veins described by Gustafson and Hunt (1975) at El Salvador, Chile. It is inferred that such veins are formed above the temperature at which the wall rocks were able to sustain continuous brittle fracture (e.g., Fournier, 1999). Planar veins with similar compositions are also abundant, indicating that the stockwork developed within a high-temperature regime during ductile-brittle transition. Vein densities typically range from 6 to 30 veins/m but reach 40 veins/m near intrusive contacts (measured in drill core; Zúñiga, 1982). It is apparent that pervasive, biotite-dominated potassic alteration accompanied a significant part of copper deposition in El Teniente. Nevertheless, sulfide-bearing veins with quartz-sericite alteration halos crosscut the potassic-altered rocks and clearly are paragenetically late relative to potassic alteration. The veins with quartz-sericite halos increase in density away from the center of the deposit and become particularly abundant on the outer edges of the orebody. According to results of fluid inclusion studies and anhydrite-chalcopyrite sulfur isotope geothermometry, sulfide deposition took place at temperatures that decreased from about 460° to 330°C (Kusakabe et al., 1984, 1990; Ip, 1987a, b; Skewes et al., 2001, 2002). O, H, and S isotope data suggest that hydrothermal water and sulfur were of magmatic origin during both potassic and quartz-sericite alteration events (Kusakabe et al., 1984, 1990; Skewes et al., 2002). Relatively sharp temperature gradients and cooling of magmatic fluids below a saturation temperature near 400°C were probably key requirements for sulfide deposition at El Teniente, as described for the Bajo de La Alumbrera porphyry Cu-Au deposit, Argentina (Ulrich and Heinrich, 2001). Most ore deposition appears to have taken place over a temperature range higher than the closure temperature of micas with respect to the K-Ar system (380°–250°C; e.g., Chesley, 1999), which is consistent with the results of our $^{40}\text{Ar}/^{39}\text{Ar}$ dating (see below).

Pervasive, biotite-dominated potassic alteration is widespread within the andesites of the mine and deep portions of the Sewell stock and other intrusions of the eastern parts of the orebody, whereas potassic alteration of the Teniente dacite porphyry is dominated by perthitic K-feldspar with only relatively minor secondary, fine-grained biotite dissemination in the groundmass (Ossandón, 1974; Camus, 1975). However, microcrystalline biotite aggregates forming pseudomorphs after amphibole also occur, and metasomatism produced Ti depletion (due to sagenite formation; Rabbia, 2002) and Mg enrichment of biotite phenocrysts (Miranda, 2002). Quartz-sericite halos to quartz-sulfide-sulfate veins within peripheral parts of the orebody overprint the dominant potassic alteration, particularly within zones of dense stockwork. Pervasive quartz-sericite alteration is largely restricted to the uppermost 500-m portion of the Sewell stock and the apophyses of similar composition in the eastern part of the deposit (Camus, 1975), but drill core data indicate potassic alteration within these intrusions at depth beneath currently exploited mine levels (Villalobos, 1975; Guzmán, 1991). Pervasive alteration dominated by quartz-sericite-chlorite-tourmaline-montmorillonite also occurs throughout the Marginal breccia and the Braden pipe (Vega and Makshev, 2003). Propylitic alteration is largely peripheral to ore-grade rocks at El Teniente (Cuadra, 1986).

The evolution of El Teniente has traditionally been divided into three main hypogene stages: (1) early hydrothermal associated with potassic alteration; (2) main hydrothermal related to superimposed veining with quartz-sericite halos; and (3) late hydrothermal related to the quartz-sericite alteration of the Marginal breccia, the Braden pipe, and the tourmaline breccia in the carapace of the Sewell stock (e.g., Camus, 2003). However, the Sewell stock seemingly developed a distinct phase of potassic alteration (Cuadra, 1986), and hydrothermal breccias associated with potassic alteration show stockwork veining with potassic and/or quartz-sericite alteration halos, indicating the existence of superimposed hydrothermal episodes (Arredondo, 1994). In addition, a number of separate porphyry intrusions were emplaced, altered, and mineralized, further confirming that the deposit was formed by multistage processes (Skewes and Stern, 1995; Skewes et al., 2002). Superimposed hydrothermal episodes suggest a complex evolution of veins and breccias formed in different stages, sometimes including reopening of previously formed veins, which make difficult the interpretation of the evolution of this supergiant orebody based solely on crosscutting vein relationships.

Geochronology

We combine SHRIMP U-Pb, Re-Os, $^{40}\text{Ar}/^{39}\text{Ar}$, and fission-track apatite dating methods to resolve the age of crystallization of intrusions and of ore deposition in this supergiant ore-forming system. The implications of the new chronology for the evolution of El Teniente are discussed.

SHRIMP U-Pb dating

A sensitive high resolution ion microprobe (SHRIMP) was used for U-Pb dating of zircon crystals from six samples of the main, mineralized, felsic intrusive rocks from El Teniente. Zircon separation, mounting, and analytical work were done

at the Australian National University, using the procedures outlined in Compston et al. (1992). The objective was to resolve the crystallization ages of the altered and mineralized intrusions that are genetically related to copper-molybdenum mineralization and associated hydrothermal alteration within the orebody.

The U-Pb system in zircon is a robust method for accurately assessing the crystallization ages of igneous rocks affected by extreme hydrothermal alteration because of the overall chemical resistance of zircon (e.g., Davis and Krogh, 2000). In addition, zircon has the highest known closure temperature for Pb diffusion, which exceeds 900°C for zircons of typical sizes (Cherniak and Watson, 2000, and references therein). Furthermore, in situ microanalyses of the type provided by SHRIMP that have allowed detection of inherited zircon cores from other Chilean porphyry copper deposits (e.g., Zentilli et al., 1994; Richards et al., 1999) have also revealed similar features in at least one sample from El Teniente.

Samples of the Sewell stock, Northern and Central quartz diorite-tonalite, the Teniente dacite porphyry, and a dacite dike were collected in the underground mine, and a sample of the A porphyry was obtained from drill core. Gabbroic host rocks were also sampled, but attempts to extract zircons were unsuccessful. All samples were collected from zones containing >0.75 percent copper, with their descriptions provided in [Appendix 1](#). Randomly selected zircons were analyzed (17–21 spots for each sample) in order to define crystallization ages and to detect possible inherited zircon cores.

The new zircon geochronologic results are summarized in [Table 1](#), and sample locations are shown projected to the Teniente 4 LHD level (2354 m) in [Figure 6](#). The $^{206}\text{Pb}/^{238}\text{U}$ ages ($\pm 2\sigma$) and representative U-Pb Tera-Wasserburg concordia plots are shown in [Figures 7, 8, and 9](#).

Zircons from the mineralized Sewell stock in the southeastern part of the El Teniente orebody (TT-101; [Fig. 6](#)) yielded a $^{206}\text{Pb}/^{238}\text{U}$ age of 6.07 ± 0.12 Ma considering all analyzed spots. However, a bimodal distribution of $^{206}\text{Pb}/^{238}\text{U}$ ages is apparent, with a peak of 6.15 ± 0.08 for the dominant population and 5.59 ± 0.17 Ma for the subordinate population ([Fig. 7a](#)). Zircons from the A porphyry (TT-150; [Fig. 6](#)) yielded a $^{206}\text{Pb}/^{238}\text{U}$ age of 6.27 ± 0.19 Ma considering all analyzed spots. However, a bimodal distribution of $^{206}\text{Pb}/^{238}\text{U}$ ages is also apparent, with a peak of 6.46 ± 0.11 Ma for the dominant population and 5.67 ± 0.19 Ma for the subordinate population ([Fig. 7b](#)). The bimodal distribution of U-Pb ages results from different spot U-Pb ages yielded by individual zircon crystals (i.e., a mixture of zircons is discarded). Thus two distinct events appear to be recorded by the U-Pb system of these zircon samples.

Zircons from the Northern quartz diorite-tonalite (TT-102; [Fig. 6](#)) yielded a $^{206}\text{Pb}/^{238}\text{U}$ age of 5.91 ± 0.19 Ma. Again, bimodal distribution of $^{206}\text{Pb}/^{238}\text{U}$ ages is apparent, with a peak of 6.11 ± 0.13 Ma for the dominant group and 5.48 ± 0.19 Ma for the subordinate one ([Fig. 8a](#)). The zircon crystals from this intrusion include inherited cores and thin overgrowths that contain one order of magnitude higher U and Th contents than the crystal body ([Table 1](#)). Zircons of the Central quartz diorite-tonalite (TT-90; [Fig. 6](#)) yielded a skewed distribution of U-Pb ages with an overall U-Pb age of 6.08 ± 0.22

TABLE 1. SHRIMP U-Pb Zircon Data

Sample TT-150 (A porphyry)

(DDH-1337, 384 m; sample level 2,044 m, northing: 110N/easting: 1735E)

Grain spot	U (ppm)	Th (ppm)	Th/U	²⁰⁶ Pb (ppm)	²⁰⁴ Pb/ ²⁰⁶ Pb	F ₂₀₆ (%)	Total		Radiogenic		Age (Ma)			
							²³⁸ U/ ²⁰⁶ Pb	±1σ	²⁰⁷ Pb/ ²⁰⁶ Pb	±1σ	²⁰⁶ Pb/ ²³⁸ U	±1σ	²⁰⁶ Pb/ ²³⁸ U	±2σ
1.1	62	48	0.78	0.06	0.018871	6.99	910.2	47.2	0.1014	0.0183	0.00102	0.00006	6.6	0.8
2.1	227	106	0.47	0.21	0.006531	0.76	930.5	32.3	0.0522	0.0091	0.00107	0.00004	6.9	0.6
2.2	209	118	0.57	0.19	0.008686	3.21	946.1	45.7	0.0715	0.0106	0.00102	0.00005	6.6	0.6
3.1	76	62	0.82	0.07	-	2.89	915.4	42.0	0.0690	0.0135	0.00106	0.00005	6.8	0.6
4.1	73	60	0.82	0.07	0.019001	8.01	923.0	43.4	0.1094	0.0174	0.00100	0.00005	6.4	0.6
5.1	784	235	0.30	0.59	0.001842	0.69	1137.1	26.2	0.0516	0.0040	0.00087	0.00002	5.6	0.2
5.2	64	52	0.81	0.05	-	4.36	1075.3	59.0	0.0806	0.0215	0.00089	0.00005	5.7	0.8
6.1	542	920	1.70	0.47	0.002206	<0.01	990.2	18.3	0.0461	0.0042	0.00101	0.00002	6.5	0.2
7.1	53	32	0.60	0.05	0.008029	5.91	996.5	58.2	0.0929	0.0243	0.00094	0.00006	6.1	0.8
8.1	54	28	0.52	0.05	-	9.02	1015.9	58.5	0.1174	0.0218	0.00090	0.00006	5.8	0.8
9.1	75	47	0.63	0.07	0.021152	1.96	985.1	52.2	0.0617	0.0147	0.00100	0.00006	6.4	0.8
10.1	2692	2691	1.00	2.30	0.000548	0.58	1005.9	18.3	0.0507	0.0020	0.00099	0.00002	6.4	0.2
11.1	36	18	0.51	0.04	-	8.95	876.8	57.1	0.1168	0.0249	0.00104	0.00008	6.7	1.0
11.2	1624	801	0.49	1.79	0.012548	31.08	777.6	10.3	0.2916	0.0157	0.00089	0.00003	5.7	0.4
12.1	46	33	0.73	0.04	-	3.33	909.8	56.1	0.0725	0.0334	0.00106	0.00008	6.8	1.0
13.1	1192	459	0.39	1.01	0.004267	-0.19	1009.3	14.7	0.0447	0.0031	0.00099	0.00002	6.4	0.2
13.2	69	58	0.84	0.06	-	4.04	991.9	49.8	0.0780	0.0177	0.00097	0.00005	6.2	0.6
Older population, 13 spots							MSWD = 0.62		Weighted mean		6.46	0.11		
Younger population, 4 spots							MSWD = 0.084		Weighted mean		5.67	0.19		

Sample TT-101 (Sewell stock)

(Level Teniente 4, 2,347 m, northing: -265N/easting: 1365E)

Grain spot	U (ppm)	Th (ppm)	Th/U	²⁰⁶ Pb (ppm)	²⁰⁴ Pb/ ²⁰⁶ Pb	F ₂₀₆ (%)	Total		Radiogenic		Age (Ma)			
							²³⁸ U/ ²⁰⁶ Pb	±1σ	²⁰⁷ Pb/ ²⁰⁶ Pb	±1σ	²⁰⁶ Pb/ ²³⁸ U	±1σ	²⁰⁶ Pb/ ²³⁸ U	±2σ
1.1	3616	2782	0.77	5.1	0.018725	39.50	611.2	9.1	0.3581	0.0100	0.00099	0.00003	6.4	0.4
1.2	45	24	0.55	0.0	0.034134	6.25	999.7	62.5	0.0955	0.0208	0.00094	0.00006	6.0	0.8
2.1	4160	3481	0.84	3.9	0.006246	10.92	907.6	10.5	0.1324	0.0101	0.00098	0.00002	6.3	0.2
2.2	292	289	0.99	0.2	-	3.77	1027.1	28.9	0.0759	0.0090	0.00094	0.00003	6.0	0.4
3.1	89	41	0.46	0.1	-	4.73	1066.0	48.9	0.0835	0.0156	0.00089	0.00005	5.8	0.6
3.2	68	54	0.79	0.1	-	5.82	964.9	49.1	0.0921	0.0174	0.00098	0.00005	6.3	0.8
4.1	1125	329	0.29	1.1	0.012160	25.91	857.8	11.2	0.2508	0.0070	0.00086	0.00002	5.6	0.2
4.2	53	42	0.78	0.0	-	8.46	932.6	52.4	0.1130	0.0215	0.00098	0.00006	6.3	0.8
5.1	101	71	0.70	0.1	-	2.38	1136.7	49.1	0.0649	0.0131	0.00086	0.00004	5.5	0.6
6.1	2164	2892	1.34	1.8	0.001128	0.83	1031.7	11.1	0.0527	0.0023	0.00096	0.00001	6.2	0.2
6.2	112	49	0.44	0.1	-	5.06	1031.7	41.1	0.0861	0.0127	0.00092	0.00004	5.9	0.6
7.1	2587	1101	0.43	2.1	0.000345	0.49	1057.1	10.7	0.0500	0.0021	0.00094	0.00001	6.1	0.2
7.2	93	71	0.77	0.1	-	4.65	1100.2	54.3	0.0829	0.0158	0.00087	0.00005	5.6	0.6
8.1 ¹	87	30	0.35	0.1	-	1.92	945.5	42.6	0.0614	0.0117	0.00104	0.00005	6.7	0.6
8.2	41	18	0.43	0.0	-	12.01	973.1	62.5	0.1410	0.0285	0.00090	0.00007	5.8	0.8
9.1	3848	2519	0.65	3.5	0.006545	11.70	945.1	14.3	0.1386	0.0121	0.00093	0.00002	6.0	0.2
9.2	155	158	1.02	0.1	0.001266	0.32	1027.3	35.0	0.0487	0.0095	0.00097	0.00004	6.3	0.4
10.1	362	298	0.82	0.3	0.005079	1.03	1036.8	25.7	0.0543	0.0096	0.00095	0.00003	6.2	0.4
¹ Excluded spot							MSWD = 0.80		Weighted mean		6.15	0.08		
Older population, 12 spots							MSWD = 0.18		Weighted mean		5.59	0.17		
Younger population, 5 spots														

Sample TT-90 (Central quartz diorite-tonalite)

(Level UCL Esmeralda, 2,192 m, northing: 250N/easting: 1325E)

Grain spot	U (ppm)	Th (ppm)	Th/U	²⁰⁶ Pb (ppm)	²⁰⁴ Pb/ ²⁰⁶ Pb	F ₂₀₆ (%)	Total		Radiogenic		Age (Ma)			
							²³⁸ U/ ²⁰⁶ Pb	±1σ	²⁰⁷ Pb/ ²⁰⁶ Pb	±1σ	²⁰⁶ Pb/ ²³⁸ U	±1σ	²⁰⁶ Pb/ ²³⁸ U	±2σ
1.1	52	25	0.48	0.04	0.017020	18.86	1058.3	134.7	0.19508	0.07479	0.00077	0.00013	4.9	1.8
2.1	181	129	0.71	0.15	-	3.26	1012.2	37.1	0.07189	0.00952	0.00096	0.00004	6.2	0.4
2.2	78	38	0.48	0.07	-	5.48	999.5	52.9	0.08948	0.01669	0.00095	0.00005	6.1	0.6
3.1	85	45	0.53	0.08	0.009764	5.47	952.6	64.2	0.08941	0.01570	0.00099	0.00007	6.4	1.0
3.2	57	34	0.61	0.04	-	9.09	1209.4	126.7	0.11795	0.02813	0.00075	0.00008	4.8	1.0
4.1	101	46	0.46	0.08	-	3.13	1142.7	57.9	0.07088	0.01331	0.00085	0.00005	5.5	0.6
5.1	85	78	0.91	0.06	0.037995	10.90	1128.5	70.8	0.13227	0.02003	0.00079	0.00005	5.1	0.8

TABLE 1. (Cont.)

Sample TT-90 (Central quartz diorite-tonalite) (cont.)

(Level UCL Esmeralda, 2,192 m, northing: 250N/easting: 1325E)

Grain spot	U (ppm)	Th (ppm)	Th/U	²⁰⁶ Pb (ppm)	²⁰⁴ Pb/ ²⁰⁶ Pb	F ₂₀₆ (%)	Total		Radiogenic		Age (Ma)			
							²³⁸ U/ ²⁰⁶ Pb	±1σ	²⁰⁷ Pb/ ²⁰⁶ Pb	±1σ	²⁰⁶ Pb/ ²³⁸ U	±1σ	²⁰⁶ Pb/ ²³⁸ U	±2σ
5.2	71	45	0.63	0.06	0.018672	5.00	1087.8	55.3	0.08565	0.01684	0.00087	0.00005	5.6	0.6
6.1	95	66	0.70	0.09	-	2.96	960.7	40.3	0.06956	0.01237	0.00101	0.00005	6.5	0.6
7.1 ¹	88	30	0.34	0.08	-	1.42	905.1	38.7	0.05738	0.01121	0.00109	0.00005	7.0	0.6
8.1	62	50	0.82	0.05	-	0.86	1125.8	62.2	0.05298	0.01208	0.00088	0.00005	5.7	0.6
9.1	110	103	0.93	0.09	-	0.02	1057.2	43.9	0.04628	0.01175	0.00095	0.00004	6.1	0.6
10.1	431	472	1.10	0.36	0.002397	<0.01	1031.3	21.5	0.04411	0.00465	0.00097	0.00002	6.3	0.2
11.1	54	33	0.61	0.05	-	2.96	915.7	48.9	0.06955	0.01507	0.00106	0.00006	6.8	0.8
11.2	45	22	0.50	0.04	0.025892	5.30	1016.3	64.0	0.08800	0.02017	0.00093	0.00006	6.0	0.8
12.1	98	62	0.63	0.08	0.014571	8.86	1037.4	49.0	0.11612	0.01624	0.00088	0.00005	5.7	0.6
13.1	82	61	0.75	0.07	-	6.70	1050.9	50.6	0.09909	0.01754	0.00089	0.00005	5.7	0.6
14.1	52	42	0.81	0.05	0.026613	2.91	963.2	54.5	0.06914	0.01740	0.00101	0.00006	6.5	0.8
15.1	48	24	0.49	0.04	-	4.70	1014.1	61.5	0.08329	0.01863	0.00094	0.00006	6.1	0.8
16.1	47	25	0.53	0.05	0.021668	10.47	870.5	48.5	0.12890	0.02331	0.00103	0.00007	6.6	0.8
17.1	43	26	0.61	0.04	-	3.76	950.3	96.6	0.07588	0.01923	0.00101	0.00011	6.5	1.4

¹ Excluded spotOlder population, 12 spots
Younger population, 8 spotsMSWD = 0.50
MSWD = 0.65Weighted mean
Weighted mean6.28 0.16
5.50 0.24

Sample TT-102 (Northern quartz diorite-tonalite)

(Level Teniente 6 UCL, 2,161 m, northing: 1016N/easting: 1110 E)

Grain spot	U (ppm)	Th (ppm)	Th/U	²⁰⁶ Pb (ppm)	²⁰⁴ Pb/ ²⁰⁶ Pb	F ₂₀₆ (%)	Total		Radiogenic		Age (Ma)			
							²³⁸ U/ ²⁰⁶ Pb	±1σ	²⁰⁷ Pb/ ²⁰⁶ Pb	±1σ	²⁰⁶ Pb/ ²³⁸ U	±1σ	²⁰⁶ Pb/ ²³⁸ U	±2σ
1.1	80	37	0.46	0.07	-	1.11	1001.9	46.0	0.0549	0.0118	0.00099	0.00005	6.4	0.6
2.1	55	37	0.68	0.05	-	4.65	916.3	49.0	0.0829	0.0173	0.00104	0.00006	6.7	0.8
3.1	174	133	0.76	0.14	0.012840	2.14	1061.6	42.9	0.0631	0.0114	0.00092	0.00004	5.9	0.6
4.1	95	51	0.53	0.08	0.019964	8.90	993.2	43.2	0.1165	0.0164	0.00092	0.00005	5.9	0.6
5.1	142	87	0.61	0.11	-	2.82	1081.6	39.9	0.0684	0.0108	0.00090	0.00004	5.8	0.4
5.2	62	49	0.79	0.06	-	5.01	934.1	50.7	0.0857	0.0319	0.00102	0.00007	6.6	1.0
6.1	185	148	0.80	0.22	0.009806	0.17	714.7	29.1	0.0476	0.0064	0.00140	0.00006	9.0	0.8
6.1 ¹	67	38	0.57	0.05	-	4.49	1106.1	59.4	0.0816	0.0170	0.00086	0.00005	5.6	0.6
7.1	80	44	0.55	0.07	-	6.80	968.1	44.7	0.0999	0.0160	0.00096	0.00005	6.2	0.6
8.1	138	86	0.62	0.11	-	1.67	1075.1	43.9	0.0594	0.0105	0.00091	0.00004	5.9	0.6
8.2 ¹	511	235	0.46	1.89	-	<0.01	232.6	2.5	0.0428	0.0023	0.00432	0.00005	27.8	0.6
9.1	105	55	0.53	0.08	-	4.81	1116.6	47.7	0.0841	0.0141	0.00085	0.00004	5.5	0.6
10.1	101	61	0.60	0.09	0.009181	1.22	970.9	84.0	0.0558	0.0103	0.00102	0.00009	6.6	1.2
11.1	381	252	0.66	4.08	0.000624	0.52	80.2	0.7	0.0517	0.0016	0.01240	0.00012	79.4	1.4
11.2 ¹	1569	564	0.36	1.27	-	0.08	1058.8	16.1	0.0468	0.0024	0.00094	0.00001	6.1	0.2
12.1	575	386	0.67	0.43	0.001739	1.89	1154.5	22.4	0.0611	0.0050	0.00085	0.00002	5.5	0.2
12.2	60	34	0.56	0.05	-	11.79	1065.0	60.8	0.1393	0.0260	0.00083	0.00006	5.3	0.8
13.1	566	209	0.37	0.48	-	0.96	1013.6	26.6	0.0538	0.0046	0.00098	0.00003	6.3	0.4

¹ Inherited population excludedOlder population, 11 spots
Younger population, 4 spotsMSWD = 0.96
MSWD = 0.074Weighted mean
Weighted mean6.11 0.13
5.49 0.19

Sample TT-94 (Teniente dacite porphyry)

(Level Teniente 6, 2,161 m, northing: 1050N/easting: 450E)

Grain spot	U (ppm)	Th (ppm)	Th/U	²⁰⁶ Pb (ppm)	²⁰⁴ Pb/ ²⁰⁶ Pb	F ₂₀₆ (%)	Total		Radiogenic		Age (Ma)			
							²³⁸ U/ ²⁰⁶ Pb	±1σ	²⁰⁷ Pb/ ²⁰⁶ Pb	±1σ	²⁰⁶ Pb/ ²³⁸ U	±1σ	²⁰⁶ Pb/ ²³⁸ U	±2σ
1.1	154	107	0.70	0.1	0.011415	2.91	1156.6	42.2	0.06912	0.01067	0.00084	0.00003	5.4	0.4
2.1	146	117	0.80	0.1	-	0.46	1218.4	46.8	0.04974	0.01018	0.00082	0.00003	5.3	0.4
3.1	202	121	0.60	0.1	-	2.68	1207.6	38.9	0.06730	0.00923	0.00081	0.00003	5.2	0.4
4.1 ¹	97	56	0.57	0.1	-	7.64	1254.6	59.4	0.10644	0.01755	0.00074	0.00004	4.7	0.6
5.1 ¹	197	93	0.47	0.1	0.005197	1.04	1323.7	43.7	0.05434	0.00833	0.00075	0.00003	4.8	0.4
6.1	142	86	0.61	0.1	-	2.15	1134.9	42.9	0.06314	0.01057	0.00086	0.00003	5.6	0.4
6.2	115	87	0.75	0.1	0.019479	8.60	1169.0	90.2	0.11408	0.01584	0.00078	0.00006	5.0	0.8
7.1	239	212	0.88	0.2	0.005319	2.06	1161.1	34.2	0.06239	0.00806	0.00084	0.00003	5.4	0.4
8.1	255	318	1.25	0.2	-	1.70	1237.2	36.0	0.05959	0.00786	0.00079	0.00002	5.1	0.4
9.1 ¹	262	241	0.92	0.2	0.007535	0.79	1071.2	28.0	0.05243	0.00591	0.00093	0.00003	6.0	0.4

TABLE 1. (Cont.)

Sample TT-94 (Teniente dacite porphyry) (cont.) (Level Teniente 6, 2,161 m, northing: 1050N/easting: 450E)														
Grain spot	U (ppm)	Th (ppm)	Th/U	²⁰⁶ Pb (ppm)	²⁰⁴ Pb/ ²⁰⁶ Pb	F ₂₀₆ (%)	Total			Radiogenic			Age (Ma)	
							²³⁸ U/ ²⁰⁶ Pb	±1σ	²⁰⁷ Pb/ ²⁰⁶ Pb	±1σ	²⁰⁶ Pb/ ²³⁸ U	±1σ	²⁰⁶ Pb/ ²³⁸ U	±2σ
9.2	300	183	0.61	0.2	-	2.04	1166.0	30.2	0.06223	0.00849	0.00084	0.00002	5.4	0.4
10.1	150	90	0.60	0.1	-	4.84	1081.4	41.3	0.08435	0.01694	0.00088	0.00004	5.7	0.6
11.1	250	147	0.59	0.2	0.005863	3.23	1185.9	34.2	0.07162	0.00843	0.00082	0.00003	5.3	0.4
12.1	86	34	0.40	0.1	0.012203	5.28	1173.3	104.0	0.08783	0.01652	0.00081	0.00007	5.2	1.0
13.1	221	157	0.71	0.2	0.018332	2.02	1175.8	55.8	0.06212	0.01127	0.00083	0.00004	5.4	0.6
14.1	208	131	0.63	0.1	-	2.28	1266.4	42.8	0.06411	0.01072	0.00077	0.00003	5.0	0.4
15.1	178	104	0.59	0.1	-	2.03	1220.8	42.4	0.06215	0.00681	0.00080	0.00003	5.2	0.4
16.1	130	66	0.51	0.1	-	2.99	1226.1	50.4	0.06979	0.01752	0.00079	0.00004	5.1	0.4
17.1	206	182	0.88	0.1	0.010752	2.54	1180.8	37.3	0.06621	0.00892	0.00083	0.00003	5.3	0.4
1 Excluded spots			Single population, 16 spots					MSWD = 0.77			Weighted mean		5.28	0.10
Sample TT-91 (Dacite dike, N-S/60°-70°W, mineralized 5 m thick) (Level UCL Esmeralda, 2,192 m, northing: 310N/easting: 1030E)														
Grain spot	U (ppm)	Th (ppm)	Th/U	²⁰⁶ Pb (ppm)	²⁰⁴ Pb/ ²⁰⁶ Pb	F ₂₀₆ (%)	Total			Radiogenic			Age (Ma)	
							²³⁸ U/ ²⁰⁶ Pb	±1σ	²⁰⁷ Pb/ ²⁰⁶ Pb	±1σ	²⁰⁶ Pb/ ²³⁸ U	±1σ	²⁰⁶ Pb/ ²³⁸ U	±2σ
1.1	299	210	0.70	0.2	-	1.58	1293.3	61.9	0.05859	0.00784	0.00076	0.00004	4.9	0.4
2.1 ¹	362	275	0.76	0.2	0.007260	0.82	1417.9	41.8	0.05260	0.00652	0.00070	0.00002	4.5	0.2
3.1	485	434	0.89	0.3	0.006817	0.29	1226.1	43.2	0.04841	0.00522	0.00081	0.00003	5.2	0.4
4.1	227	160	0.70	0.1	0.007184	5.44	1302.8	46.2	0.08908	0.01077	0.00073	0.00003	4.7	0.4
4.2	77	42	0.54	0.1	-	4.98	983.6	43.1	0.08546	0.01453	0.00097	0.00005	6.2	0.6
5.1 ¹	391	264	0.68	0.3	0.003414	1.19	1264.4	31.3	0.05556	0.00611	0.00078	0.00002	5.0	0.2
6.1	368	376	1.02	0.2	0.005357	2.02	1314.1	42.8	0.06212	0.00657	0.00075	0.00003	4.8	0.4
7.1 ¹	274	172	0.63	0.2	0.007630	1.66	1449.0	43.9	0.05925	0.00823	0.00068	0.00002	4.4	0.2
8.1	295	180	0.61	0.2	0.005524	2.61	1343.4	38.0	0.06676	0.00792	0.00072	0.00002	4.7	0.2
9.1	465	401	0.86	0.3	-	1.91	1349.6	31.2	0.06119	0.00616	0.00073	0.00002	4.7	0.2
10.1	356	280	0.79	0.2	-	<0.01	1377.6	36.3	0.04345	0.00683	0.00073	0.00002	4.7	0.2
11.1	120	61	0.51	0.1	-	4.35	1259.1	53.6	0.08049	0.01326	0.00076	0.00003	4.9	0.4
12.1	272	203	0.75	0.2	-	0.57	1304.6	64.7	0.05065	0.00754	0.00076	0.00004	4.9	0.4
13.1	372	349	0.94	0.2	0.004603	0.94	1347.4	36.8	0.05359	0.00640	0.00074	0.00002	4.7	0.2
14.1	158	114	0.72	0.1	0.010024	2.86	1286.3	48.0	0.06875	0.01099	0.00076	0.00003	4.9	0.4
15.1	263	177	0.67	0.2	-	2.01	1314.0	42.2	0.06204	0.00812	0.00075	0.00003	4.8	0.4
16.1	221	133	0.60	0.1	0.007979	2.73	1270.6	40.2	0.06767	0.00885	0.00077	0.00003	4.9	0.4
17.1	215	132	0.61	0.1	0.016481	1.77	1323.2	43.3	0.06008	0.00876	0.00074	0.00003	4.8	0.4
18.1	186	111	0.60	0.1	-	3.12	1225.6	41.8	0.07081	0.01009	0.00079	0.00003	5.1	0.4
19.1	358	302	0.84	0.2	-	0.91	1391.7	36.4	0.05335	0.00844	0.00071	0.00002	4.6	0.2
20.1	355	353	1.00	0.2	0.009081	0.71	1277.9	32.6	0.05174	0.00630	0.00078	0.00002	5.0	0.2
1 Excluded spots			Single population, 18 spots					MSWD = 1.2			Weighted mean		4.82	0.09

Notes: Uncertainties for U-Pb ages given at the two standard deviation level ($\pm 2\sigma$); error in FC1, reference zircon calibration, was 0.30% for the analytical session (not included in errors of spot analyses but included in the final age estimates); F₂₀₆ (%) denotes the percentage of ²⁰⁶Pb that is common Pb; correction for common Pb made using the measured ²³⁸U/²⁰⁶Pb and ²⁰⁷Pb/²⁰⁶Pb ratios following Tera and Wasserburg (1972) as outlined in Compston et al. (1992); - = no data

Ma, but two age populations can be separated, with a peak of 6.28 ± 0.16 Ma for the dominant group and 5.50 ± 0.24 Ma for the subordinate one (Fig. 8b).

There are two possible interpretations for the bimodal U-Pb data: the older groups of spot ages may indicate that zircons were inherited from a previous deeper intrusion or crystallizing magma chamber, whereas the younger groups of ages may represent lead loss and/or magmatic zircon overgrowths during the crystallization of the quartz diorite-tonalite stocks at the orebody level; or the older groups of spot ages may indicate that zircon grew during crystallization of the stocks at

the orebody level and the younger groups may represent lead loss and/or zircon overgrowths during superimposed potassic alteration.

The second interpretation, involving a magmatic-hydrothermal evolution, is favored here, because it is consistent with recent studies that indicate that metasomatism and leaching by hot fluid circulation may partly reset the U-Pb zircon geochronometer (e.g. Geisler et al., 2001; Cocherie et al., 2002; Kaulina, 2002). We dated mineralized rocks with pervasive hydrothermal alteration (potassic, in most cases with a sericitic overprint; Appendix 1) that contain zircon crystals

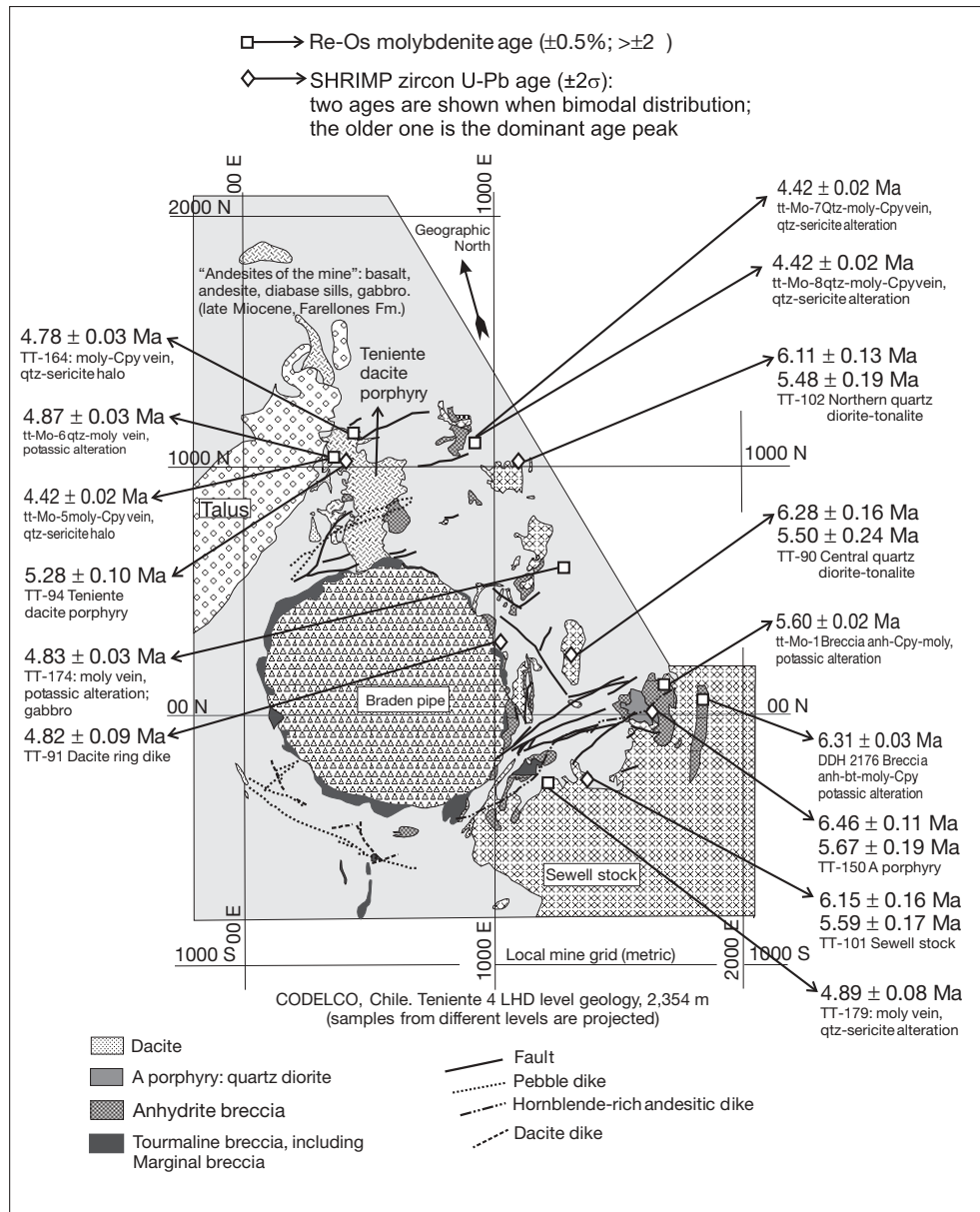


FIG. 6. Distribution of samples dated by SHRIMP U-Pb on zircon and Re-Os on molybdenite, projected to the Teniente 4 LHD level (2,354 m).

with pitted surfaces at a microscopic scale. Some crystals have thin zircon overgrowths with notably high U and Th contents that are consistent with the effects of hydrothermal activity (hydrothermal zircon; e.g., Rubín et al., 1989; Corfu and Davis, 1991; Corfu et al., 2003; Hoskin and Schaltegger, 2003). One sample (TT-102) includes inherited zircon cores, but these yielded spot ages from 79.4 ± 1.4 to 9.0 ± 0.8 Ma (Table 1). In addition, hydrothermal breccias developed within and surrounding these intrusions in the southeastern part of El Teniente yielded molybdenite Re-Os ages of 6.31 ± 0.03 and 5.60 ± 0.02 Ma (see below) that are concordant with the peaks of U-Pb ages. This indicates that the two geochronologic events recorded by the U-Pb system for the zircons correspond with hydrothermal molybdenite deposition.

In this context, the dominant peaks of $^{206}\text{Pb}/^{238}\text{U}$ ages are interpreted as crystallization ages of the mineralized Sewell stock and other quartz diorite-tonalite intrusions of the eastern part of the orebody from 6.46 ± 0.11 to 6.11 ± 0.13 Ma. These altered and mineralized stocks with porphyritic and equigranular textures may well represent separate magma injections but were emplaced within a brief period of geologic time. These intrusive bodies were customarily correlated at El Teniente, but this is the first geochronologic confirmation of the closeness of their crystallization ages.

The subordinate younger peaks of zircon U-Pb ages from 5.67 ± 0.19 to 5.48 ± 0.19 Ma for the four dated zircon samples from quartz diorite-tonalite intrusions of the eastern part of the orebody are statistically identical. This indicates that

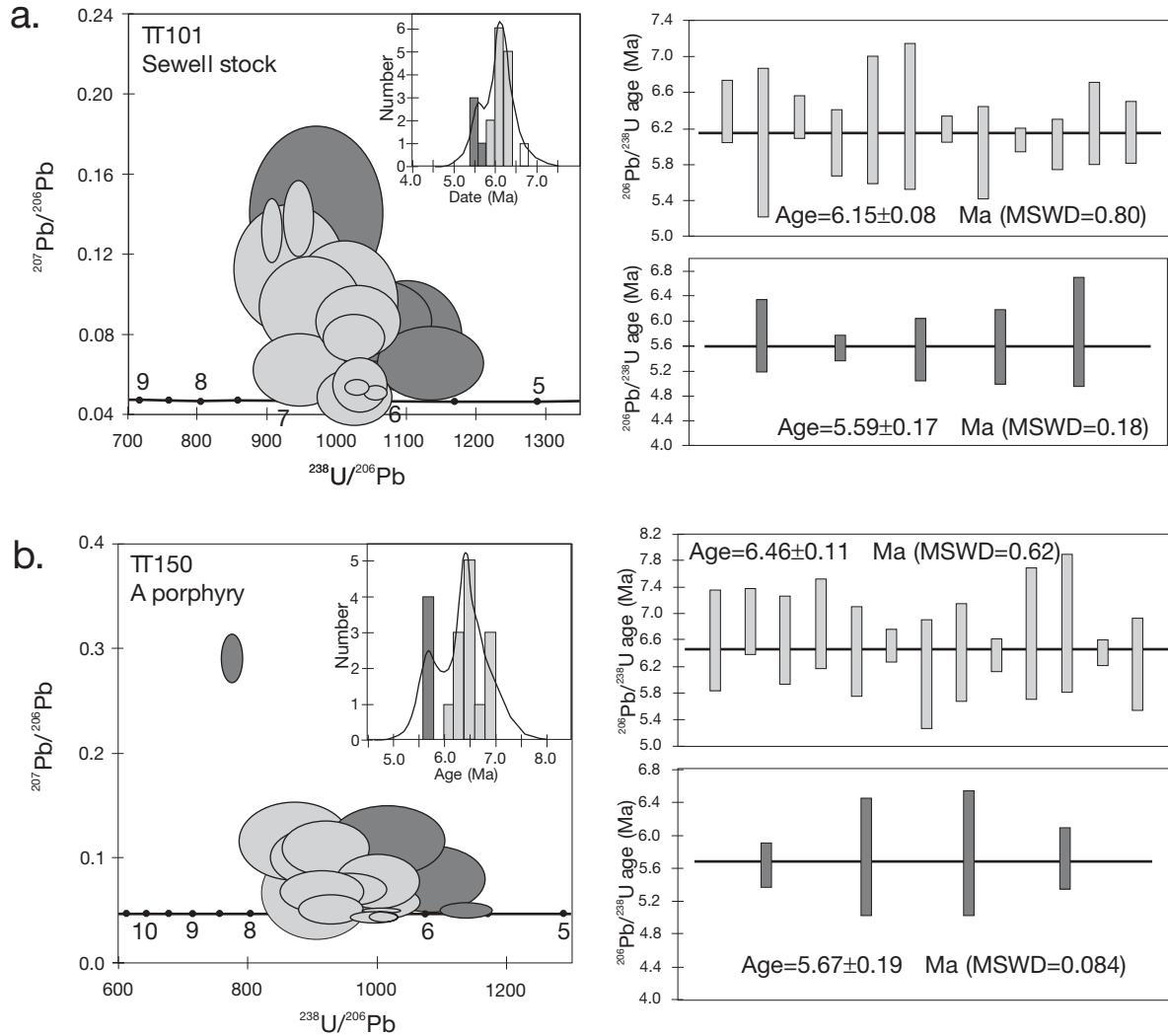


FIG. 7. Tera-Wasserburg concordia plots (Tera and Wasserburg, 1972) and weighted averages plots of SHRIMP U-Pb isotope data for (a) Sewell stock, and (b) A porphyry. Data are shown as 1σ error ellipses; error bars and U-Pb ages are $\pm 2\sigma$. Age distribution histograms shown as insets.

four separate zircon samples recorded a simultaneous episode that is consistent with a hydrothermal overprint. This episode is 0.56 ± 0.25 to 0.79 ± 0.30 m.y. younger than the crystallization ages inferred for the intrusions. Thus, the younger peaks of zircon U-Pb ages are interpreted to correspond to thin hydrothermal zircon overgrowths and inferred partial Pb loss produced by the potassic hydrothermal overprint. The time lag of 0.56 ± 0.25 to 0.79 ± 0.30 m.y. is significantly greater than the uncertainty of the U-Pb age determinations, indicating that potassic alteration was superimposed on crystallized Sewell stock and other quartz diorite-tonalite stocks at 5.67 ± 0.19 to 5.48 ± 0.19 Ma.

The $^{206}\text{Pb}/^{238}\text{U}$ ages suggest that the A porphyry crystallized before the dated portion of the Sewell stock in the southeastern part of the orebody. Although the age difference is small (0.31 ± 0.19 m.y.), the data are at variance with the observed crosscutting relationship of the A porphyry stock with the Sewell stock. Nevertheless, some parts of the Sewell stock may well have crystallized somewhat earlier than the intrusion of

the A Porphyry. The Sewell stock is probably a composite intrusion whose different pulses are masked by the superimposed potassic and quartz-sericitic alteration events.

The mineralized Teniente dacite porphyry from the northern part of the El Teniente orebody (TT-94; Fig. 6) yielded a zircon $^{206}\text{Pb}/^{238}\text{U}$ age of 5.28 ± 0.10 Ma, with a unimodal distribution of spot ages (Fig. 9a). This U-Pb age is interpreted as the crystallization age of the Teniente dacite porphyry and is slightly younger than the 5.67 ± 0.19 to 5.48 ± 0.19 Ma range of ages inferred for the potassic overprint that affected intrusions in the eastern part of El Teniente, suggesting that the eastern quartz diorite-tonalite intrusions were affected by an earlier hydrothermal event unrelated to the emplacement of the Teniente dacite porphyry. There is no contact relationship between the Teniente dacite porphyry and the eastern quartz diorite-tonalite intrusions, but its U-Pb crystallization age of 5.28 ± 0.10 Ma indicates that this dacite porphyry is a younger intrusive pulse. Our new zircon U-Pb age is older than the previously published biotite K-Ar ages for the

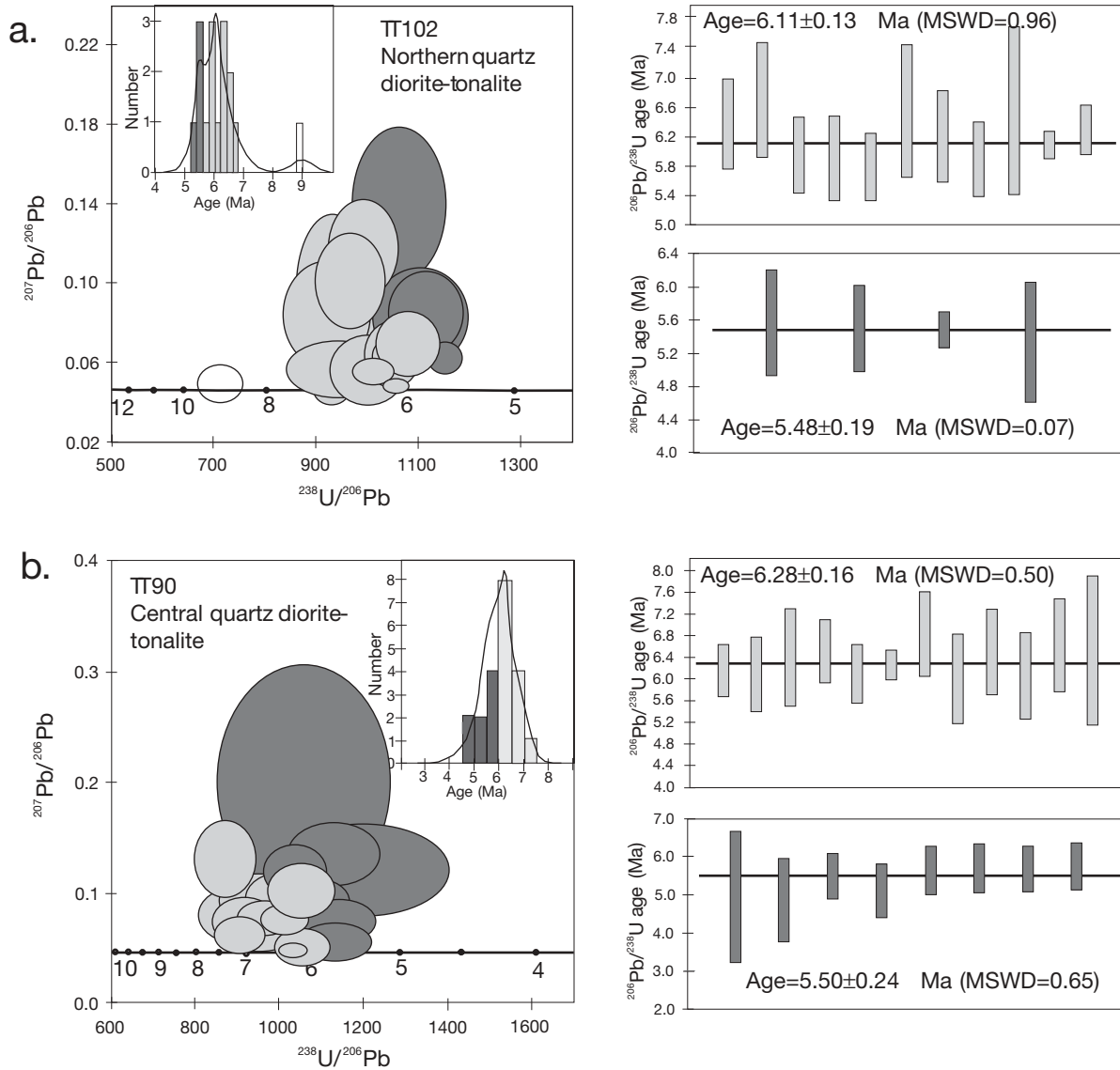


FIG. 8. Tera-Wasserburg concordia plots (Tera and Wasserburg, 1972) and weighted averages plot of SHRIMP U-Pb isotope data for (a) Northern quartz diorite-tonalite, and (b) Central quartz diorite-tonalite. Data are shown as 1σ error ellipses; error bars and U-Pb ages are $\pm 2\sigma$. Age distribution histograms shown as insets. Unshaded symbols are excluded from age calculations.

Teniente dacite porphyry, which range from 4.77 ± 0.18 to 4.6 ± 0.3 Ma (Clark et al., 1983; Cuadra, 1986), and older than our biotite and sericite $^{40}\text{Ar}/^{39}\text{Ar}$ plateau ages for this dacite porphyry, which range from 4.77 ± 0.14 to 4.57 ± 0.12 Ma (Table 2f); however, these K-Ar and $^{40}\text{Ar}/^{39}\text{Ar}$ ages on micas probably reflect high-temperature ($>350^\circ\text{C}$) hydrothermal overprints. The dated part of the Teniente dacite porphyry corresponds to the earliest, western pulse of this composite body according to the mapping of Rojas (2002) and thus defines the maximum age of the intrusion.

Zircons from one mineralized dacite ring dike that encircles the Braden pipe (TT-91; Fig. 6) yielded a $^{206}\text{Pb}/^{238}\text{U}$ age of 4.82 ± 0.09 Ma with a unimodal distribution of spot ages (Fig. 9b). This age probably represents the crystallization of the ring dikes related to a forceful emplacement of dacite magma associated

with the Braden diatreme breccia; these dacite ring dikes show pervasive quartz-sericite alteration and contain chalcopyrite-bearing stockwork veins. Other poorly mineralized dacite dikes that occur within the orebody, however may represent later dacite intrusions consistent with their $^{40}\text{Ar}/^{39}\text{Ar}$ ages (see below).

Unlike zircons of the early Sewell stock and related quartz diorite-tonalite intrusions that recorded their U-Pb crystallization age and a subsequent overprint (bimodal distribution of U-Pb ages), the zircons of the younger dacite intrusions show unimodal distribution of U-Pb ages, which simply record their crystallization age. This suggests that a change in physicochemical conditions took place during the evolution of the ore-forming system, which may have been related to the explosive formation of the Braden pipe in the center of the deposit, but this remains uncertain at present.

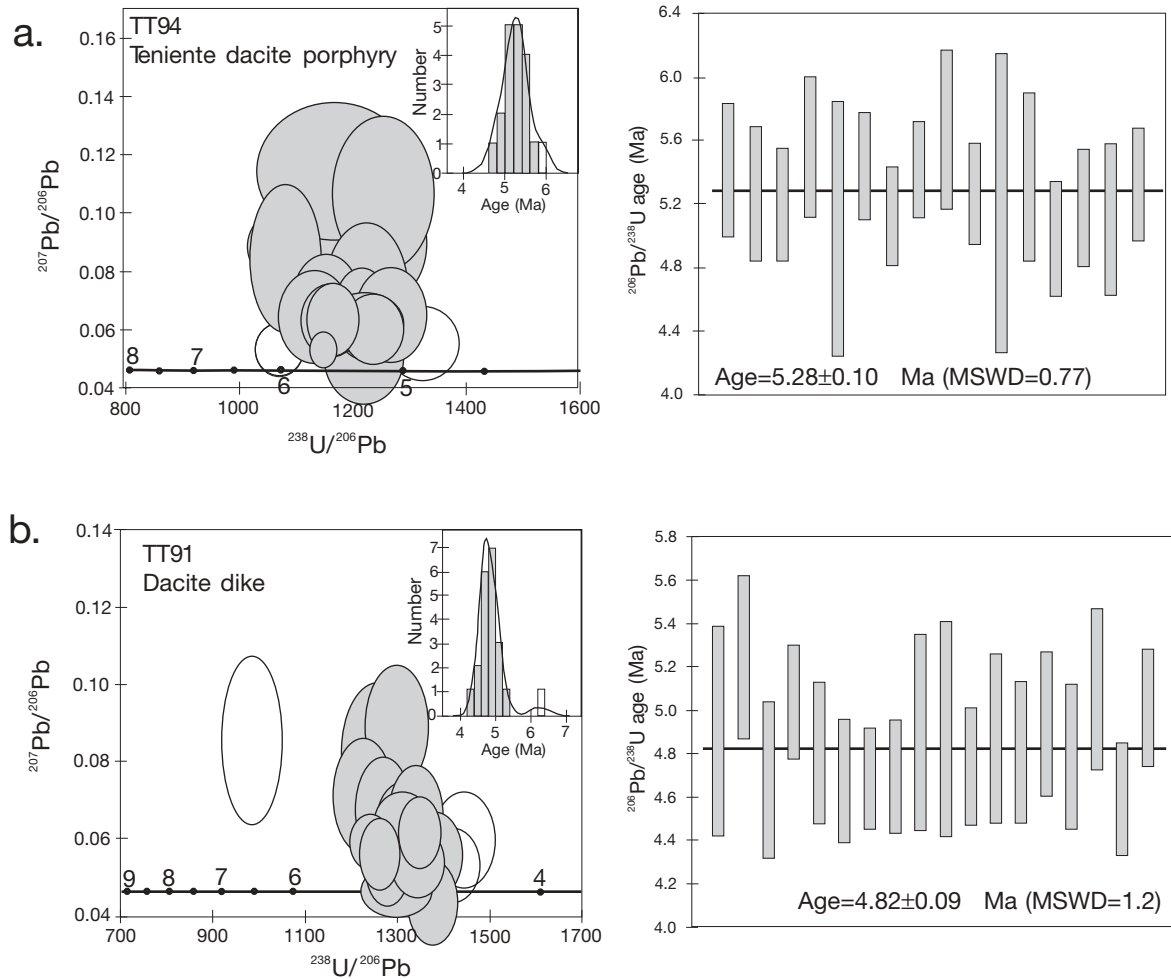


FIG. 9. Tera-Wasserburg concordia plots (Tera and Wasserburg, 1972) and weighted averages plot of SHRIMP U-Pb isotope data for (a) Teniente dacite porphyry, and (b) Dacite dike. Data are shown as 1σ error ellipses; error bars and U-Pb ages are $\pm 2\sigma$. Age distribution histograms shown as insets. Unshaded symbols are excluded from age calculations.

Molybdenite Re-Os dating

Molybdenum mineralization at El Teniente occurred in all alteration and mineralization events recognized in the deposit (Hernández et al., 1980; Cuadra, 1986), and molybdenite frequently occurs intergrown with copper sulfides. We collected samples of molybdenite-bearing veins and breccias from drill core throughout the deposit and used Re-Os systematics in molybdenite to resolve the age of ore deposition within the deposit. Analytical work was done at the University of Arizona, Tucson. Because the geology of the system is complicated and many events are superimposed, we used molybdenite ages and compared them to the alteration and crystallization ages determined from alteration silicates and zircon, respectively, so as to unravel the complex, intertwined hydrothermal evolution of the deposit.

The most robust technique for analyzing Re-Os in molybdenite is debated elsewhere (Stein et al., 2001; Kosler et al., 2003). These studies identified age variability within the same samples and suggested that analyses should either be carried

out at the microscale (0.001 g) or the samples should be homogenized. For the analysis we used approximately 0.1 g of homogenized handpicked sample, which was digested by the carius tube method (Shirley and Walker, 1995) and heated overnight at 230°C to ensure complete sample dissolution. We added 2 ml of hydrogen peroxide to the carius tube to increase oxidation and Os yield throughout the purification of the Os during the distillation process (Frei et al., 1998). Re was separated through column chemistry. Molybdenite ages were calculated using an ^{187}Re decay constant of $1.666 \times 10^{-11} \text{ y}^{-1}$ (Smoliar et al., 1996). Molybdenite Re-Os ages are reported with a conservative total error of 0.5 percent (greater than the conventional 2σ), which is the upper limit of reported Re-Os analyses, considering uncertainties from under/over spiking, instrumental counting statistics, uncertainties in spike calibrations, and in the ^{187}Re decay constant (0.31%). All Re and Os in molybdenite samples were measured with Faraday collectors; all measured Os is assumed to be radiogenic ^{187}Os (assuming no initial Os in molybdenite). Blank corrections are insignificant for molybdenite.

TABLE 2. Summary of $^{40}\text{Ar}/^{39}\text{Ar}$ Step-Heating Ages for El Teniente

2a. $^{40}\text{Ar}/^{39}\text{Ar}$ step-heating ages for biotitized host rocks (andesites of the mine) of El Teniente										
Sample no.	Drill hole no.	Depth (m)	Material dated	Plateau age (Ma $\pm 2\sigma$)	Isochron age (Ma $\pm 2\sigma$)	MSWD	Isochron fit	Total gas age (Ma $\pm 2\sigma$)	Comments	
TT-74	DDH-1309	140.8	WR biotite	4.78 \pm 0.14	4.69 \pm 0.08	4.28	Bad	5.63 \pm 0.92	Biotitized andesite	
TT-15	DDH-1891	87.5	Biotite	4.69 \pm 0.10	4.72 \pm 0.12	1.94	Good	4.64 \pm 0.12	Biotitized andesite	
TT-56	DDH-1300	374.9	Biotite	4.68 \pm 0.10	4.68 \pm 0.12	1.87	Good	4.73 \pm 0.14	Coarse-grained biotite-quartz vein within biotitized andesite	
TT-1673	880N	1640E	WR biotite	4.46 \pm 0.22	4.51 \pm 0.24	1.05	Good	4.81 \pm 0.88	Gabbro with potassic alteration (biotite-magnetite)	
2b. $^{40}\text{Ar}/^{39}\text{Ar}$ step-heating ages for the Sewell stock										
DDH-2176	DDH-2176	73	Biotite	5.69 \pm 0.08	5.69 \pm 0.10	0.80	Good	5.47 \pm 0.38	Anhydrite matrix hydrothermal breccia hosted by the Sewell stock with a molybdenite Re-Os age of 6.31 \pm 0.03 Ma	
DDH-1116	DDH-1116	432.8	Biotite	5.63 \pm 0.12	5.51 \pm 0.46	1.74	Good	5.44 \pm 0.16	Unmineralized tonalite beyond the limit of the orebody	
DDH-1140	DDH-1140	501.7	Biotite	5.47 \pm 0.12	5.49 \pm 0.16	0.45	Good	5.30 \pm 0.26	Unmineralized tonalite beyond the limit of the orebody	
TT-01	DDH-1334	360	Biotite	5.06 \pm 0.12	5.06 \pm 0.12	3.26	Bad	4.98 \pm 0.18	Coarse-grained hydrothermal biotite vein hosted by the Sewell stock	
TT-09	DDH-1337	291.4	Biotite	4.74 \pm 0.10	4.74 \pm 0.10	0.88	Good	4.66 \pm 0.14	Coarse-grained hydrothermal biotite	
TT-108	DDH-1091A	941.2	Biotite	4.62 \pm 0.12	4.66 \pm 0.26	1.68	Good	4.58 \pm 0.16	Potassic alteration (biotite-magnetite)	
DDH-1091A	DDH-1091A	905.2	WR biotite	4.69 \pm 0.10	4.52 \pm 0.38	0.54	Good	5.69 \pm 0.16	Whole-rock biotite K-Ar of 7.1 \pm 1.0 Ma; Cuadra (1986)	
TT-81	DDH-1311	669	WR sericite	4.37 \pm 0.10	4.37 \pm 0.12	0.85	Good	4.23 \pm 0.12	Pervasive quartz-sericite-smectite alteration	
TT-50	DDH-1309	146.6	WR sericite	4.62 \pm 0.12	4.51 \pm 0.36	5.44	Bad	4.58 \pm 0.16	Pervasive quartz-sericite alteration	
TT-64	DDH-1309	98.1	WR sericite	4.55 \pm 0.12	4.56 \pm 0.14	0.7	Good	4.53 \pm 0.12	Pervasive quartz-sericite alteration	
TT-69	DDH-1309	157.7	WR sericite	4.54 \pm 0.12	4.54 \pm 0.14	1.27	Good	4.50 \pm 0.18	Coarse-grained sericite; pervasive quartz-sericite alteration	
TT-60	DDH-1309	68.6	WR sericite	4.47 \pm 0.10	4.37 \pm 0.14	0.22	Good	4.31 \pm 0.18	Coarse-grained sericite; pervasive quartz-sericite alteration	
2c. $^{40}\text{Ar}/^{39}\text{Ar}$ Step-heating age for the A porphyry										
Sample no.	Northing (m)	Easting (m)	Level (m)	Material dated	Plateau age (Ma $\pm 2\sigma$)	Isochron age (Ma $\pm 2\sigma$)	MSWD	Isochron fit	Total gas age (Ma $\pm 2\sigma$)	Comments
TT-101	-265N	1365E	2347	Biotite	4.72 \pm 0.12	4.72 \pm 0.14	1.54	Good	4.72 \pm 0.12	Sample that yielded zircon U-Pb ages of 6.15 \pm 0.08 and 5.59 \pm 0.17 Ma
2d. $^{40}\text{Ar}/^{39}\text{Ar}$ step-heating age for the Central quartz diorite-tonalite										
Sample no.	Drill hole no.	Depth (m)	Material dated	Plateau age (Ma $\pm 2\sigma$)	Isochron age (Ma $\pm 2\sigma$)	MSWD	Isochron fit	Total gas age (Ma $\pm 2\sigma$)	Comments	
TT-150	DDH-1337	384	Biotite	4.93 \pm 0.12	4.95 \pm 0.24	1.67	Good	4.69 \pm 0.16	Sample that yielded zircon U-Pb ages of 6.46 \pm 0.11 and 5.67 \pm 0.19 Ma	
TT-39	DDH-1333	126.5	WR sericite	4.55 \pm 0.10	4.53 \pm 0.10	0.79	Good	4.40 \pm 0.24	Pervasive quartz-sericite-smectite alteration	

TABLE 2. (Cont.)

2e. $^{40}\text{Ar}/^{39}\text{Ar}$ step-heating ages for the Northern quartz diorite-tonalite											
Sample no.	Northing (m)	Easting (m)	Depth (m)	Level (m)	Material dated	Plateau age (Ma \pm 2 σ)	Isochron age (Ma \pm 2 σ)	MSWD	Isochron fit	Total gas age (Ma \pm 2 σ)	Comments
TT-102	1016N	1110E	2161	WR sericite	4.74 \pm 0.12	4.70 \pm 0.18	1.16	Good	4.66 \pm 0.20	Sample that yielded zircon U-Pb ages of 6.11 \pm 0.13 and 5.48 \pm 0.19 Ma	
2f. $^{40}\text{Ar}/^{39}\text{Ar}$ step-heating ages for the Teniente dacite porphyry											
Sample no.	Drill hole no.	Depth (m)	Material dated	Plateau age (Ma \pm 2 σ)	Isochron age (Ma \pm 2 σ)	MSWD	Isochron fit	Total gas age (Ma \pm 2 σ)	Comments		
TT-19	DDH-1514	522.2	Biotite	4.77 \pm 0.14	4.79 \pm 0.16	0.90	Good	4.79 \pm 0.36	Fine-grained hydrothermal biotite		
TT-19	DDH-1514	522.2	Sericite	4.40 \pm 0.10	4.39 \pm 0.32	8.84	Bad	4.36 \pm 0.16	Fine-grained hydrothermal biotite		
TT-18	DDH-1514	521.7	Sericite	4.69 \pm 0.12	4.72 \pm 0.14	0.65	Good	4.52 \pm 0.14	Coarse-grained hydrothermal sericite		
TT-21	DDH-1514	371	Biotite	4.69 \pm 0.12	4.43 \pm 0.48	3.18	Good	4.58 \pm 0.16	Coarse-grained biotite		
TT-22	DDH-1514	302	Sericite	4.65 \pm 0.12	4.73 \pm 0.18	1.12	Good	4.76 \pm 0.12	Sericite halo of quartz-chalcopyrite-molybdenite vein		
TT-21	DDH-1514	371	Sericite	4.61 \pm 0.14	4.57 \pm 0.24	0.17	Good	4.57 \pm 0.18	Quartz-sericite vein		
tt-Mo-5	DDH-1514	462	Sericite	4.57 \pm 0.12	4.56 \pm 0.14	0.70	Good	4.54 \pm 0.34	Sericite halo of molybdenite-chalcopyrite vein with molybdenite Re-Os age of 4.42 \pm 0.02 Ma		
2g. $^{40}\text{Ar}/^{39}\text{Ar}$ step-heating ages for the Braden pipe and Marginal breccia											
Sample no.	Northing (m)	Easting (m)	Level (m)	Material dated	Plateau age (Ma \pm 2 σ)	Isochron age (Ma \pm 2 σ)	MSWD	Isochron fit	Total gas age (Ma \pm 2 σ)	Comments	
T-7 #10	985N	530E	2942	Biotite	4.69 \pm 0.18	4.68 \pm 0.72	2.18	Good	3.87 \pm 0.24	Biotite K-Ar 4.6 \pm 0.3 Ma; Cuadra (1986)	
TT-93	225N	820E	2160	WR sericite	4.81 \pm 0.10	4.81 \pm 0.12	2.32	Good	4.70 \pm 0.12	Sericitized halo of chalcopyrite vein hosted by the Braden pipe	
TT-138	378N	835E	2210	Sericite	4.75 \pm 0.12	4.74 \pm 0.16	1.24	Good	4.81 \pm 0.14	Sericite alteration of fragment; Braden pipe	
TT-135	220N	975E	2210	WR sericite	4.68 \pm 0.12	4.74 \pm 0.22	22.42	Bad	4.59 \pm 0.10	Tourmalinized breccia from Braden pipe	
LHD-3	404N	983E	2372	WR sericite	4.67 \pm 0.22	4.78 \pm 0.38	0.57	Good	4.97 \pm 0.22	Sericitized border of andesite fragment from Marginal breccia; whole-rock K-Ar 4.7 \pm 0.3 Ma; Cuadra (1986)	
TT-137	301N	890E	2210	WR sericite	4.60 \pm 0.10	4.62 \pm 0.30	30.48	Bad	4.51 \pm 0.10	Sericite alteration of fragment from Marginal breccia	
T-5-214	360N	495E	2284	WR sericite	4.60 \pm 0.06	4.57 \pm 0.06	0.27	Good	4.66 \pm 0.06	Sericitized border of andesite fragment from Braden pipe; WR K-Ar age 4.5 \pm 0.2 Ma; Cuadra (1986)	
TT-136	240N	975E	2210	WR sericite	4.58 \pm 0.12	4.59 \pm 0.12	1.13	Good	4.46 \pm 0.12	Bedded horizon of the Braden pipe	
TT-134	102N	975E	2210	WR sericite	4.49 \pm 0.10	4.49 \pm 0.12	1.34	Good	4.48 \pm 0.10	Hydrothermal breccia within Braden pipe	

TABLE 2. (Cont.)

2h. $^{40}\text{Ar}/^{39}\text{Ar}$ step-heating ages for late dacite stocks and dikes										
Sample no.	Drill hole no.	Depth (m)	Material dated	Plateau age (Ma \pm 2 σ)	Isochron age (Ma \pm 2 σ)	MSWD	Isochron fit	Total gas age (Ma \pm 2 σ)	Comments	
TT-43	DDH-1407	271.8	Sericite	4.61 \pm 0.12	4.61 \pm 0.20	1.36	Good	4.67 \pm 0.12	Dike with pervasive quartz-sericite alteration	
TT-105	DDH-1068	976.9	Biotite	4.58 \pm 0.10	4.57 \pm 0.12	2.11	Good	4.66 \pm 0.14	Magmatic biotite of relatively fresh dacite that underlies the Braden pipe.	
TT-46	DDH-1409	468.5	Sericite	4.56 \pm 0.12	4.56 \pm 0.12	1.09	Good	4.60 \pm 0.12	Dike with quartz-sericite-carbonate alteration	
TT-30	DDH-1414	369.4	Sericite	4.52 \pm 0.12	4.53 \pm 0.18	0.40	Good		Sericitized halo of quartz vein within dike	
TT-143	DDH-2008	157.6	Sericite	4.46 \pm 0.10	4.47 \pm 0.12	0.74	Good	4.44 \pm 0.10	Poorly mineralized stock with quartz-sericite alteration	
Sample no.	Northing (m)	Easting (m)	Level (m)	Material dated	Plateau age (Ma \pm 2 σ)	Isochron age (Ma \pm 2 σ)	MSWD	Isochron fit	Total gas age (Ma \pm 2 σ)	Comments
TT-144	430N	471E	1980	Sericite	4.55 \pm 0.12	4.56 \pm 0.16	0.15	Good	4.44 \pm 0.14	Poorly mineralized stock with quartz-sericite alteration
2i. $^{40}\text{Ar}/^{39}\text{Ar}$ step-heating age for post-mineralization hornblende-rich andesite dike										
TT-141	-249.7N	1133.5E	2452	Hornblende	3.85 \pm 0.18	4.28 \pm 1.22	22.24	Bad	3.33 \pm 0.36	Postmineralization dike that crosscuts the southeastern part of the orebody
2j. $^{40}\text{Ar}/^{39}\text{Ar}$ step-heating age for dacite from the La Huifa breccia pipe, 2 km north from El Teniente										
Sample no.	UTM north coord. (m)	UTM east coord. (m)	Material dated	Plateau age (Ma \pm 2 σ)	Isochron age (Ma \pm 2 σ)	MSWD	Isochron fit	Total gas age (Ma \pm 2 σ)	Comments	
E-1359	6231700	377920	Biotite	6.97 \pm 0.10	6.91 \pm 0.14	0.71	Good	7.05 \pm 0.14	K-Ar age of 7.0 \pm 0.4 Ma; Cuadra (1986)	

Notes: $^{40}\text{Ar}/^{39}\text{Ar}$ step-heating analysis at the Geochronology Laboratory, Stanford University
 Abbreviations: MSWD = mean standard weighted deviation, WR = whole-rock

Aside from resolving the analytical procedures for Re-Os analysis, there have been discussions regarding the reliability of the Re-Os geochronometer and its ease of disturbance. McCandless et al. (1993) and Suzuki et al. (2000) indicated that the Re-Os systematics within samples can be disturbed after deposition and suggested microprobe analysis of samples to look for possible alteration silicates that could be indicative of postdepositional isotopic disturbance. In contrast, Stein et al. (2001) and Selby and Creaser (2001) proposed that the Re-Os system is extremely robust and that high-grade metamorphism, deformation, and postore hydrothermal fluids do not disturb the Re-Os geochronometer. In this study we present Re-Os ages on molybdenite that overlap both alteration and crystallization ages of other minerals found in the deposit, as determined using other isotopic systems. This overlap indicates that the Re-Os system in molybdenite throughout the porphyry copper deposit does not appear to be disturbed by subsequent, local, high-temperature (>350°C) hydrothermal events.

Re-Os age determinations of nine molybdenite samples are presented in Table 3. This table includes data already reported by Mathur et al. (2001) plus new Re-Os determinations. Sample locations are shown in Figure 6 projected to the Teniente 4 LHD level (2,354 m).

The oldest molybdenite Re-Os age of 6.31 ± 0.03 Ma was obtained from a hydrothermal breccia with coarse-grained matrix of biotite, anhydrite, chalcocopyrite, and molybdenite (DDH-2176; sample provided by José Seguel); the breccia is hosted by the potassic-altered Sewell stock, near the eastern limit of the orebody (Fig. 6). The age is in excellent agreement with the zircon U-Pb crystallization ages (6.46 ± 0.11 – 6.11 ± 0.13 Ma) obtained for the quartz diorite-tonalite intrusions of this part of the deposit. This result is consistent with an early ore-depositing event related to crystallization of these intrusions in the eastern part of the orebody (Fig. 6). This Re-Os molybdenite age supports conclusions of previous studies that related the earliest stage of significant potassic alteration and mineralization at El Teniente to the emplacement of quartz diorite-tonalite intrusions (e.g., Howell and Molloy, 1960; Camus, 1975; Cuadra, 1986).

A hydrothermal breccia with a coarse-grained matrix of anhydrite, chalcocopyrite, and molybdenite hosted by the potassic-altered Sewell stock (sample tt-Mo-1), near the contact with the A porphyry in the southeastern part of the orebody, yielded a molybdenite Re-Os age of 5.60 ± 0.02 Ma (the replicate analysis yielded an identical age; Table 3). This molybdenite Re-Os age agrees with the youngest peaks in the zircon SHRIMP U-Pb ages obtained for the Sewell stock and

TABLE 3. Molybdenite Re-Os Data for El Teniente

Sample no.	Drill hole (DDH)	Depth (m)	$^{187}\text{Os}^1$ (ppb)	Re (ppm)	^{187}Re (ppm)	Age ² (Ma)	Comments
DDH-2176	2176	73	7.58	73	45.698	6.31 ± 0.03	Breccia with coarse-grained anhydrite, biotite, chalcocopyrite, and molybdenite hosted by Sewell stock with potassic alteration; biotite $^{40}\text{Ar}/^{39}\text{Ar}$ plateau age of 5.69 ± 0.08 Ma
tt-Mo-1	1334	355.8	10.75	182.26	114.59	5.60 ± 0.02	Breccia with coarse-grained anhydrite, chalcocopyrite, and molybdenite hosted by Sewell stock with potassic alteration
tt-Mo-1	1334	355.8	10.95	184.19	115.80	5.60 ± 0.02	Replicated analysis
TT-179	1556	551	8.8	168.7	104.59	4.89 ± 0.08	Molybdenite vein hosted by Sewell stock with pervasive quartz-sericite alteration
tt-Mo-6	1514	185	59.09	1153.66	725.26	4.87 ± 0.03	Quartz-molybdenite vein hosted by Teniente dacite porphyry with potassic alteration
TT-174	2181	65	3.66	72.54	45.60	4.83 ± 0.03	Molybdenite vein hosted by biotitized gabbro (andesites of the mine)
TT-164	1303	228.6	10.79	220.06	138.35	4.78 ± 0.03	Molybdenite-chalcocopyrite vein with sericite alteration halo hosted by Teniente dacite porphyry
tt-Mo-5	1514	462	11.57	249.52	156.87	4.42 ± 0.02	Molybdenite vein with minor chalcocopyrite and sericite alteration halo hosted by Teniente dacite porphyry; sericite $^{40}\text{Ar}/^{39}\text{Ar}$ plateau age of 4.57 ± 0.12
tt-Mo-7	1309	298	14.68	319.93	201.14	4.42 ± 0.02	Quartz-molybdenite-chalcocopyrite vein hosted by Northern quartz diorite-tonalite porphyry with pervasive quartz-sericite alteration and abundant chalcocopyrite dissemination
tt-Mo-8	1309	169	11.81	254.81	160.20	4.42 ± 0.02	Quartz vein with molybdenite and chalcocopyrite hosted by Northern quartz diorite-tonalite porphyry with quartz-sericite pervasive alteration

Notes: Analysis at University of Arizona Laboratory by Ryan Mathur

¹ All measured Os is radiogenic ^{187}Os (assuming no initial Os)

² Molybdenite Re-Os dates are reported with a conservative total error of 0.5% (greater than the conventional 2σ), which is the upper limit of reported Re-Os analyses, considering uncertainties from under/over spiking, instrumental counting statistics, uncertainties in spike calibrations and in the ^{187}Re decay constant (0.31%)

the A porphyry (5.59 ± 0.17 and 5.67 ± 0.19 Ma, respectively), which are interpreted to be the result of hydrothermal overprinting of zircon crystals (see above). This suggests a separate superimposed ore depositional event, associated with potassic alteration, in the quartz diorite-tonalite intrusions in the southeastern part of the orebody. Cannell et al. (2003) reported a molybdenite Re-Os age of 5.89 Ma for a sample from the same breccia body; although the analytical uncertainty was not reported; this age is somewhat older than our Re-Os and U-Pb results.

Cannell et al. (2003) also reported three Re-Os ages from 5.01 to 4.96 Ma for molybdenite associated with potassic alteration at El Teniente (analytical uncertainty and sample locations not reported). These molybdenite Re-Os ages are younger than the 5.28 ± 0.10 Ma U-Pb maximum crystallization age that we resolved for the Teniente dacite porphyry, but they could represent molybdenite deposition following the crystallization of this composite intrusion.

A quartz-molybdenite vein (sample tt-Mo-6) hosted by the potassic altered Teniente dacite porphyry yielded a molybdenite Re-Os age of 4.87 ± 0.03 Ma, whereas a molybdenite vein (sample TT-174) hosted by a strongly biotitized gabbro (“Andesites of the mine”) yielded a molybdenite Re-Os age of 4.83 ± 0.03 Ma. A molybdenite vein (sample TT-179) hosted by the Sewell stock displaying pervasive quartz-sericite alteration yielded a molybdenite Re-Os age of 4.89 ± 0.08 Ma, and a molybdenite-chalcopyrite vein (sample TT-164) with a quartz-sericite alteration halo hosted by the Teniente dacite porphyry yielded a molybdenite Re-Os age of 4.78 ± 0.03 Ma. These ages indicate that molybdenite deposition associated with potassic alteration took place from 4.87 ± 0.03 to 4.83 ± 0.03 Ma in the Teniente dacite porphyry and gabbroic host rocks, whereas molybdenite deposition at 4.78 ± 0.03 Ma was associated with quartz-sericite alteration in the dacite porphyry. This is consistent with the paragenetic relationships, which indicate that quartz-sericite alteration is superimposed on a former potassic assemblage (e.g., Camus, 2003). However, in the Sewell stock 1 km to the southeast (Fig. 6), molybdenite deposition appears associated with quartz-sericite alteration at 4.89 ± 0.08 Ma. It overlaps temporally with potassic alteration of the dacite porphyry but is consistent with zoning of alteration types at that moment in time. These four Re-Os age determinations for molybdenite from veins suggest a hydrothermal ore depositional event (4.89 ± 0.08 – 4.78 ± 0.03 Ma) that is represented in different parts of the orebody (Fig. 6). In addition, Cannell et al. (2003) mentioned four other concurrent Re-Os ages ranging from 4.89 to 4.70 Ma for molybdenite associated with quartz-sericite alteration (analytical uncertainties and sample locations not reported). These Re-Os age determinations reveal an ore depositional event between 4.89 and 4.70 Ma that concurs with the zircon U-Pb crystallization age (4.82 ± 0.09 Ma) for a mineralized dacite ring dike encircling the Braden pipe.

It is uncertain at present whether the 5.01 to 4.96 Ma (Cannell et al., 2003) and the 4.89 to 4.70 Ma time intervals resolved by Re-Os dating represent two separate molybdenite depositional events or a single extended hydrothermal episode. They are herein treated as separate episodes, as details about the samples dated by Cannell et al. (2003) are unavailable.

A molybdenite veinlet with minor chalcopyrite (sample tt-Mo-5) possessing a sericitic alteration halo in a sample from the Teniente dacite porphyry yielded a molybdenite Re-Os age of 4.42 ± 0.02 Ma; sericite from the alteration selvage of this veinlet yielded an $^{40}\text{Ar}/^{39}\text{Ar}$ plateau age of 4.57 ± 0.12 Ma (Table 2f). Other quartz-molybdenite-chalcopyrite veins (samples tt-Mo-7 and tt-Mo-8) hosted by the Northern quartz diorite-tonalite affected by pervasive quartz-sericite alteration produced two identical molybdenite Re-Os ages of 4.42 ± 0.02 Ma. These ages (Fig. 6) indicate that a late ore depositional event related to quartz-sericite alteration was superimposed on these intrusions.

$^{40}\text{Ar}/^{39}\text{Ar}$ dating

Hydrothermal mica (biotite and sericite) is abundant in the El Teniente orebody and we have systematically dated these silicates by the $^{40}\text{Ar}/^{39}\text{Ar}$ method. Samples were collected from drill core from different levels and parts of the orebody. The analytical work was performed at Stanford University, using the procedures of Marsh et al. (1997), who provided a detailed discussion of the sample preparation techniques, analytical methods, and data analysis.

Initially, we completed an orientation study including 32 $^{40}\text{Ar}/^{39}\text{Ar}$ total fusion ages for sericite, biotite, and altered whole-rock samples from different lithologic units at El Teniente (Table 4), plus a reanalysis, by $^{40}\text{Ar}/^{39}\text{Ar}$ step heating, of five samples that Cuadra (1986) previously dated by the conventional K-Ar method (Fig. 10). The $^{40}\text{Ar}/^{39}\text{Ar}$ total fusion ages obtained a range from 12.26 ± 0.74 to 4.39 ± 0.34 Ma (Table 4) but showed a marked statistical peak at 4.7 ± 0.1 Ma and a subordinate peak at 5.3 ± 0.1 Ma, preliminarily suggesting two separate hydrothermal events (Maksaev et al., 2001).

Four samples of Cuadra (1986) reanalyzed during this study yielded plateau ages that replicate previous K-Ar ages (Fig. 10). In contrast, one biotitized whole-rock sample (DDH-1091A) from the Sewell stock, with a K-Ar age of 7.1 ± 1.0 Ma (Cuadra, 1986), yielded a U-shaped apparent age spectrum and an inverse isochron $^{40}\text{Ar}/^{36}\text{Ar}$ intercept of 308.0 ± 13.2 , indicative of excess ^{40}Ar (Fig. 10); when corrected for extraneous Ar, this sample produced an $^{40}\text{Ar}/^{39}\text{Ar}$ plateau age of 4.69 ± 0.10 Ma ($\pm 2\sigma$). This result demonstrates that even minor extraneous Ar in the young minerals at El Teniente may significantly affect the accuracy of conventional K-Ar or $^{40}\text{Ar}/^{39}\text{Ar}$ total fusion ages, which at times are older than the geologic age of the samples. Extraneous ^{40}Ar could be trapped in fluid inclusions that are abundant within hydrothermal minerals at El Teniente. In fact, subsequent reanalysis of samples dated initially by $^{40}\text{Ar}/^{39}\text{Ar}$ total fusion, using $^{40}\text{Ar}/^{39}\text{Ar}$ step heating, showed good correlation for reanalyses of pure biotite separates ($R^2 = 0.9706$) but very poor correlation for reanalyses of altered whole-rock and sericite samples ($R^2 = 0.0496$). The latter produced a number of $^{40}\text{Ar}/^{39}\text{Ar}$ total fusion and K-Ar ages that are systematically older than the $^{40}\text{Ar}/^{39}\text{Ar}$ plateau ages that are almost invariant (Fig. 11). This bias reflects the influence of extraneous Ar in whole-rock samples and sericite. Thus, conventional K-Ar and $^{40}\text{Ar}/^{39}\text{Ar}$ total fusion from El Teniente, which do not provide information about possible extraneous argon, must be taken with extreme caution when interpreting the chronologic evolution of

TABLE 4. Total Fusion $^{40}\text{Ar}/^{39}\text{Ar}$ Ages for El Teniente

Sample no.	Drill hole	Depth (m)	Age (Ma $\pm 2\sigma$)	Mineral	Rad. Ar (%)	Rock unit	Comments
TT-15	1891	87.5	4.76 \pm 0.12	Biotite	45.5	Biotitized andesite	Brown biotite (phlogopite)
TT-14	1891	53.3	5.09 \pm 0.12	Whole-rock biotite	56.0	Biotitized andesite	Greenish-brown biotite
TT-20	1514	543.3	5.58 \pm 0.14	Sericite	84.7	Biotitized andesite	Sericite vein
TT-23	1891	354.8	4.76 \pm 0.10	Biotite	87.2	Biotitized andesite	Brown biotite (phlogopite)
TT-44	1407	275.2	4.85 \pm 0.10	Whole-rock sericite	83.6	Biotitized andesite	Quartz-sericite halo of quartz-chalcopyrite vein
TT-56	1300	374.9	4.73 \pm 0.18	Biotite	29.2	Biotitized andesite	Coarse-grained biotite-quartz vein; brown biotite
TT-74	1309	391.8	5.50 \pm 0.24	Biotite	58.4	Biotitized andesite	Quartz vein with molybdenite suture and biotite halo
TT-04	1337	216.0	4.93 \pm 0.14	Biotite	0.07	Biotitized andesite	Greenish-brown biotite
TT-93 ¹	225N	820E	5.42 \pm 0.12	Whole-rock sericite	84.0	Braden pipe	Sericite halo of a chalcopyrite vein
TT-33	1323	188.1	4.66 \pm 0.10	Whole-rock sericite	56.8	Central quartz diorite-tonalite	Quartz-sericite alteration
TT-39 ¹	1333	163.4	4.80 \pm 0.18	Whole-rock sericite	45.5	Central quartz diorite-tonalite	Sericite-smectite-calcite alteration
TT-50 ¹	1309	146.6	10.07 \pm 0.62	Whole-rock sericite	69.2	Northern quartz diorite-tonalite	Quartz-sericite alteration
TT-65	1309	116.0	5.94 \pm 0.44	Whole-rock sericite	48.3	Northern quartz diorite-tonalite	Strong sericitization (coarse-grained sericite)
TT-69 ¹	1309	157.7	5.26 \pm 0.82	Whole-rock sericite	10.3	Northern quartz diorite-tonalite	Coarse-grained greenish sericite; quartz-sericite alteration
TT-64 ¹	1309	98.1	5.25 \pm 0.36	Whole-rock sericite	37.4	Northern quartz diorite-tonalite	Strong sericitization (coarse-grained sericite)
TT-60 ¹	1309	68.6	5.07 \pm 0.22	Whole-rock sericite	64.4	Northern quartz diorite-tonalite	Strong sericitization (coarse-grained sericite), local chlorite
TT-49	1309	267.3	4.67 \pm 0.18	Sericite	57.0	Northern quartz diorite-tonalite	Sericite halo of quartz vein; weakly sericitized rock
TT-01 ¹	1334	360.0	5.27 \pm 0.08	Biotite	41.6	Sewell stock	Coarse-grained biotite-anhydrite-chalcopyrite vein
TT-01 ¹	1334	360.0	5.32 \pm 0.10	Biotite	50.1	Sewell stock	Replicate dating
TT-05	1307	227.4	4.91 \pm 0.20	Sericite	36.8	Sewell stock	Quartz-sericite alteration
TT-09 ¹	1337	149.5	4.71 \pm 0.08	Biotite	61.6	Sewell stock	Coarse-grained biotite-anhydrite-chalcopyrite vein
TT-81 ¹	1311	669.0	12.26 \pm 0.74	Whole-rock sericite	63.3	Sewell stock	Quartz-sericite alteration
TT-10	1554	41.7	4.94 \pm 0.14	Sericite	57.3	Teniente dacite porphyry	Coarse-grained sericite from a pyrite-sericite vein
TT-17	1514	497.0	5.40 \pm 0.42	Biotite	30.9	Teniente dacite porphyry	Partly chloritized biotite
TT-18 ¹	1514	521.7	4.60 \pm 0.08	Sericite	90.9	Teniente dacite porphyry	Coarse-grained sericite vein
TT-19 ¹	1514	522.2	5.10 \pm 0.28	Sericite	35.3	Teniente dacite porphyry	Quartz-sericite-molybdenite vein
TT-21 ¹	1514	371.7	6.35 \pm 0.62	Sericite	42.1	Teniente dacite porphyry	Quartz-sericite vein
TT-21 ¹	1514	371.0	4.93 \pm 0.24	Biotite	29.4	Teniente dacite porphyry	Biotite phenocrysts
TT-22 ¹	1514	302.0	5.09 \pm 0.32	Sericite	49.0	Teniente dacite porphyry	Sericite halo of a quartz-chalcopyrite-molybdenite vein
TT-24	1891	247.2	4.68 \pm 0.06	Sericite	82.5	Teniente dacite porphyry	Sericite-pyrite vein
TT-30 ¹	1414	369.4	4.39 \pm 0.34	Sericite	24.9	Dacite dike	Sericite-clay-carbonate alteration
TT-43 ¹	1407	270.1	8.40 \pm 1.40	Sericite	10.9	Dacite dike	Quartz-sericite alteration; quartz-molybdenite vein
TT-46 ¹	1409	468.5	4.80 \pm 0.14	Sericite	77.9	Dacite dike	Pervasive sericitization and carbonate alteration

¹ Re-analyzed sample

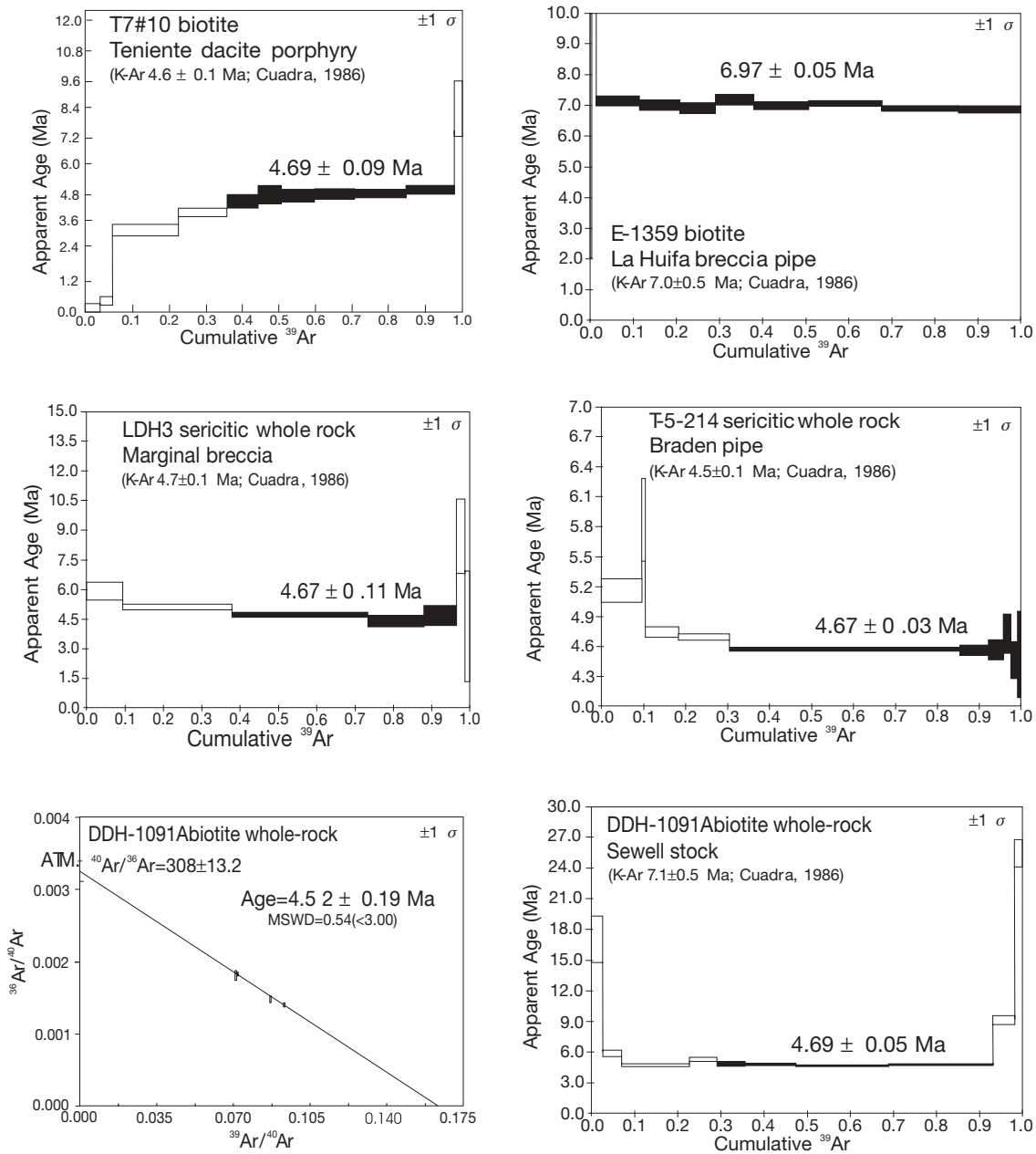


FIG. 10. Apparent $^{40}\text{Ar}/^{39}\text{Ar}$ age spectra ($\pm 1\sigma$) of samples originally dated by conventional K-Ar by Cuadra (1986), re-analyzed by $^{40}\text{Ar}/^{39}\text{Ar}$ step heating (furnace). The upper four plateaus replicate the original K-Ar ages, but the lower U-shaped spectrum of a biotite-altered whole rock yielded a younger $^{40}\text{Ar}/^{39}\text{Ar}$ plateau age and an inverse isochron $^{40}\text{Ar}/^{36}\text{Ar}$ intercept of 308.0 ± 13.2 , indicative of excess ^{40}Ar .

the deposit. Therefore, these types of age dates are excluded from our further geochronologic analysis.

Our oldest $^{40}\text{Ar}/^{39}\text{Ar}$ plateau age of 6.97 ± 0.10 Ma on hydrothermal biotite ($\pm 2\sigma$; Table 2j) was obtained by reanalysis of a sample of porphyry from the La Huifa breccia pipe (located 2 km north of the El Teniente mine), which originally yielded a biotite K-Ar age of 7.0 ± 0.4 Ma (Cuadra, 1986). This result suggests that hydrothermal activity in the district had commenced by 6.97 ± 0.10 Ma; although, such early hydrothermal activity is not recorded by any of the ages obtained by step heating from the El Teniente orebody.

In a second stage, we completed 39 additional $^{40}\text{Ar}/^{39}\text{Ar}$ step-heating determinations, with careful handpicking after mineral separation to avoid materials (sulfides, sulfates, apatite, quartz, etc.) that might contribute extraneous Ar; this procedure was even adopted for altered whole-rock samples. The results for each lithologic unit are summarized in Table 2, locations of the dated samples are projected to the Teniente 4 LHD level (2,354 m) in Figures 12 and 13, and apparent $^{40}\text{Ar}/^{39}\text{Ar}$ age spectra are presented in Appendix 2.

The oldest $^{40}\text{Ar}/^{39}\text{Ar}$ plateau ages for El Teniente were obtained from samples from the easternmost portion of the

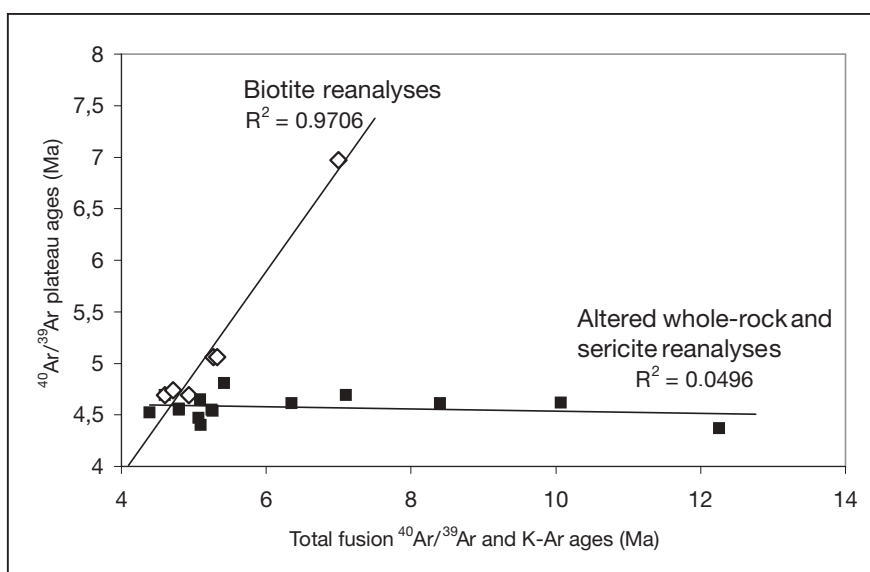


FIG. 11. Plot of $^{40}\text{Ar}/^{39}\text{Ar}$ plateau ages of reanalyzed samples (furnace step heating) against ages obtained originally either by conventional K-Ar or total fusion $^{40}\text{Ar}/^{39}\text{Ar}$; fitted lines are shown for biotite (correlation coefficient; $r^2 = 0.9706$) and altered whole-rock and sericite samples (correlation coefficient; $r^2 = 0.0496$). The near-horizontal line for altered whole-rock and sericite samples shows that some samples with essentially invariant $^{40}\text{Ar}/^{39}\text{Ar}$ plateau ages show a significant spread to older values when analyzed by conventional K-Ar of total fusion $^{40}\text{Ar}/^{39}\text{Ar}$, due to excess ^{40}Ar that cannot be detected by these methods.

deposit. Coarse-grained hydrothermal biotite from a sample (DDH-2176; Fig. 12) of mineralized breccia hosted by the Sewell stock on the eastern border of the mineralized body yielded an $^{40}\text{Ar}/^{39}\text{Ar}$ plateau age of 5.69 ± 0.08 Ma. The biotite is from the same hydrothermal breccia sample that yielded a molybdenite Re-Os age of 6.31 ± 0.03 Ma. The $^{40}\text{Ar}/^{39}\text{Ar}$ plateau age of the biotite is concurrent with the potassic overprint that affected the Sewell stock and the A porphyry in the same part of the orebody (U-Pb: 5.59 ± 0.17 and 5.67 ± 0.19 Ma; see above), indicating that the $^{40}\text{Ar}/^{39}\text{Ar}$ system for biotite was reset during the hydrothermal overprint, whereas the Re-Os system in molybdenite was unaffected owing to its higher closure temperature. Other concurrent $^{40}\text{Ar}/^{39}\text{Ar}$ plateau ages of 5.63 ± 0.12 and 5.47 ± 0.12 Ma were obtained for magmatic biotite in unmineralized quartz diorite-tonalite samples (DDH-1116 and DDH-1140; Fig. 12) from deep drill holes immediately southeast of the orebody (Reich, 2001). This fresh, equigranular quartz diorite-tonalite is probably a separate intrusion that is temporally related to the potassic alteration overprint at about 5.6 Ma inferred from the U-Pb, Re-Os, and $^{40}\text{Ar}/^{39}\text{Ar}$ ages in the eastern part of the orebody.

A coarse-grained hydrothermal biotite vein hosted by the Sewell stock (sample TT-01; Fig. 12) yielded an $^{40}\text{Ar}/^{39}\text{Ar}$ plateau age of 5.06 ± 0.12 Ma, and hydrothermal biotite from a sample of the A porphyry (sample TT-150; Fig. 12) provided an $^{40}\text{Ar}/^{39}\text{Ar}$ plateau age of 4.93 ± 0.12 Ma (the same sample yielded zircon U-Pb ages of 6.46 ± 0.11 and 5.67 ± 0.19 Ma; see above). These biotite $^{40}\text{Ar}/^{39}\text{Ar}$ ages are concurrent with Re-Os ages from 5.01 to 4.96 Ma for molybdenite associated with potassic alteration (Cannell et al., 2003) and may represent resetting of the K-Ar system by hydrothermal circulation temporally related to the Teniente dacite porphyry (max

U-Pb age of 5.28 ± 0.10 Ma; see above). Although these biotite samples are from the southeastern part of the orebody, about 1 km from the Teniente dacite porphyry in the mine, they still seem to have recorded a thermal event that followed the emplacement of this intrusion.

A total of 38 $^{40}\text{Ar}/^{39}\text{Ar}$ step-heating age determinations on biotite and sericite samples obtained from drill core from different parts and rock units of the El Teniente orebody yielded $^{40}\text{Ar}/^{39}\text{Ar}$ plateau ages in a limited range from 4.81 ± 0.10 to 4.37 ± 0.10 Ma (Table 2; Figs. 12–13). Irrespective of the nature of biotite (hydrothermal or magmatic), sericite grain size, or the altered whole rocks dated, all these samples yielded $^{40}\text{Ar}/^{39}\text{Ar}$ plateau ages that fall within the same brief time span. These ages are also in agreement with most published K-Ar ages from El Teniente (e.g., Cuadra, 1986). Therefore, most of the mica of the deposit was either generated and/or its $^{40}\text{Ar}/^{39}\text{Ar}$ system completely reset during this time interval. Considering the approximate closure temperature of micas with respect to $^{40}\text{Ar}/^{39}\text{Ar}$ ($380^\circ\text{--}250^\circ\text{C}$), it is inferred that high-temperature fluid circulation ($>350^\circ\text{C}$) affected, either continuously or episodically, the orebody from 4.81 ± 0.10 to 4.37 ± 0.10 Ma. Except for the three above-mentioned $^{40}\text{Ar}/^{39}\text{Ar}$ biotite plateau ages of 5.6 to 4.9 Ma from the easternmost part of the orebody, the inferred high-temperature fluid circulation obliterated the $^{40}\text{Ar}/^{39}\text{Ar}$ record for previous thermal events, which are inferred on the basis of other isotopic systems and methods that possess higher closure temperatures. As a result, the $^{40}\text{Ar}/^{39}\text{Ar}$ data provide exclusively the record of the latest hydrothermal episodes and only a partial history for the development of this large ore-forming system. The susceptibility of the $^{40}\text{Ar}/^{39}\text{Ar}$ system to resetting by high-temperature fluids has been documented for other porphyry systems (e.g., Selby and Creaser, 2001).

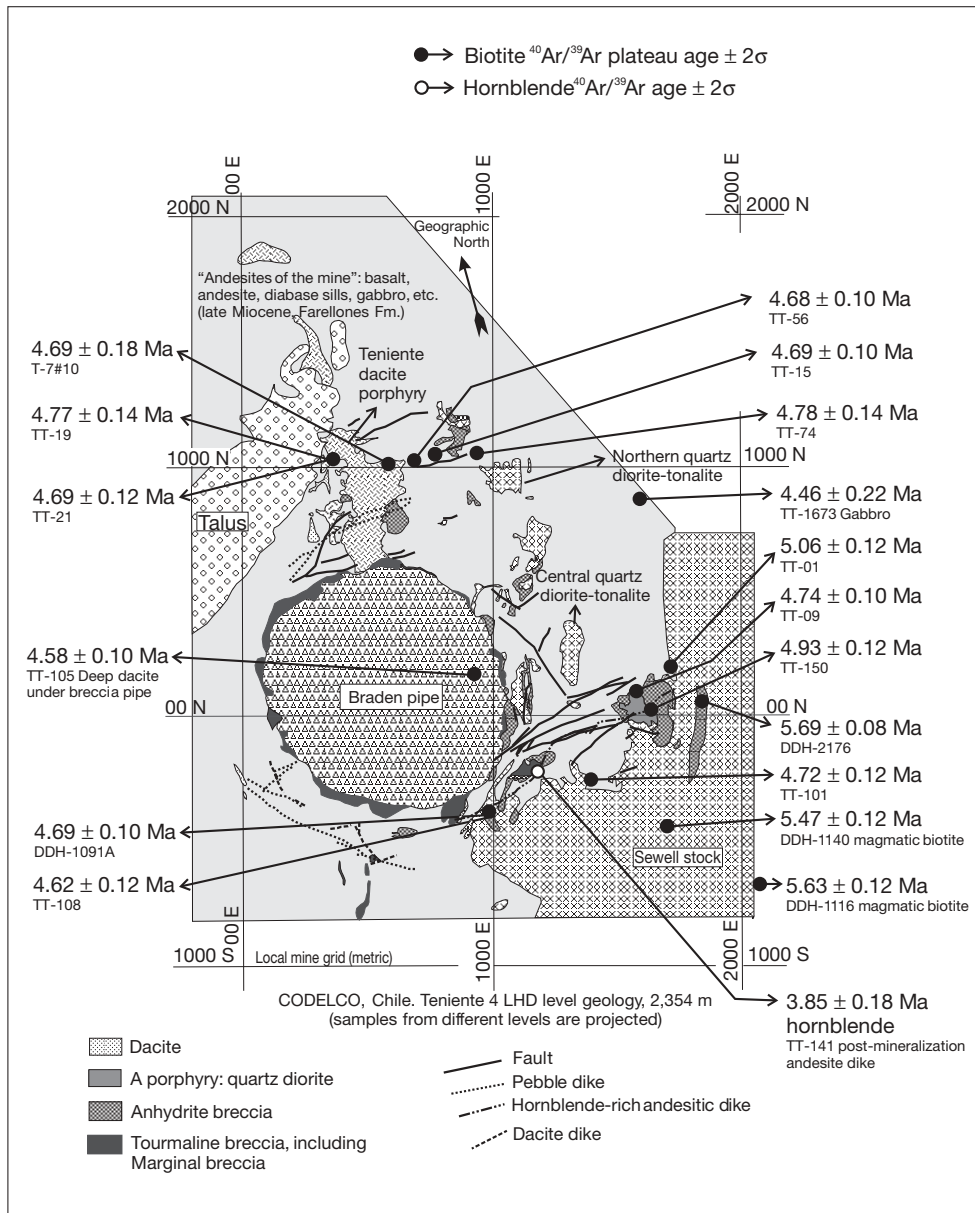


FIG. 12. Distribution of biotite samples and one hornblende sample dated by $^{40}\text{Ar}/^{39}\text{Ar}$ step heating; plateau $^{40}\text{Ar}/^{39}\text{Ar}$ ($\pm 2\sigma$) ages are shown, except for hornblende that did not define a plateau. Sample locations projected to the Teniente 4 LHD level (2,354 m).

Sericite $^{40}\text{Ar}/^{39}\text{Ar}$ ages are confined to the $4.81 \pm$ to 4.37 ± 0.10 Ma time interval and most are younger than the biotite $^{40}\text{Ar}/^{39}\text{Ar}$ ages, suggesting a transition from potassic-dominated to later quartz-sericite alteration. This is not only consistent with the paragenetic relationships of sulfide-bearing veins with quartz-sericite alteration halos, which are late relative to potassic alteration (e.g., Cuadra, 1986; Camus, 2003), but it is also in agreement with our Re-Os ages between 4.89 ± 0.08 and 4.42 ± 0.02 Ma for molybdenite-bearing veins with quartz-sericite selvages.

Sericite $^{40}\text{Ar}/^{39}\text{Ar}$ ages from 4.81 ± 0.12 to 4.49 ± 0.10 Ma were obtained for altered samples from the Braden pipe, indicating that the diatreme already existed at that time. This pipe

was clearly formed after intrusion of the Teniente dacite porphyry (U-Pb 5.28 ± 0.10 Ma), probably at 4.82 ± 0.09 Ma, which is the zircon U-Pb age of an encircling dacite ring dike. The formation of the diatreme in the center of the ore-forming system coincided with the onset of quartz-sericite alteration in the orebody, according to the sericite $^{40}\text{Ar}/^{39}\text{Ar}$ ages and Re-Os ages of molybdenite-bearing veins with sericitic halos. The Braden pipe clearly controlled further hydrothermal circulation along its shattered margins, but the quartz-sericitic overprint suggests a change in physicochemical conditions that could be related to the sudden decompression of the porphyry system after brecciation. In fact, the formation of the breccia pipe may have also influenced magma degassing and ore deposition.

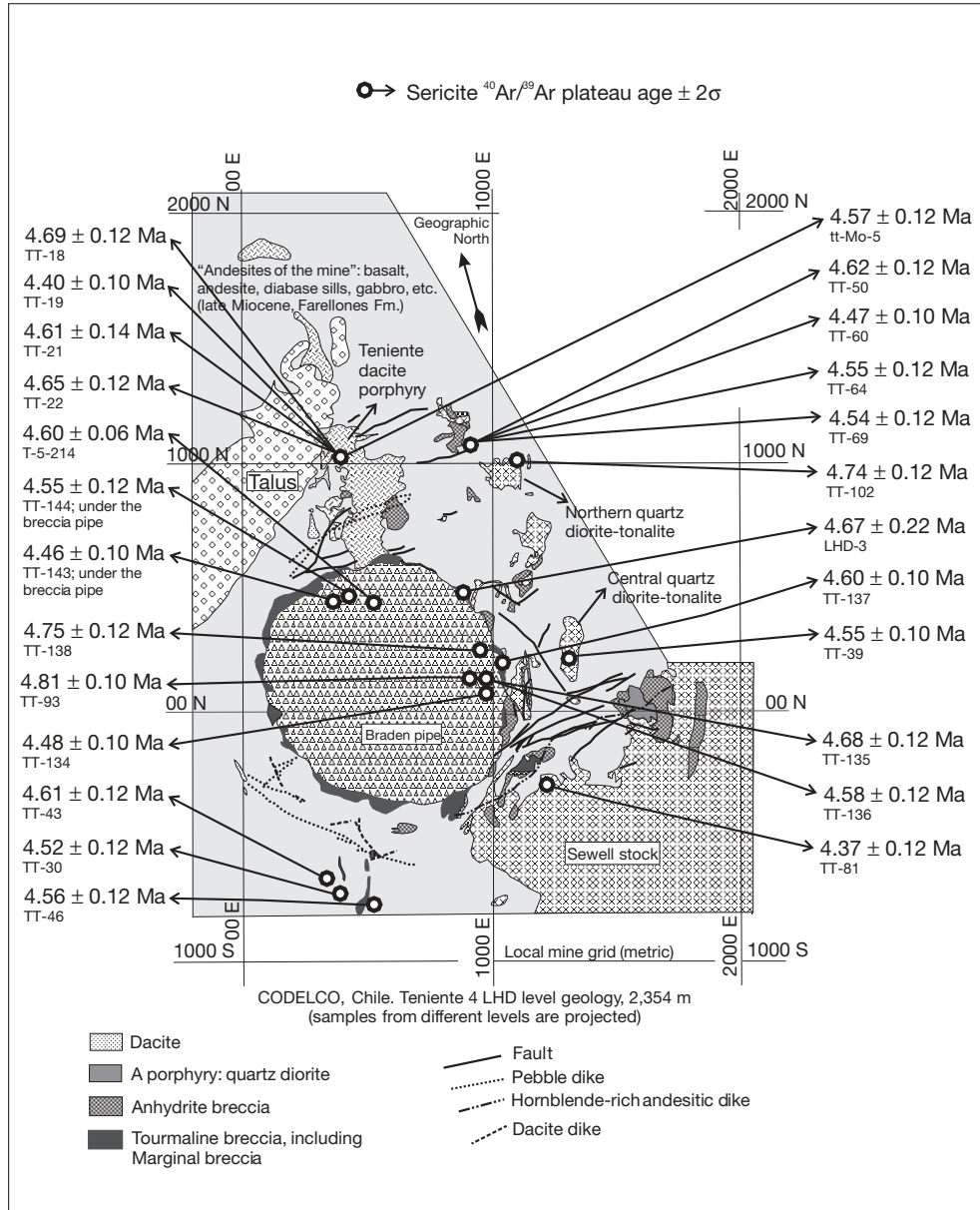


FIG. 13. Distribution of sericite and sericitic samples dated by $^{40}\text{Ar}/^{39}\text{Ar}$ step heating; plateau $^{40}\text{Ar}/^{39}\text{Ar}$ ages are shown ($\pm 2\sigma$). Sample locations projected to the Teniente 4 LHD level (2,354 m).

Poorly mineralized dacite intrusions and dikes represent a late intrusive event. A dacite sample collected from the roots of the Braden pipe yielded an $^{40}\text{Ar}/^{39}\text{Ar}$ plateau age of 4.58 ± 0.10 Ma for biotite (1,006-m level from a deep drill hole in the center of the pipe). Also an altered, but largely unmineralized, dacite stock that underlies the northern part of the Braden pipe yielded sericite $^{40}\text{Ar}/^{39}\text{Ar}$ plateau ages between 4.56 ± 0.12 and 4.46 ± 0.10 Ma. This late dacite intrusive event is concurrent with the molybdenite depositional episode dated at 4.42 ± 0.02 Ma by the Re-Os method and with a sericitic overprint of the Teniente dacite porphyry, according to sericite $^{40}\text{Ar}/^{39}\text{Ar}$ plateau ages of 4.57 ± 0.12 and 4.40 ± 0.10 Ma.

A postore, hornblende-rich andesitic dike that crosscuts the southeastern part of the orebody yielded the youngest $^{40}\text{Ar}/^{39}\text{Ar}$ age of 3.85 ± 0.18 Ma at El Teniente (App. 2.5). This dike marks the end of igneous activity within the El Teniente orebody and postdates all hydrothermal alteration and mineralization processes within the deposit.

Biotite and sericite are demonstrated to be prone to resetting by high-temperature fluids ($>350^\circ\text{C}$), so the $^{40}\text{Ar}/^{39}\text{Ar}$ plateau ages are mostly grouped between 4.81 ± 0.10 and 4.37 ± 0.10 Ma. Systematic $^{40}\text{Ar}/^{39}\text{Ar}$ step-heating determinations on these minerals revealed that hydrothermal circulation extended either continuously or episodically from 5.69 ± 0.08 to 4.37 ± 0.10 Ma. Nevertheless, $^{40}\text{Ar}/^{39}\text{Ar}$ dating clearly

underestimates the total life span of the ore-forming system, which was already active at ~ 6.3 Ma according to the Re-Os and U-Pb data. Selby and Creaser (2001) showed a similar behavior of the $^{40}\text{Ar}/^{39}\text{Ar}$ system in the Endako porphyry molybdenum deposit.

Fission-track dating

Samples from the El Teniente deposit and vicinity were collected for apatite fission-track dating to study the low-temperature cooling history of the system. Analytical work was carried out at the Fission Track Laboratory of Dalhousie University, Halifax, Canada. Fission-track ages were determined using the external detector method (Hurford and Carter, 1991).

Apatite samples from the El Teniente deposit contain ubiquitous fluid and zircon inclusions, dislocations, and/or pitting,

unfortunately rendering most unusable for dating, but track length data were obtained (Fig. 14). Only two apatite crystals from the Teniente dacite porphyry (sample TT-95; Table 5; Fig 14d) were analyzed, yielding a fission-track age of 4.2 ± 5.6 Ma ($\pm 2\sigma$). Because of the very limited count data, this date should just be considered only as a rough estimate. The measured mean confined track length of the apatite sample is 13.36 ± 0.24 μm , with a unimodal track length distribution, consistent with a simple cooling history (i.e., no reheating is apparent). The age estimate and the measured track length distribution were combined to model the thermal evolution of the sample (Fig. 14e), which is consistent with the porphyry cooling quickly below the apatite closure temperature for fission tracks ($105^\circ \pm 20^\circ\text{C}$), before emplacement of the postore andesitic dike with a hornblende $^{40}\text{Ar}/^{39}\text{Ar}$ age of 3.85 ± 0.18 Ma.

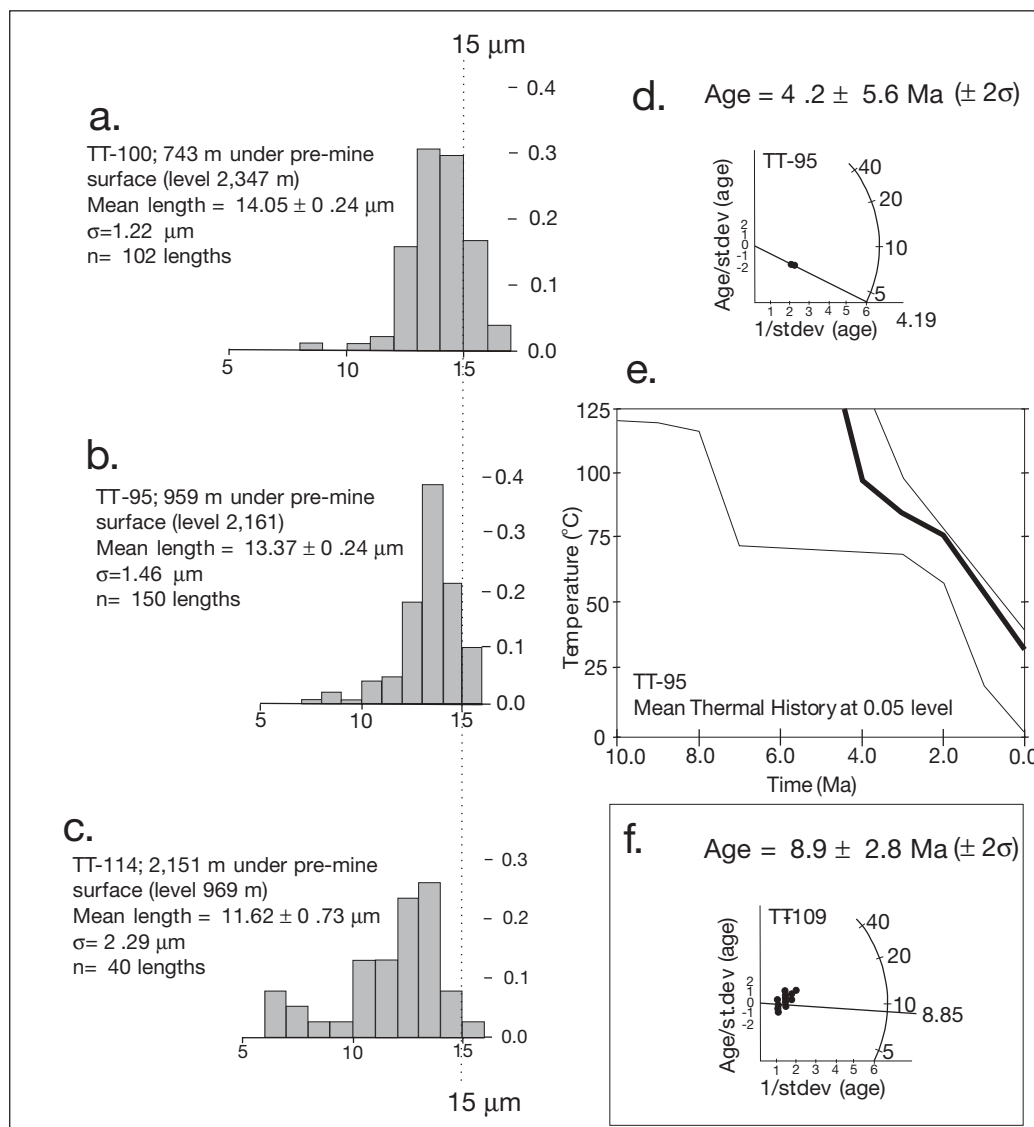


FIG. 14. Apatite fission-track data for intrusive rocks at El Teniente. a, b, c. Track length distribution histograms shown relative to their altitude. d. Radial plot of fission-track age estimation (4.2 ± 5.6 Ma) for the Teniente dacite porphyry. e. Thermal model that fits to the track length distribution and fission-track age of the sample. f. (inset) Radial plot of apatite fission-track age estimates (8.9 ± 2.8 Ma) for a basic sill 5 km west of the mine.

TABLE 5. Apatite Fission Track Age Data

Sample no.	Unit	Grains	ρ_s	N_s	ρ_i	N_i	χ^2	ρ_d	N_d	Pooled age (Ma $\pm 2\sigma$)
TT-95	Teniente dacite porphyry	2 ¹	0.179	9	8.14	417	89.0	1.10	4916	4.2 \pm 5.6
TT-109	Mafic sill 5 km west from El Teniente	27	0.034	42	0.738	922	96.1	1.10	4916	8.9 \pm 2.8

Notes: Analyses by A.M. Grist at Fission Track Laboratory, Dalhousie University; samples passed the chi-squared test at the 95% confidence level (i.e., a single age population is apparent); a value of 353.5 ± 7.1 (CN-5) was used for the zeta calibration factor; the ages reported in the table are the pooled ages

Abbreviations: ρ_s , ρ_i , and ρ_d are the density of spontaneous, induced, and flux dosimeter tracks, respectively ($?10^6/\text{cm}^2$); N_s , N_i , and N_d are the number of spontaneous, induced, and glass dosimeter (CN5) tracks, respectively

¹ Samples with most apatite grains with numerous inclusions and/or ubiquitous pitting making them unusable for dating, thus only two grains were counted

There is a consistent track length variation in apatites with sample depth: the shortest mean confined track length measured is $11.62 \pm 0.73 \mu\text{m}$ (TT-114; level 969 m) in a sample from 2,150 m beneath the premine surface; this deep sample shows a spread of track lengths and a bimodal distribution with a peak in short tracks (Fig. 14c), consistent with the sample remaining for a certain period within the lower part of the partial annealing zone of apatite. In contrast, samples of the Dacite Teniente Porphyry and the Sewell stock show unimodal track length distributions, and their mean track lengths are $13.36 \pm 0.24 \mu\text{m}$ (TT-95; level 2,161 m), and $14.05 \pm 0.24 \mu\text{m}$ (TT-100; level 2,347 m), respectively.

An apatite sample (TT-109) from a diabase sill emplaced within the volcanic sequence of the Miocene Farellones Formation, 5 km west of the mine, yielded a fission-track age of 8.9 ± 2.8 Ma (Table 5; Fig. 14f). This sill, according to Skewes et al. (2002), extends continuously to El Teniente. Its fission-track age agrees with the range of K-Ar ages for the host volcanic succession (12.0 ± 0.7 – 6.6 ± 0.4 Ma; Cuadra, 1986; Godoy and Köeppen, 1993). The mean track length of the apatite sample is $13.38 \pm 1.07 \mu\text{m}$, with a unimodal distribution of track lengths, consistent with a simple cooling history. These characteristics indicate that the sill was emplaced within the volcanic pile and cooled above the fission-track annealing zone of apatite. Therefore, exhumation in the El Teniente district is <3 to 4 km since the late Miocene, assuming a $30^\circ\text{C}/\text{km}$ paleogeothermal gradient, consistent with preservation of the upper Miocene volcanic sequence in the region.

Porphyry Copper or Breccia-Hosted Deposit Model: Implications for Geochronologic Data Interpretation

The El Teniente Cu-Mo orebody has traditionally been viewed as “a model porphyry copper deposit” (Howell and Molloy, 1960, p. 901), with primary sulfide mineralization genetically related to the emplacement of porphyritic felsic intrusions and associated pervasive potassic alteration with a subordinate quartz-sericitic overprint. The porphyry model is recognized by most published studies referring to El Teniente (e.g., Camus, 1975, 2003; Gustafson and Hunt, 1975; Cuadra, 1986; Ip, 1987a, b; Makshev et al., 2001, 2002; Cannell et al., 2003). However, Skewes et al. (2002) argued that felsic intrusion at El Teniente is confined to small, late, copper-poor stocks that merely redistributed earlier copper mineralization. They depicted El Teniente as a breccia-hosted ore deposit; calling attention to unmapped, biotite-bearing breccias,

which according to their interpretation began with the intrusion of a basic laccolith, before the emplacement of felsic porphyritic stocks (see also Skewes and Arévalo, 2000). Main-stage ore deposition was interpreted to be related to early-formed breccia pipes, hypothetically generated by fluid discharge from unexposed, basic intrusions interacting with a crystallizing felsic magma chamber at depth.

The pervasively altered felsic porphyry intrusions at El Teniente with hypogene copper mineralization in stockworks of veins widely exceed 1.0 percent Cu and cannot be explained merely by copper redistribution. These porphyries were originally injected as silicate melts at igneous temperatures and high pressure; probably well below the ductile-brittle transition (cf., Fournier, 1999). Thus, hydrothermal fluid must have flowed away from the crystallizing intrusions (i.e., down-pressure gradients) and not into the stocks to introduce ore components from outside the intrusions. This is further substantiated by the relatively homogeneous initial $^{187}\text{Os}/^{188}\text{Os}$ ratios for cogenetic chalcopyrite, bornite, and sphalerite from El Teniente (0.17–0.22), suggesting that most Os was provided by the causal intrusions and not from the surrounding country rocks (Freydier et al., 1997). In addition, a recent investigation of trace elements in rutile and anatase from El Teniente concluded that the felsic intrusions were a source of metals (specifically Mo), whereas the biotitized host rocks and parts of the Sewell stock (Fig. 2) acted passively as host rocks (Rabbia, 2002).

The minimum age for main-stage ore deposition at El Teniente was ascribed by Skewes et al. (2002) to be 7.1 Ma, based on the whole-rock K-Ar age of 7.1 ± 1.0 Ma reported by Cuadra (1986) for the Sewell stock. However, our step-heating reanalysis of the same sample (DDH-1091A) yielded an $^{40}\text{Ar}/^{39}\text{Ar}$ plateau age of 4.69 ± 0.05 (Fig. 10) and showed that the 7.1 ± 1.0 Ma K-Ar age was an analytical artifact of excess ^{40}Ar (see above).

Skewes et al. (2002) emphasized the occurrence of angular biotitized inclusions of mineralized host rocks within a dacite intrusion at El Teniente as evidence that main-stage ore deposition preceded the intrusion of all the felsic intrusive bodies. This observation is certainly indicative of superimposed events during the evolution of this supergiant deposit, which are also demonstrated by brecciation of mineralized rocks and superimposition of stockworks on hydrothermal breccias throughout the deposit (e.g., Arredondo, 1994; our observations). Nevertheless, the Teniente dacite porphyry and dacite

ring dikes are clearly hydrothermally altered and mineralized by stockworks of sulfide-bearing veins. Thus, there is no basis for considering the ages of felsic intrusions as minimum ages for mineralization.

Our new U-Pb geochronologic data provide for the first time a precise and accurate estimate of the crystallization age of the altered and mineralized felsic intrusions at El Teniente, the timing of molybdenite deposition, and the age of hydrothermal alteration silicates. Aside from the purely hypothetical model for existence of basic magma at depth, the genetic relationship of the felsic intrusions with Cu-Mo ore-forming hydrothermal processes is strongly supported by the agreement of zircon U-Pb and molybdenite Re-Os ages and the partial overlap with $^{40}\text{Ar}/^{39}\text{Ar}$ ages of biotite and sericite (consistent with their lower closure temperatures). Thus, crystallization ages of felsic intrusions at El Teniente, inferred from their zircon U-Pb ages, represent maximum ages for hydrothermal alteration, brecciation, and ore deposition genetically associated with each intrusive pulse.

Duration of Hydrothermal Activity

Lifespans of hydrothermal systems are a fundamental metallogenic question, particularly for supergiant deposits. Our new geochronologic data set for El Teniente ranges from 6.46 ± 0.11 to 4.37 ± 0.10 Ma, indicating evolution of the ore-forming system during a period of 2.09 ± 0.21 m.y. This is consistent with the constraints imposed by the K-Ar ages for the country rocks in the district (12.0 ± 0.7 – 6.6 ± 0.4 Ma; Cuadra, 1986; Godoy and Köeppen, 1993) and by the hornblende $^{40}\text{Ar}/^{39}\text{Ar}$ age of 3.85 ± 0.18 Ma for a postore andesitic dike. The latter age suggests a maximum lifespan of 2.75 ± 0.58 m.y. for all hydrothermal and mineralizing processes. Detailed $^{40}\text{Ar}/^{39}\text{Ar}$ step-heating dating of hydrothermal biotite, sericite, and strongly altered whole-rock samples from El Teniente yielded 40 plateau ages spanning the range from 5.06 ± 0.12 to 4.37 ± 0.10 Ma. These isotopic ages for hydrothermal micas reveal a period of hydrothermal activity at El Teniente corresponding to the time of dacite magma intrusion, which extended either continuously or episodically for at least 0.69 ± 0.22 m.y. ($\pm 2\sigma$). Three mineralization episodes are resolved by molybdenite Re-Os dating within the same period, at 5.01 to 4.96, 4.89 to 4.78, and 4.42 Ma. Thus, we conclude that individual hydrothermal mineralization episodes lasted considerably $<0.69 \pm 0.22$ m.y. When $^{40}\text{Ar}/^{39}\text{Ar}$ plateau ages of biotite are considered, they range from 5.06 ± 0.12 to 4.58 ± 0.10 Ma, indicating a duration of at least 0.48 ± 0.22 m.y., whereas in the case of sericite the ages range from 4.75 ± 0.12 to 4.46 ± 0.10 Ma (sericitized whole-rock samples excluded), representing a duration of at least 0.29 ± 0.22 m.y. The duration of hydrothermal mica formation inferred from $^{40}\text{Ar}/^{39}\text{Ar}$ plateau ages of hydrothermal minerals from El Teniente is comparable to the 0.50 ± 0.32 m.y. that Parry et al. (2001) estimated for hydrothermal biotite formation at Bingham. We infer that three short-lived episodes of high-temperature ($>350^\circ\text{C}$) fluid circulation took place during the time span from 5.06 to 4.37 Ma within the large (~ 7 km³) El Teniente orebody, according to the $^{40}\text{Ar}/^{39}\text{Ar}$ ages for micas and molybdenite Re-Os ages. In addition, concurrence of published K-Ar ages (Clark et al., 1983, Cuadra, 1986) and most of the molybdenite Re-Os ages

of El Teniente (Cannell et al., 2003; our data) probably indicate that the main mineralizing period at El Teniente took place during this time interval (5.06–4.37 Ma). Mineralization was linked to a large ore-forming system temporally related to the emplacement of successive batches of dacite magma and the interrelated explosive activity that originated the Braden pipe. However, two preceding mineralizing stages, related to quartz diorite-tonalite intrusions, at 6.31 and 5.60 Ma are inferred from U-Pb and Re-Os dating in the southeastern part of the deposit.

Cooling Rates

Estimating a cooling rate from the El Teniente deposit is made difficult by successive thermal overprinting, but the agreement of U-Pb zircon and Re-Os molybdenite ages suggests that ore deposition occurred immediately after the felsic intrusions crystallized, implying very fast cooling. After a comparison of the 4.82 ± 0.09 Ma zircon U-Pb age for a mineralized dacite dike and the 4.74 ± 0.10 Ma $^{40}\text{Ar}/^{39}\text{Ar}$ plateau age of coarse hydrothermal biotite at El Teniente, we conclude that cooling took place from about 800° (zircon U-Pb closure temperature) to 300°C (biotite $^{40}\text{Ar}/^{39}\text{Ar}$ closure temperature) within $\sim 80,000$ yr. Similarly, a comparison of the 5.28 ± 0.10 Ma U-Pb zircon age for the Teniente dacite porphyry and the $^{40}\text{Ar}/^{39}\text{Ar}$ plateau age of 5.06 ± 0.12 Ma for hydrothermal biotite suggests cooling within $\sim 220,000$ yr, leading to cooling rates in excess of $1,000^\circ\text{C}/\text{m.y.}$ This is faster than, but of the same order as, the rates for discrete intrusions at the Chuquicamata porphyry copper deposit (Ballard, et al., 2001). The high cooling rates we infer for El Teniente agree with model calculations by Cathles et al. (1997, and references therein) for kilometer-scale, shallow-level intrusions. The strong associated thermal gradients may have greatly contributed to rapid deposition of copper sulfide minerals to create the high hypogene copper grades at El Teniente, as temperature is the fundamental variable controlling the solubility of copper in magmatic-hydrothermal fluids (e.g., Hemley et al., 1992).

Multiple Discrete Overprinting Events of Hydrothermal Mineralization: A Characteristic of El Teniente and Other Supergiant Porphyry Copper Deposits

The new geochronologic data indicate that El Teniente was generated by at least five superimposed mineralizing events temporally related to the intrusion of felsic magma. According to the available Re-Os data for molybdenite, each was linked to hydrothermal episodes at 6.31 ± 0.03 , 5.60 ± 0.02 , 5.01 to 4.96 , 4.89 ± 0.08 to 4.78 ± 0.03 , and 4.42 ± 0.02 Ma. Hydrothermal overprinting by overlapping mineralization events has also been suggested on the basis of geochronologic studies at the Chuquicamata (Reynolds et al., 1998; Ballard et al., 2001; Ossandón et al., 2001), Río Blanco-Los Bronces (Serrano et al., 1996; Deckart et al., 2003), Los Pelambres (Stein et al., 2002; Bertens et al., 2003), and La Escondida porphyry copper deposits (Padilla et al., 2001). It would appear that superimposed mineralization events within a single orebody are required to generate supergiant porphyry Cu-Mo deposits. Although the hypothetical role of especially copper rich hydrothermal fluid cannot be overlooked (e.g., Clark,

1993), overprinting of ore deposition is believed to be one of the fundamental controls on deposit size. Large-scale tectonic and local structural control is of utmost importance in focusing magma injection and hydrothermal fluid flow, but repeated and probably efficient ore deposition, associated with injection of felsic magma in epizonal levels, is characteristic of these supergiant porphyry deposits. Although, at present we cannot rule out that the latter characteristic is common to all porphyry copper deposits, we provide for the first time a precise and accurate estimate of five discrete mineralizing stages in the world's largest deposit of this type. In addition, recently released U-Pb and $^{40}\text{Ar}/^{39}\text{Ar}$ data for the Río Blanco supergiant porphyry copper deposit (Fig. 1) show that it developed episodically from 6.32 to 4.37 Ma; thus the two largest porphyry deposits in central Chile are essentially coeval within analytical uncertainty of the geochronologic methods (Deckart et al., 2003).

Conclusions

Combined isotopic dating methods indicate a succession of felsic intrusions in the El Teniente orebody. The oldest pulses are the mineralized quartz diorite-tonalite stocks in the eastern part of the system, which according to zircon U-Pb ages crystallized from 6.46 ± 0.11 to 6.11 ± 0.13 Ma. These stocks were emplaced within late Miocene country rocks, according to an apatite fission-track age of 8.9 ± 2.8 Ma from a basic sill, in agreement with the previous K-Ar age data (12.0 ± 0.7 – 6.6 ± 0.4 Ma) for volcanic rocks in the district (Cuadra 1986; Godoy and Köeppen, 1993).

A second pulse of quartz diorite-tonalite is inferred from an unaltered equigranular intrusion intercepted by drilling immediately southeast of the orebody, with magmatic biotite yielding plateau $^{40}\text{Ar}/^{39}\text{Ar}$ ages of 5.63 ± 0.12 and 5.47 ± 0.12 Ma. This intrusion is temporally related to the potassic alteration overprint that produced zircon overgrowths and inferred Pb loss between 5.67 ± 0.19 and 5.48 ± 0.19 Ma (U-Pb) in quartz diorite-tonalite stocks of the eastern part of the deposit. The overprint is further substantiated by the concordance of a plateau $^{40}\text{Ar}/^{39}\text{Ar}$ age of 5.69 ± 0.08 Ma that was obtained for coarse hydrothermal biotite and a molybdenite Re-Os age of 5.60 ± 0.02 Ma for mineralized breccia hosted by the Sewell stock in the easternmost part of the orebody.

The Teniente dacite porphyry represents a third composite, mineralized intrusive pulse, with earliest facies crystallizing at 5.28 ± 0.10 Ma according to a zircon U-Pb age. A fourth intrusive event gave rise to the mineralized dacite ring dikes encircling the Braden pipe, which crystallized at 4.82 ± 0.09 Ma according to a zircon U-Pb age. A fifth intrusive event appears to be represented by poorly mineralized barren late dacite intrusions and dikes, which have yielded a biotite $^{40}\text{Ar}/^{39}\text{Ar}$ plateau age of 4.58 ± 0.10 Ma and sericite $^{40}\text{Ar}/^{39}\text{Ar}$ plateau ages between 4.56 ± 0.12 and 4.46 ± 0.10 Ma.

Concurrent with the five intrusive events, ore deposition episodes are documented by molybdenite Re-Os ages of 6.30 ± 0.03 , 5.60 ± 0.02 , 5.01 to 4.96 , 4.89 ± 0.08 to 4.78 ± 0.03 , and 4.42 ± 0.02 Ma. The older mineralizing episodes are in overall agreement with the zircon $^{206}\text{Pb}/^{238}\text{U}$ ages for mineralized intrusive bodies. The oldest Re-Os molybdenite ages (6.31 ± 0.03 and 5.60 ± 0.02 Ma) were obtained exclusively in the easternmost portion of the orebody where they are

spatially and temporally related to the oldest intrusive rocks dated in the deposit. In contrast, the 4.89 ± 0.08 to 4.42 ± 0.02 Ma molybdenite Re-Os ages are from different parts of the orebody, suggesting that a more widespread, high-temperature fluid circulated throughout this supergiant Cu-Mo deposit. This is substantiated by $^{40}\text{Ar}/^{39}\text{Ar}$ plateau ages ranging from 5.06 ± 0.12 to 4.37 ± 0.10 Ma for biotite, sericite, and altered whole-rock samples collected throughout the orebody. Because of the susceptibility of mica to resetting, the $^{40}\text{Ar}/^{39}\text{Ar}$ system provides a record of only the latest high-temperature ($>350^\circ\text{C}$) fluid circulation events and, therefore, a partial developmental history for the entire ore-forming system.

The superimposition of ore depositional episodes may account for the extremely large volume and high hypogene grades at El Teniente. Successive intrusions and crystallization of felsic bodies were immediately followed by genetically related cycles of molybdenum sulfide deposition, each associated with concomitant hydrothermal alteration, stockwork development, and hydrothermal brecciation. Exceptionally large volumes of copper-rich hydrothermal fluid circulated episodically through ~ 7 km³ of rock to generate the world's largest Cu-Mo orebody. Strong thermal gradients related to small, shallow-level intrusions may have been important for rapid and efficient deposition of copper-bearing sulfides to create the high hypogene copper grades that characterize El Teniente. Petrographic evidence indicates that copper mineralization accompanied the molybdenite introduction events resolved by the Re-Os dating at El Teniente.

The preservation of older Re-Os molybdenite ages and their correlation with zircon U-Pb ages for intrusions indicates that the Re-Os system is resistant to resetting by high-temperature fluid in this large porphyry system and was not disturbed by episodic high-temperature fluid circulation that reset the $^{40}\text{Ar}/^{39}\text{Ar}$ systems of micas.

The three earliest ore depositional events (6.30 ± 0.03 , 5.60 ± 0.02 , 5.01 to 4.96 Ma) are associated with potassic alteration, whereas from 4.89 ± 0.08 to 4.78 ± 0.03 Ma both potassic and quartz-sericite alteration accompanied molybdenite deposition. The final ore depositional event at 4.42 ± 0.02 Ma appears to have been accompanied exclusively by quartz-sericite alteration. The superimposition of a number of potassic alteration events, substantiated by intertwined relationships between stockwork development and brecciation, contrasts with the traditional view of continuum from an early potassic stage followed immediately by development of quartz-sericite alteration. The multistage evolution inferred from our systematic dating study was not apparent from previous geochronologic data but is inferred to have contributed to the enormous volume and richness of the deposit.

The formation of the Braden pipe occurred as a single cataclysmic synmineralization event, probably related in time to the injection of the dacite ring dikes at 4.82 ± 0.09 Ma (zircon U-Pb age) that encircle it. Breccia pipe formation was followed by hydrothermal circulation within and peripheral to the breccia between 4.81 ± 0.12 and 4.37 ± 0.10 Ma, according to sericite $^{40}\text{Ar}/^{39}\text{Ar}$ ages. The effect of diatreme formation was probably a sudden decompression of the porphyry system, and this structure controlled further hydrothermal circulation along its shattered margins; it may also have

influenced further ore deposition and magma degassing. The quartz-sericitic alteration that immediately followed pipe formation appears to reflect changes of physicochemical conditions induced by the brecciation process.

The youngest molybdenite Re-Os ages of 4.42 ± 0.02 Ma represent a late ore depositional event temporally related to the youngest dacite intrusions underlying the Braden pipe, which yielded biotite and sericite $^{40}\text{Ar}/^{39}\text{Ar}$ plateau ages between 4.58 ± 0.10 and 4.46 ± 0.10 Ma. Sericite $^{40}\text{Ar}/^{39}\text{Ar}$ plateau ages of 4.57 ± 0.12 and 4.40 ± 0.10 Ma were also obtained from the Teniente dacite porphyry.

A postore hornblende-rich andesitic dike, with a hornblende $^{40}\text{Ar}/^{39}\text{Ar}$ age of 3.85 ± 0.18 Ma, cuts the southern portion of the orebody and marks the end of igneous activity within the deposit. An imprecise apatite fission-track age of 4.2 ± 5.6 Ma from the Teniente dacite porphyry combined with the track length distribution generated a thermal model that suggests that the porphyry system cooled exceedingly rapidly to below $105^\circ \pm 20^\circ\text{C}$ (apatite fission-track closure temperature). Fission-track data are compatible with <3 km of denudation since the late Miocene in the El Teniente district.

Acknowledgments

CONICYT, Chile, through Fondecyt 1000932 grant to V. Maksaev and F. Munizaga (Universidad de Chile), supported this geochronologic project at El Teniente. CODELCO-Chile funded the zircon SHRIMP U-Pb dating. Special thanks are due to Francisco Camus (Exploration Manager), Jorge Skármeta, and Miguel Hervé. We are particularly indebted to Patricio Zúñiga (Geology Manager, El Teniente) for granting access to the mine and drill core. The assistance, guidance, and helpful instruction in the mine by geologists Alejandra Arévalo, Ricardo Floody, José Seguel, Andrés Brzovic, Omar Quezada, and other personnel of CODELCO El Teniente Division are truly appreciated, yet the interpretation of the data remain the sole responsibility of the writers. Thorough reviews by Eric Seedorff and Alan Clark significantly improved the final manuscript.

REFERENCES

- Arredondo, C.S., 1994, Distribución, caracterización y génesis de los cuerpos de brecha ubicados en el sector central-este del yacimiento El Teniente: Unpublished B.Sc. thesis, Santiago, Universidad de Chile, 137 p.
- Atkinson, W.W., Jr., Souviron, A., Vehrs, T.I., and Faunes, A., 1996, Geology and mineral zoning of the Los Pelambres porphyry copper deposit, Chile: Society of Economic Geologists Special Publication 5, p. 131–155.
- Ballard, J.R., Michael-Palin, J., Williams, I.S., Campbell, I.H., and Faunes, A., 2001, Two ages of porphyry intrusion resolved for the super-giant Chuquicamata copper deposit of northern Chile by ELA-ICP-MS and SHRIMP: *Geology*, v. 29, p. 383–386.
- Bertens, A., Deckart, K., and Gonzalez, A., 2003, Geocronología U-Pb, Re-Os y $^{40}\text{Ar}/^{39}\text{Ar}$ del pórfido Cu-Mo Los Pelambres, Chile central: Congreso Geológico Chileno, 10th, Concepción, 2003, CD-ROM, 5 p.
- Bissig, T., Clark, A.H., Lee, J.K.W., and Heather, K.B., 2001, The Neogene history of volcanism and hydrothermal alteration in the central Andean flat-slab region: New $^{40}\text{Ar}/^{39}\text{Ar}$ constraints from the El Indio-Pascua Au (Ag, Cu) belt, III/IV region, Chile, provincia San Juan, Argentina: *International Geology Review*, v. 43, p. 312–340.
- Bissig, T., Clark, A.H., Lee, J.K.W., and Hogson, J., 2002, Miocene landscape evolution and geomorphologic controls on epithermal processes in the El Indio-Pasuca Au-Ag-Cu belt, Chile and Argentina: *Economic Geology*, v. 97, p. 971–996.
- Camus, F., 1975, Geology of the El Teniente orebody with emphasis on wall-rock alteration: *Economic Geology*, v. 70, p. 1342–1372.
- 2003, Geología de los sistemas porfíricos en los Andes de Chile: Santiago, Chile, Servicio Nacional de Geología y Minería, 267 p.
- Cannell, J., Cooke, D.R., Stein, H.J., and Markey, R., 2003, New paragenetically constrained Re-Os molybdenite ages for El Teniente Cu-Mo porphyry deposit, central Chile: Biennial Society for Geology Applied to Mineral Deposits Meeting, Athens, 2003, 7th, Proceedings, v. 1, p. 255–258.
- Cathles, L.M., Erendi, A.H.J., Thayer, J.B., and Barrie, T., 1997, How long can a hydrothermal system be sustained by a single intrusion event?: *Economic Geology*, v. 92, p. 766–771.
- Charrier, R., and Munizaga, F., 1979, Edades K-Ar de volcanitas cenozoicas del sector cordillerano del río Cachapoal, Chile ($34^\circ 15'$ Lat. S): *Revista Geológica de Chile*, no. 7, p. 41–51.
- Charrier, R., Baeza, O., Elgueta, S., Flynn, J.J., Gans, P., Kay, S.M., Muñoz, N., Wyss, A.R., and Zurita, E., 2002, Evidence for Cenozoic extensional basin development and tectonic inversion south of the flat-slab segment, southern Central Andes, Chile ($33^\circ\text{--}36^\circ\text{S.L.}$): *Journal of South American Earth Sciences*, v. 15, p. 117–139.
- Cherniak, D.J., and Watson, E.B., 2000, Pb diffusion in zircon: *Chemical Geology*, v. 172, p. 5–24.
- Chesley, J.T., 1999, Integrative geochronology of ore deposits: New insights into the duration and timing of hydrothermal circulation: *Reviews in Economic Geology*, v. 12, p. 115–141.
- Clark, A.H., 1993, Are outsized porphyry copper deposits either anatomically or environmentally distinctive?: Society of Economic Geologists Special Publication 2, p. 213–283.
- Clark, A.H., Farrar, E., Camus, F., and Quirt, G.S., 1983, K-Ar data for El Teniente porphyry copper deposit, central Chile: *Economic Geology*, v. 78, p. 1003–1006.
- Cocherie, A., Rossi, P., Fanning, C.M., and Deloule, E., 2002, Accretion and splitting within the Permian Pangea recorded by episodic metamorphic zircon growth [abs.]: *Geochimica et Cosmochimica Acta*, v. 66, Special Supplement S1, p. A146.
- Compston, W., Williams, I.S., Kirschvink, J.L., Zhang Zichao, and Ma Gougan, 1992, Zircon U-Pb dates for the Early Cambrian time-scale: *Journal of the Geological Society [London]*, v. 149, p. 171–184.
- Corfu, F., and Davis, D.W., 1991, Comment on “Archean hydrothermal zircon in the Abitibi greenstone belt: Constraints on the timing of gold mineralization” by J.C. Clauoué-Long, R.W. King, and R. Kerrich: *Earth and Planetary Science Letters*, v. 104, p. 545–552.
- Corfu, F., Hanchar, J.M., Hoskin, P.W.O., and Kinny, P., 2003, Atlas of zircon textures: *Reviews in Mineralogy and Geochemistry*, v. 53, p. 469–500.
- Cuadra, P., 1986, Geocronología K-Ar del yacimiento El Teniente y áreas adyacentes: *Revista Geológica de Chile*, no. 27, p. 3–26.
- Davidson, J., and Mpodozis, C., 1991, Regional geologic setting of epithermal gold deposits, Chile: *Economic Geology*, v. 86, p. 1174–1186.
- Davis, D.W., and Krogh, T.E., 2000, Preferential dissolution of ^{234}U and radiogenic Pb from α -recoil-damaged lattice sites in zircon: Implications for thermal histories and Pb isotopic fractionation in the near surface environment: *Chemical Geology*, v. 172, p. 41–58.
- Deckart, K., Clark, A.H., Aguilar, C., Vargas, R., Serrano, L., and Ortega, H., 2003, Geochronology of the Río Blanco porphyry Cu(-Mo) deposit, Principal Cordillera, central Chile ($33^\circ 08'\text{S}$) [abs.]: Congreso Geológico Chileno, 10th, Concepción, 2003, CD-ROM, 1 p.
- Faunes, A., 1981, Caracterización de la mineralogía y de alteración en un sector del stock tonalítico del yacimiento El Teniente: Unpublished B.Sc. thesis, Santiago, Universidad de Chile, 175 p.
- Fournier, R.O., 1999, Hydrothermal processes related to movement of fluid from plastic into brittle rock in the magmatic-epithermal environment: *Economic Geology*, v. 94, p. 1193–1212.
- Frei, R., Nagler, T., Schonberg, R., and Kramers, J., 1998, Re-Os, Sm-Nd, U-Pb, and stepwise lead leaching isotope systematics in shear zone hosted gold mineralization: Genetic tracing and age constraints of crustal hydrothermal activity: *Geochimica et Cosmochimica Acta*, v. 62, p. 1925–1936.
- Freydier, C., Ruiz, J., Chesley, J., McCandless, T., and Munizaga, F., 1997, Re-Os isotope systematics of sulfides from felsic igneous rocks: Application to base metal porphyry mineralization in Chile: *Geology*, v. 25, p. 775–778.
- Geisler, T., Ulonska, M., Schleicher, H., Pidgeon, R.T., and Van Bronswijk, W., 2001, Leaching and differential recrystallization of metamict zircon under experimental hydrothermal conditions: *Contributions to Mineralogy and Petrology*, v. 141, p. 53–65.
- Godoy, E., and Köppen, R., 1993, Geología del área entre los ríos Claro del Maipo y Cachapoal, Informe Final: Santiago, CODELCO-SERNA-GEOMIN, unpublished report, 68 p.

- Gröpper, H., Calvo, M., Crespo, H., Bisso, C.R., Cuadra, W.A., Dunkerley, P.M., and Aguirre, E., 1991, The epithermal gold-silver deposit of Choque-limpie, northern Chile: *Economic Geology*, v. 86, p. 1206–1221.
- Gustafson, L.B., and Hunt, J.P., 1975, The porphyry copper deposit at El Salvador, Chile: *Economic Geology*, v. 70, p. 857–912.
- Guzmán, C., 1991, Alteración y mineralización de los pórfidos dioríticos del sector central, yacimiento El Teniente: Unpublished B.Sc. thesis, Santiago, Universidad de Chile, 145 p.
- Hemley, J.J., Cygan, G.L., Fein, J.B., Robinson, G.R., and D'Angelo, W.M., 1992, Hydrothermal ore-forming processes in the light of studies in rock-buffered systems: I. Iron-copper-zinc-lead sulfide solubility relations: *Economic Geology*, v. 87, p. 1–22.
- Hernández, E., Letelier, C., Letelier, O., Mestre, A., and Portigliati, C., 1980, Geología, distribución y cálculo de reservas de molibdeno en El Teniente: Anales del Congreso del Cincuentenario 1930–1980, Minería de cobres porfíricos: Santiago, Chile, Instituto de Ingenieros de Minas, v. 2, p. 364–383.
- Hoskin, P.W.O., and Schaltegger, U., 2003, The composition of zircons and igneous and metamorphic petrogenesis: *Reviews in Mineralogy and Geochemistry*, v. 53, p. 27–62.
- Howell, F.H., and Molloy, J.S., 1960, Geology of the Braden orebody, Chile, South America: *Economic Geology*, v. 55, p. 863–905.
- Hurford, A.J., and Carter, A., 1991, The role of fission track dating in discrimination of provenance: *Geological Society [London], Special Publication* 57, p. 67–78.
- Ip, L., 1987a, Estudio de inclusiones fluidas en vetillas de la etapa hidrotermal temprana e hidrotermal principal del sector nor-oeste del yacimiento El Teniente: Unpublished B.Sc. thesis, Santiago, Universidad de Chile, 120 p.
- 1987b, Estudio de inclusiones fluidas en vetillas tempranas del sector noroeste del yacimiento "El Teniente": *Comunicaciones [Universidad de Chile]*, no. 38, p. 27–45.
- Kaulina, T.V., 2002, Metasomatic alteration of zircons from potassic granites [abs.]: *Geochimica et Cosmochimica Acta*, v. 66, Special Supplement S1, p. A387.
- Kay, S.M., and Kurtz, A.C., 1995, Magmatic and tectonic characterization of El Teniente region., Santiago, CODELCO-Chile, unpublished report to División El Teniente, 180 p.
- Kosler, J., Simonetti, A., Sylvester, P.J., Cox, R.A., Tubrett, M.N., and Wilton, D.H.C., 2003, Laser-ablation ICP-MS measurements of Re/Os in molybdenite and implications for Re-Os geochronology: *Canadian Mineralogist*, v. 41, p. 307–320.
- Kusakabe, M., Nakagawa, S., Hori, M., Matsuhita, Y., Ojeda, J., and Serrano, L., 1984, Oxygen and sulfur isotopic compositions of quartz, anhydrite, and sulfide minerals from El Teniente and Río Blanco porphyry copper deposits, Chile: *Bulletin of Geological Survey of Japan*, v. 35, no. 11, p. 583–614.
- Kusakabe, M., Hori, M., and Matsuhita, Y., 1990, Primary mineralization-alteration of the El Teniente and Río Blanco porphyry copper deposits, Chile. Stable isotopes, fluid inclusions, and $Mg^{2+}/Fe^{2+}/Fe^{3+}$ ratios of hydrothermal biotite: Perth, University of Western Australia Press Publication 23, p. 244–259.
- Lindgren, W., and Bastin, E.S., 1922, Geology of the Braden mine, Rancagua, Chile: *Economic Geology*, v. 17, p. 75–99.
- Maksaev, V., Munizaga, F., McWilliams, M., Thiele, K., Arévalo, A., Zúñiga, P., and Floody, R., 2001, $^{40}Ar/^{39}Ar$ geochronology of the El Teniente porphyry copper deposit [ext. abs.]: *South American Symposium on Isotope Geology*, 3rd, Santiago, Sociedad Geológica de Chile, Extended Abstract Volume (CD-ROM), p. 496–499.
- Maksaev, V., Munizaga, F., McWilliams, M., Fanning, M., Mathur, R., Ruiz, J., and Thiele, K., 2002, El Teniente porphyry copper deposit in the Chilean Andes: New geochronological time frame and duration of hydrothermal activity [abs.]: *Geological Society of America Abstracts with Programs*, v. 34, no. 6, p. 336.
- Marsh, T.M., Einaudi, M.T., and McWilliams, M., 1997, $^{40}Ar/^{39}Ar$ geochronology of Cu-Au and Au-Ag mineralization in the Potrerillos district, Chile: *Economic Geology*, v. 92, p. 784–806.
- Mathur, R., Ruiz, J., and Munizaga, F., 2001, Insights into Andean metallogenesis from the perspective of Re-Os analyses of sulfides: *South American Symposium on Isotope Geology*, 3rd, Santiago, Sociedad Geológica de Chile, Extended Abstract Volume (CD-ROM), p. 500–503.
- McCandless, T.E., Ruiz, J., and Campbell, A.R., 1993, Rhenium behavior in molybdenite in hypogene and near-surface environments: Implications for Re-Os geochronometry: *Geochimica et Cosmochimica Acta*, v. 57, p. 889–905.
- McKee, E.H., Robinson, A.C., Rytuba, J.J., Cuitiño, L., and Moscoso, R., 1994, Age and Sr isotopic composition of volcanic rocks in the Maricunga belt, Chile: Implications for magma sources: *Journal of South American Earth Sciences*, v. 7, p. 167–177.
- Miranda, C.E., 2002, Comparación química de biotitas de intrusivos mineralizados y no mineralizados pertenecientes a la franja del Mioceno de los Andes de Chile central: Unpublished B.Sc. thesis, Santiago, Universidad de Chile, 60 p.
- Morales, A., 1997, Geología y geotecnia del sector norte del Proyecto Esmeralda, División El Teniente: *Congreso Geológico Chileno*, 7th, Concepción, 1997, Actas, v. 2, p. 1068–1072.
- Moscoso, R., Maksaev, V., Cuitiño, L., Díaz, F., Köeppen, R.P., Tosdal, R.M., Cunningham, C.G., McKee, E.H., and Rytuba, J.J., 1993, El complejo volcánico Cerros Bravos, región de Maricunga, Chile: Geología, alteración hidrotermal y mineralización, in *Investigaciones de metales preciosos en el complejo volcánico Neógeno-Cuaternario de los Andes centrales: Bolivia, GEOBOL, SERNAGEOMIN, INGEMMET, USGS*, p. 131–165.
- Muntean, J.L., and Einaudi, M.T., 2001, Porphyry-epithermal transition: Maricunga belt, northern Chile: *Economic Geology*, v. 96, p. 743–772.
- Ortega, V.H., 1981, Geología de la chimenea Braden y su relación con el yacimiento El Teniente, Chile: Unpublished B.Sc. thesis, Antofagasta, Universidad Católica del Norte, 137 p.
- Ossandón, G., 1974, Petrografía y alteración del pórfido dacítico, yacimiento El Teniente: Unpublished B.Sc. thesis, Santiago, Universidad de Chile, 116 p.
- Ossandón, G., Fréaut, R., Gustafson, L.B., Lindsay, D.D., and Zentilli, M., 2001, Geology of the Chuquicamata mine: A progress report: *Economic Geology*, v. 96, p. 249–270.
- Padilla, R., Titley, S.R., and Pimentel, F., 2001, Geology of the Escondida porphyry copper deposit, Antofagasta region, Chile: *Economic Geology*, v. 96, p. 307–324.
- Parry, W.T., Wilson, P.N., Moser, D., and Heizler, M.T., 2001, U-Pb dating of zircon and $^{40}Ar/^{39}Ar$ dating of biotite at Bingham, Utah: *Economic Geology*, v. 96, p. 1671–1684.
- Phillips, W.J., 1973, Mechanical effects of retrograde boiling and its probable importance in the formation of some porphyry ore deposits: *Transactions of the Institution of Mining and Metallurgy Transactions*, v. 81, p. B90–B98.
- Rabbia, O., 2002, Cristalografía de rutilo y anatasa en sistemas de pórfidos cupríferos andinos: evaluación de su uso como monitores de la actividad de metales en fluidos hidrotermales corticales: Unpublished Ph.D. thesis, Santiago, Universidad de Chile, 147 p.
- Reich, M., 2001, Estudio petrográfico, mineraloquímico y geoquímico de los cuerpos intrusivos de Sewell y La Huifa, Yacimiento El Teniente, VI Región, Chile: Unpublished B.Sc. thesis, Concepción, Universidad de Concepción, 124 p.
- Reynolds, P., Ravenhurst, C., Zentilli, M., and Lindsay, D., 1998, High-precision $^{40}Ar/^{39}Ar$ dating of two consecutive hydrothermal events in the Chuquicamata porphyry copper system, Chile: *Chemical Geology*, v. 148, p. 45–60.
- Richards, J.P., Noble, S.R., and Pringle, M., 1999, A revised late Eocene age for porphyry Cu magmatism in the Escondida area, northern Chile: *Economic Geology*, v. 94, p. 1231–1248.
- Rivano, S., Godoy, E., Vergara, M., and Villarreal, R., 1990, Redefinición de la Formación Farellones en la Cordillera de los Andes de Chile Central (32°–34°S): *Revista Geológica de Chile*, v. 17, p. 205–214.
- Riveros, M., 1991, Geología del pórfido latítico del sector sur del yacimiento El Teniente: Unpublished B.Sc. thesis, Santiago, Universidad de Chile, 140 p.
- Rojas, A., 2002, Petrografía y geoquímica del pórfido dacítico Teniente, yacimiento El Teniente, Provincia Cachapoal, VI región, Chile: Unpublished B.Sc. thesis, Concepción, Universidad de Concepción, 118 p.
- Rubin, J.N., Henry, C.D., and Price, J.G., 1989, Hydrothermal zircons and zircon overgrowths, Sierra Blanca Peaks, Texas: *American Mineralogist*, v. 74, p. 865–869.
- Salazar, M.A., 2003, Aspectos geológicos en los modelos de dilución mina Esmeralda, yacimiento El Teniente, VI Región, Chile: Unpublished M.Sc. thesis, Santiago, Universidad de Chile, 136 p.
- Selby, D., and Creaser, R.A., 2001, Re-Os geochronology and systematics in molybdenite from the Endako porphyry molybdenum deposit, British Columbia, Canada: *Economic Geology*, v. 96, p. 197–204.

- Serrano, L., Vargas, R., Stambuk, V., Aguilar, C., Galeb, M., Holgrem, C., Contreras, A., Godoy, S., Vela, I., Skewes, M.A., and Stern, C.R., 1996, The late Miocene Río Blanco-Los Bronces copper deposit, central Chilean Andes: Society of Economic Geologists Special Publication 5, p. 119–130.
- Shirley, S., and Walker, R., 1995, Carius tube digestion for low blank rhenium-osmium analysis: Analytical Chemistry, v. 67, p. 2136–2141.
- Sillitoe, R.H., 1985, Ore-related breccias in volcanoplutonic arcs: Economic Geology, v. 80, p. 1467–1514.
- 1991, Gold metallogeny of Chile—an introduction: Economic Geology, v. 86, p. 1187–1205.
- Sillitoe, R.H., McKee, E.H., and Vila, T., 1991, Reconnaissance K-Ar geochronology of the Mariungta gold-silver belt, northern Chile: Economic Geology, v. 86, p. 1261–1270.
- Skewes, M.A., and Arévalo, A., 1997, “Andesitas de la Mina” El Teniente: Congreso Geológico Chileno, 8th, Antofagasta, 1997, Actas, v. 2, p. 1162–1164.
- 2000, El complejo de gabros y diabasas que hospeda a las brechas mineralizadas del depósito de cobre El Teniente, Chile central: Congreso Geológico Chileno, 9th, Puerto Varas, Actas, v. 1, p. 380–384.
- Skewes, M.A., and Stern, C.R., 1995, Genesis of the giant late Miocene to Pliocene copper deposits of central Chile in the context of Andean magmatic and tectonic evolution: International Geology Review, v. 37, p. 893–909.
- Skewes, M.A., Arévalo, A., Holgrem, C., and Stern, C.R., 2001, Stable isotope evidence for formation from magmatic fluids of the mineralized breccias in the Los Bronces and El Teniente copper deposits, central Chile: South American Symposium on Isotope Geology, 3rd, Santiago, Sociedad Geológica de Chile, Extended Abstract Volume (CD-ROM), p. 531–534.
- Skewes, M.A., Arévalo, A., Floody, R., Zúñiga, P., and Stern, C.R., 2002, The giant El Teniente breccia deposit: Hypogene copper distribution and emplacement: Society of Economic Geologists Special Publication 9, p. 299–332.
- Smoliar, M.I., Walker, R.J., and Morgan, J.W., 1996, Re-Os ages of group IIA, IIIA, IVA and IVB iron meteorites: Science, v. 271, p. 1099–1102.
- Stein, H.J., Markey, R.J., Morgan, J.W., Hannah, J.L., and Scherstén, A., 2001, The remarkable Re-Os geochronometer in molybdenite: How and why it works: Terra Nova, v. 13, p. 479–486.
- Stein, H.J., Sillitoe, R.H., and Perelló, J., 2002, Discerning the lifespan of a giant porphyry Cu deposit: Re-Os dating at Los Pelambres, Chile [abs.]: Geochimica et Cosmochimica Acta, v. 66, Special Supplement S1, p. A738.
- Strecheisen, A., 1976, To each plutonic rock its proper name: Earth Science Reviews, v. 12, p. 1–33.
- Suzuki, K., Kagi, H., Nara, M., Tacaño, B., and Nozaki, Y., 2000, Experimental alteration in molybdenite: Evaluation of the Re-Os system, infrared spectroscopic profile and polytype: Geochimica et Cosmochimica Acta, v. 64, p. 223–232.
- Tera, F., and Wasserburg, G.J., 1972, U-Th-Pb systematics in three Apollo 14 basalts and the problem of initial Pb in lunar rocks: Earth and Planetary Science Letters, v. 14, p. 281–304.
- Thiele, R., 1980, Hoja Santiago, Región Metropolitana: Instituto de Investigaciones Geológicas, Carta Geológica de Chile 39, 51 p.
- Ulrich, T., and Heinrich, C.A., 2001, Geology and alteration geochemistry of the porphyry Cu-Au deposit at Bajo de la Alumbrera, Argentina: Economic Geology, v. 96, p. 1719–1742.
- Valenzuela, R., 2003, Mineralización sulfurada hipógena de cobre en el sector central del yacimiento El Teniente, VI región: Unpublished B.Sc. thesis, Concepción, Universidad de Concepción, 118 p.
- Vega, E., 2004, Estudio geológico de la chimenea Braden y su relación con el yacimiento de cobre-molibdeno El Teniente, VI región de Chile: Unpublished M.Sc. thesis, Santiago, Universidad de Chile, 140 p.
- Vega, E., and Maksaev, V., 2003, La chimenea Braden: Nuevos antecedentes geológicos y geocronológicos: Congreso Geológico Chileno, 10th, Concepción, 2003, CD-ROM, 6 p.
- Villalobos, J., 1975, Alteración hidrotermal en las andesitas del yacimiento El Teniente, Chile: Unpublished Ph.D. thesis, Santiago, Universidad de Chile, 125 p.
- Zentilli, M., Krogh, T., Maksaev, V., and Alpers, C., 1994, Uranium-lead dating of zircons from the Chuquicamata and La Escondida porphyry copper deposits, Chile: Inherited zircon cores of Paleozoic age with Tertiary overgrowths: Comunicaciones [Universidad de Chile], no. 45, p. 101–110.
- Zúñiga, P., 1982, Alteración y mineralización en el sector oeste del yacimiento El Teniente: Unpublished B.Sc. thesis, Santiago, Universidad de Chile, 104 p.

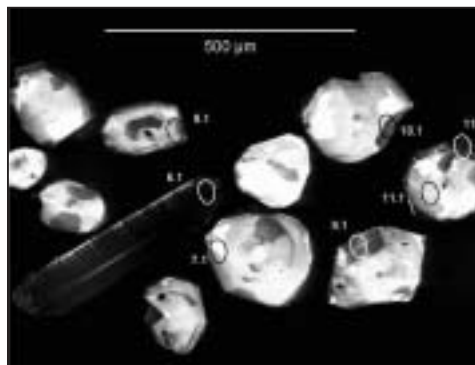
APPENDIX 1

Petrographic Descriptions of U-Pb Dated Samples and Cathodoluminescence Images of Zircon Crystals

TT-150. A *porphyry*, from drill core DDH 1337, 384 m. Small, vertical, fine-grained gray porphyritic mineralized stock that intrudes the Sewell stock in the southeastern part of the deposit. Next to its contacts contains abundant equigranular tonalite inclusions; the stock is surrounded by breccias with matrices of anhydrite, biotite, and Cu and Mo sulfides. At the mined levels, the stock has pervasive quartz-sericite alteration, but in the sampled drill core intense potassic alteration occurs.

Microscopic: Quartz diorite with partially destroyed porphyritic texture by intense potassic alteration; plagioclase phenocrysts (20%) up to 2 mm long within a groundmass composed of a microcrystalline aggregate of plagioclase and quartz, with abundant hydrothermal anhydrite, quartz, chalcopyrite, and chloritized biotite. Some plagioclase crystals are altered to sericite and smectite.

Zircon crystals with minor hydrothermal overgrowths with high content of U and Th.

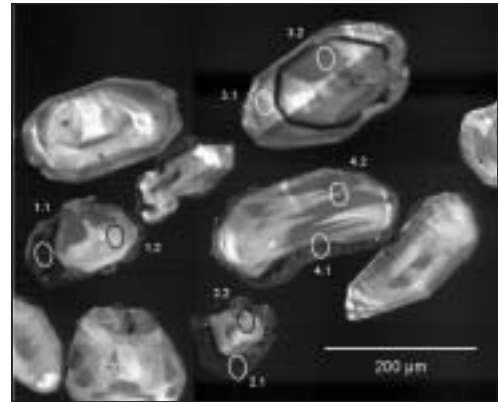


APPENDIX 1 (Cont.)

TT-101. *Sewell stock*, from Teniente 4 level, 2,347 m, northing: -265S/easting: 1365E. The largest stock that intrudes the biotitized host rocks in the southeastern part of the orebody. It shows pervasive quartz-sericite alteration and chalcopryite-dominated stockwork mineralization at the exploitation levels. The stock had also a carapace breccia with tourmaline matrix at the already exploited higher levels; the stockwork decreases in intensity and the Cu grades decline at depth, and the alteration changes to potassic.

Microscopic: Quartz diorite, porphyritic but almost hypidionomorphic granular texture, composed mainly of subhedral plagioclase 1 to 3 mm long, with varied intensity of sericite and calcite replacements, interstitial quartz, and minor K-feldspar. Potassic alteration with fine-grained hydrothermal biotite, anhydrite, and chalcopryite disseminations; strong overprint of quartz-sericite and calcite alteration. Quartz-anhydrite-chalcopryite veins.

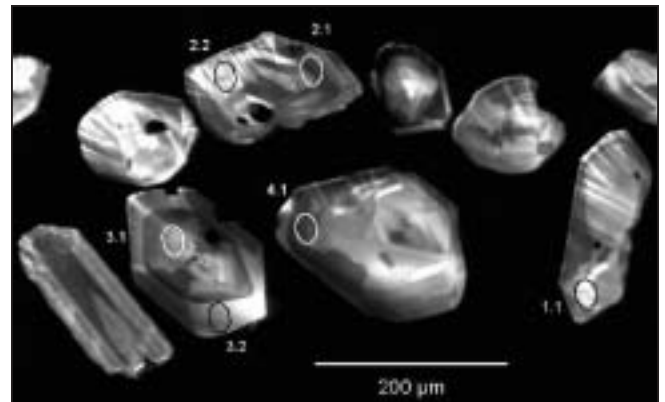
Zircon crystals with hydrothermal overgrowths that contain one order of magnitude higher U and Th contents.



TT-90. *Central quartz diorite-tonalite*, from UCL Esmeralda level, 2,192 m, northing: 250N/easting: 1,325E. Stock in the central part of the deposit; it shows pervasive quartz-sericite alteration at the exploitation levels and chalcopryite-dominated stockwork mineralization.

Microscopic: Intensely altered porphyritic rock to quartz-sericite; most of the original texture and composition are obliterated, but faint plagioclase phenocrysts and relict biotite occur within a microcrystalline quartz-sericite groundmass. Abundant anhydrite, chalcopryite and pyrite, and minor tourmaline. Anhydrite and calcite veins.

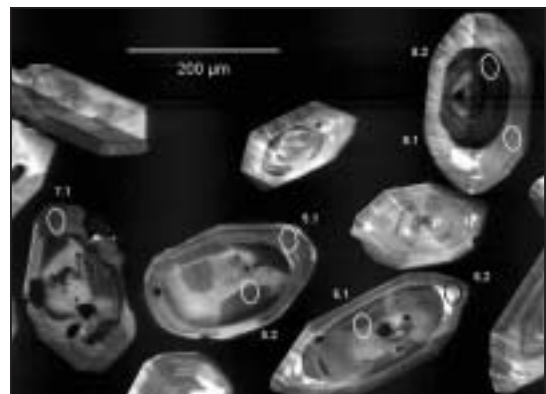
Zircons crystals without overgrowths.



TT-102. *Northern quartz diorite-tonalite*, from Teniente 6 UCL level, 2,161 m, northing: 1016N/easting: 1110E. Northernmost quartz diorite-tonalite stock in the eastern part of the orebody. It shows intense quartz-sericite alteration and rich chalcopryite-dominated stockwork mineralization.

Microscopic: Strongly altered rock to quartz-sericite but recognizable porphyritic texture and quartz phenocrysts (10%). Most of the rock is formed by a quartz-sericite-chlorite-anhydrite-chalcopryite aggregate. Anhydrite-chalcopryite veins.

Zircons crystals with older inherited cores and minor thin hydrothermal overgrowths with high U and Th contents.

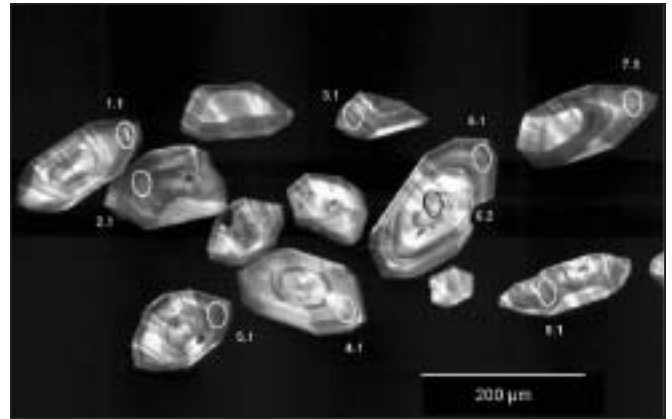


APPENDIX 1 (Cont.)

TT-94. *Teniente dacite porphyry*, from Teniente 6 level, 2,161 m, northing: 1050N/easting: 450E. North-south-trending intrusion in the northern part of the orebody. It shows dominant potassic alteration and bornite-chalcopyrite-dominated stockwork mineralization.

Microscopic: Porphyritic texture, plagioclase phenocrysts (60%) up to 4 mm long with incipient sericite and calcite replacements, biotite phenocrysts (10%) 2 to 3 mm long, some altered to chlorite, calcite, and white mica, minor perthitic K-feldspar and quartz. Aplitic groundmass with dissemination of anhydrite, chalcopyrite, and fine-grained hydrothermal biotite.

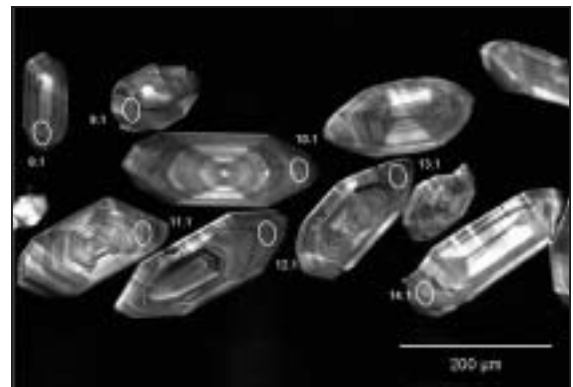
Zoned magmatic zircon crystals.



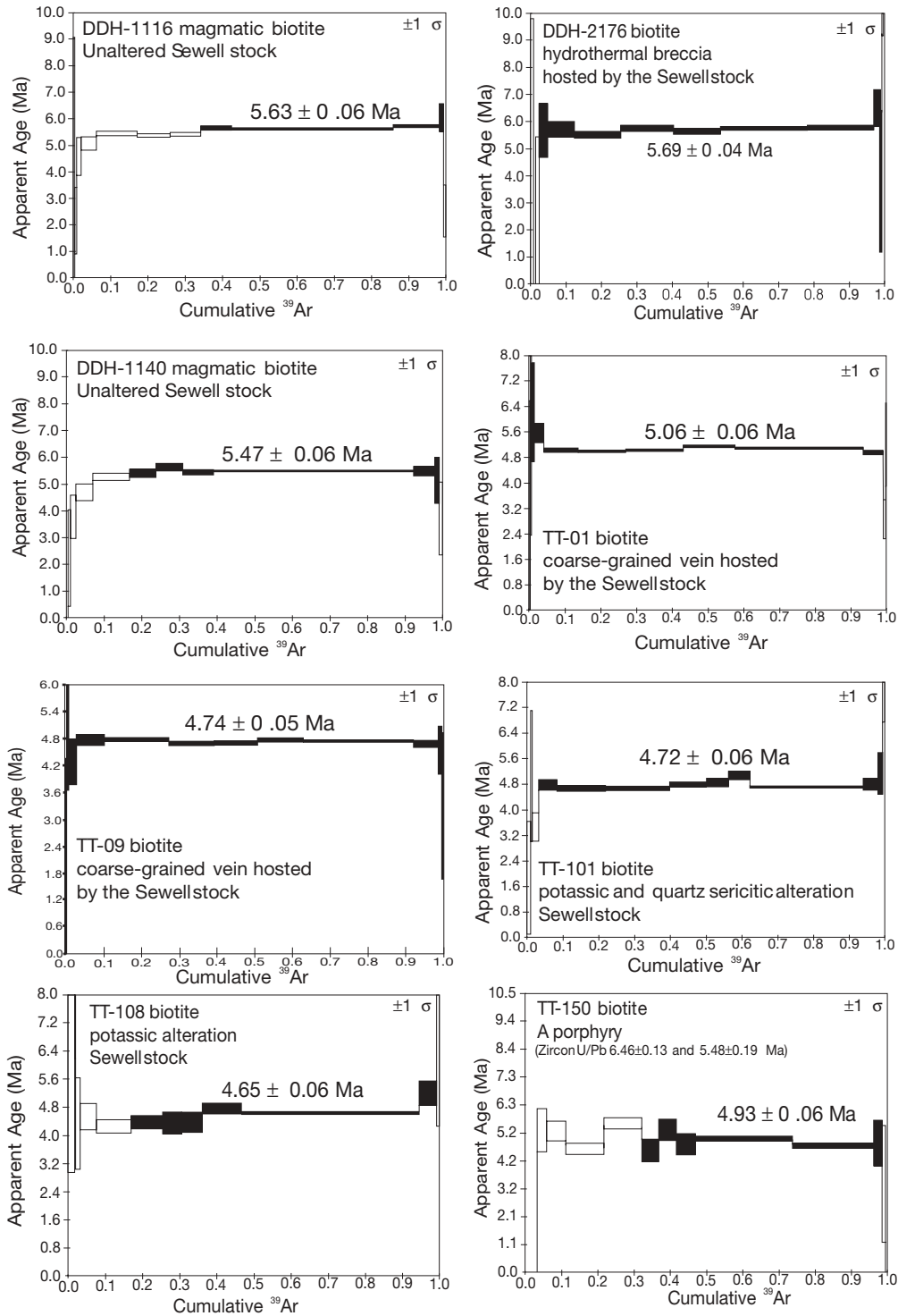
TT-91. *Dacite dike*, from UCL Esmeralda level, 2,192 m, northing: 310N/easting: 1030E. Ring dike that surrounds the Braden pipe along its eastern side; it shows pervasive quartz-sericite alteration and chalcopyrite-dominated stockwork mineralization.

Microscopic: Porphyritic texture, zoned plagioclase phenocrysts (30%) up to 4 mm long, fragmented and with partial sericitization on their borders, biotite phenocrysts mostly transformed to white mica and chlorite, and minor sericitized K-feldspar phenocrysts. Microcrystalline groundmass composed of sericitized plagioclase and replaced by calcite, chlorite, and smectite. Disseminated anhydrite, chalcopyrite and pyrite, and minor tourmaline.

Zoned magmatic zircon crystals.

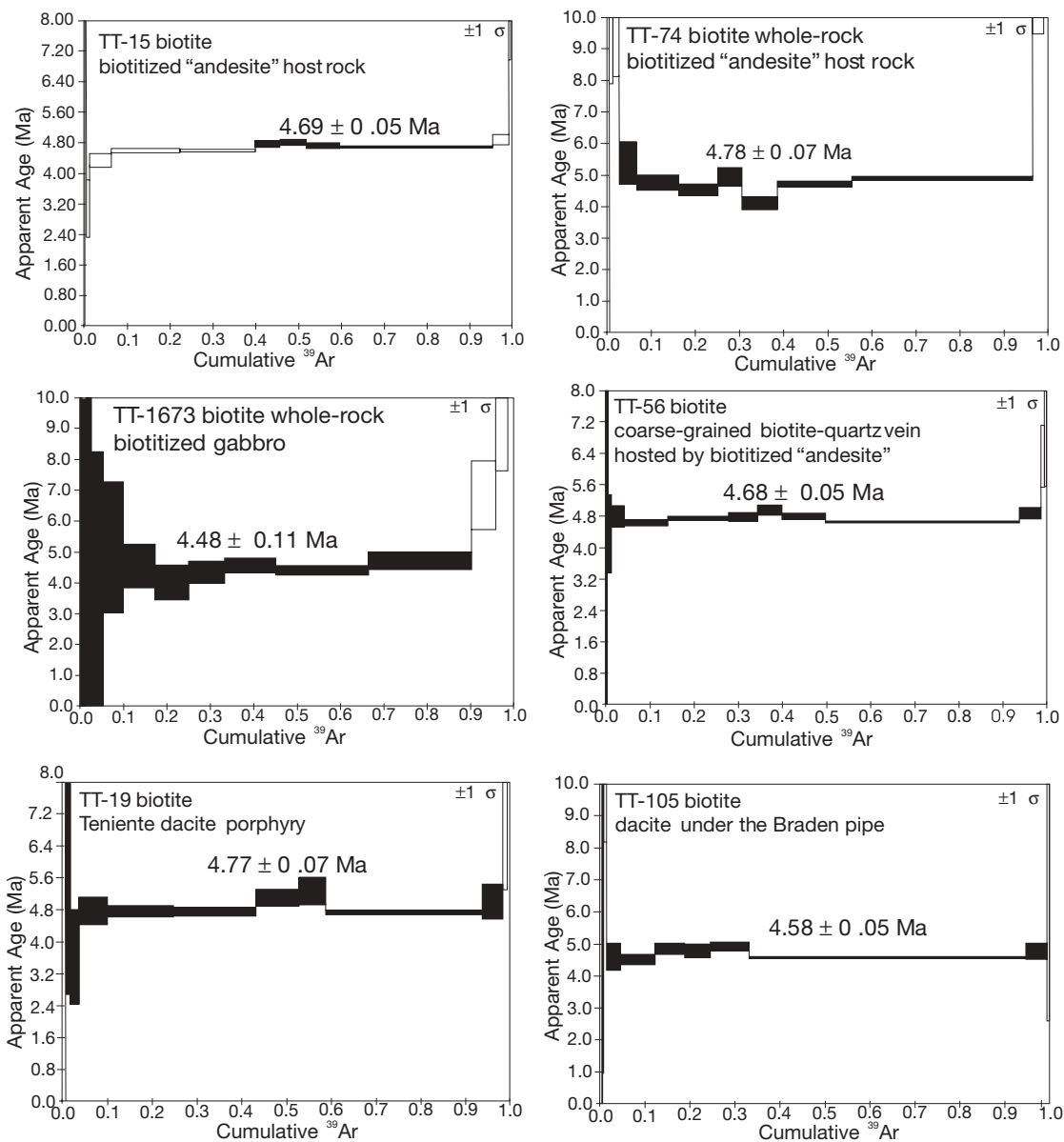


APPENDIX 2



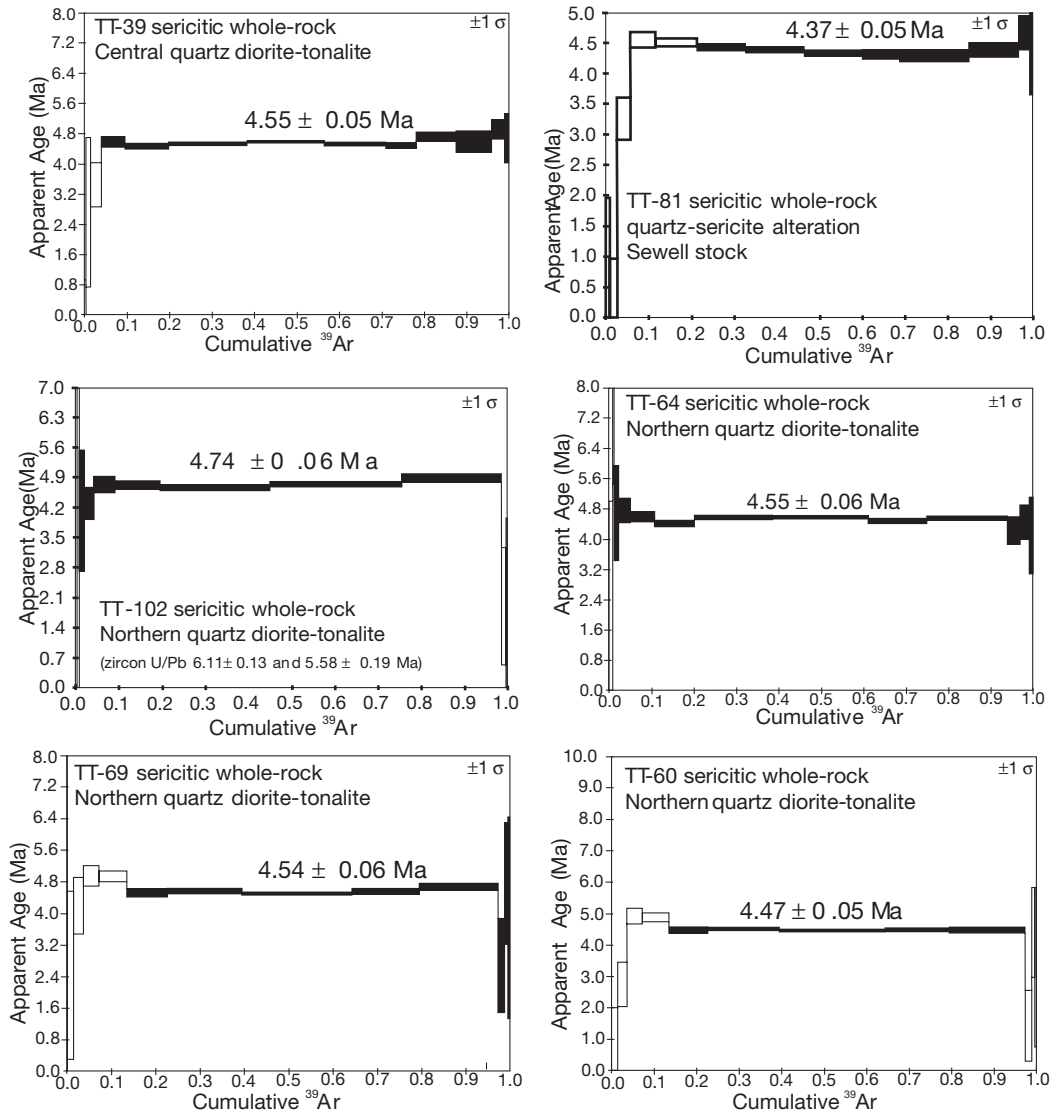
Appendix 2.1. Apparent $^{40}\text{Ar}/^{39}\text{Ar}$ Age Spectra ($\pm 1\sigma$) of Biotite Samples from the Sewell Stock and the A Porphyry (plateau $^{40}\text{Ar}/^{39}\text{Ar}$ ages ($\pm 1\sigma$) are shown)

APPENDIX 2 (Cont.)



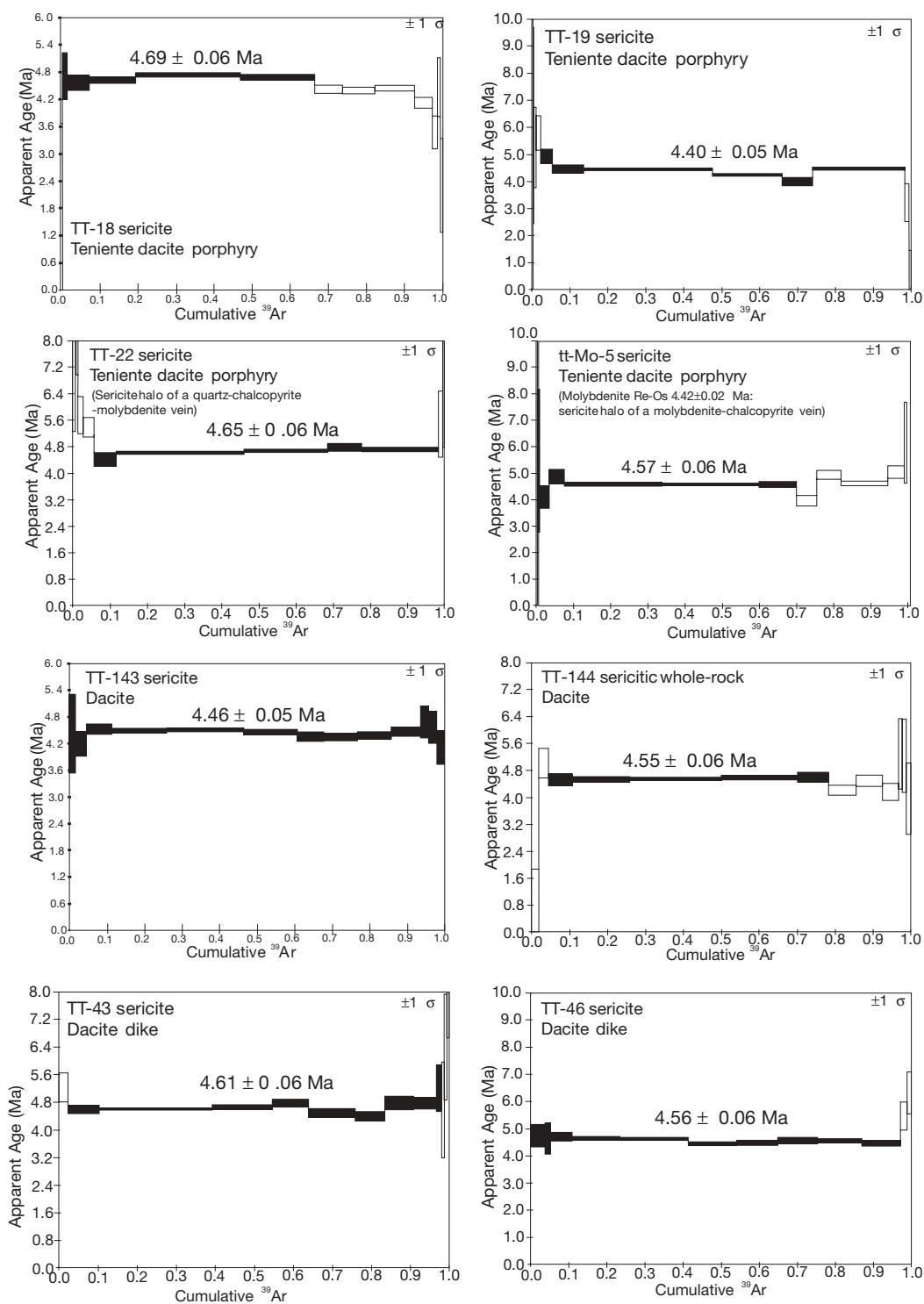
Appendix 2.2 Apparent $^{40}\text{Ar}/^{39}\text{Ar}$ Age Spectra ($\pm 1\sigma$) for Biotite and Biotitic Whole-Rock Samples from the Altered Andesite of the Mine Host Rocks, Including Biotitized Gabbro, Teniente Dacite Porphyry, and a Dacite under the Braden Pipe (plateau $^{40}\text{Ar}/^{39}\text{Ar}$ ages ($\pm 1\sigma$) are shown)

APPENDIX 2 (Cont.)



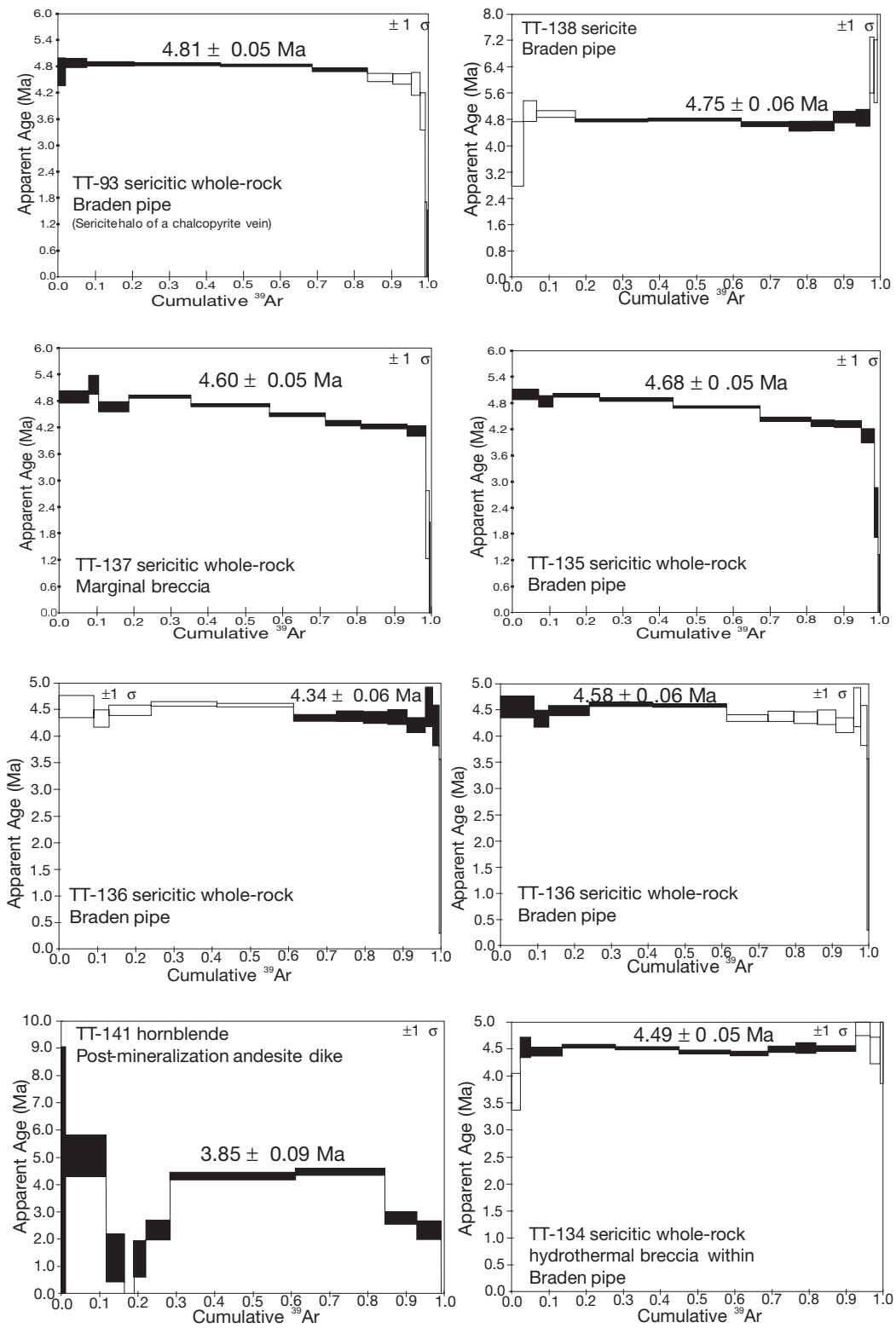
Appendix 2.3. Apparent $^{40}\text{Ar}/^{39}\text{Ar}$ Age Spectra ($\pm 1\sigma$) for Sericitic Whole-Rock Samples of the Central Quartz Diorite-Tonalite, Sewell Stock, and Northern Quartz Diorite-Tonalite (plateau $^{40}\text{Ar}/^{39}\text{Ar}$ ages ($\pm 1\sigma$) are shown)

APPENDIX 2 (Cont.)



Appendix 2.4. Apparent $^{40}\text{Ar}/^{39}\text{Ar}$ Age Spectra ($\pm 1\sigma$) for Sericite and Sericitic Whole-Rock Samples from the Teniente Dacite Porphyry and the Dacite Dikes and Other Dacite Intrusions (plateau $^{40}\text{Ar}/^{39}\text{Ar}$ ages ($\pm 1\sigma$) are shown)

APPENDIX 2 (Cont.)



Appendix 2.5. Apparent $^{40}\text{Ar}/^{39}\text{Ar}$ Age Spectra ($\pm 1\sigma$) for Sericitic Whole-Rock Samples and Sericite from the Braden Pipe and Marginal Breccia and the Age Spectra ($\pm 1\sigma$) for Hornblende from a Postore Andesitic Dike and Sericitic Whole-Rock from a Hydrothermal Breccia Hosted by the Braden Pipe (plateau $^{40}\text{Ar}/^{39}\text{Ar}$ ages ($\pm 1\sigma$) are shown, except for the TT-141 hornblende sample that does not define a plateau)

APPENDIX 3

Sampled Drill Hole Locations

Sampled drill hole	Drill hole collar			Azimuth	Inclination
	Northing ¹ (m)	Easting (m)	Level (m)		
DDH 1068	217.695	755.098	1982	91°	-85°
DDH 1091A	215.661	753.924	1983	195°	-62°
DDH 1116	-325	1790	2161	128°35'	-22°
DDH 1140	-107.043	1494.399	2400	128°35'	-45°
DDH 1300	1058.598	741.937	2282.905	0	-90°
DDH 1307	-415.610	1351.892	2607.223	0	-90°
DDH 1303	1170.328	457.015	2282.115	0	-90°
DDH 1309	1078.674	914.685	2283.224	0	-90°
DDH 1311	-304.542	1210.329	2606.672	0	-90°
DDH 1323	1665.925	168.462	2165.260	83°35'	17°
DDH 1333	224.746	1454.045	2375.695	265°13'	17°
DDH 1334	109.159	1515.361	2358.996	70°08'30"	-45°
DDH 1337	108.659	1515.437	2358.818	89°35'	-55°
DDH 1407	-421.342	419.551	2283.802	192°18'	-13°
DDH 1409	-385.602	644.634	2284.908	194°25'	-25°
DDH 1414	-365.716	462.982	2357.335	190°33'	-27°
DDH 1514	1018.637	388.080	2282.115	0	-90°
DDH 1554	1028.038	468.701	2282.596	0	-90°
DDH 1556	-164.498	1216.335	2283	128°35'	-84°
DDH 1891	1084.175	919.092	2075.513	270°	9°
DDH 2008	399.422	246.419	2100	91°	-72°
DDH 2176	98.948	1821.69		90°	-35°

¹ Local mine grid of the El Teniente mine (metric)